(1, 1, 1-trifluoroacetylacetonato)silver(I) Used for Photochemical and Thermal Deposition of Silver and Silver Oxide Film and its Kinetics

by

Hai Xiong (Hanson) Ruan
B. Eng. East China University of Science and Technology, 1992

THESIS SUBMITTED IN PARTIAL FULFILLMENT OF
THE REQUIREMENTS FOR THE DEGREE OF

MASTER OF SCIENCE

In the
Department
of
Chemistry

SIMON FRASER UNIVERSITY

Summer 2007

APPROVAL

Name: Hai-Xiong(Hanson) Ruan

Degree: Master of Science

Title of Thesis: (1,1,1-trifluoroacetylacetonato)silver(I) used for photochemical and thermal deposition of silver and silver oxide film and its kinetics

Examining Committee:

Dr. George R. Agnes
Chair
Professor, Department of Chemistry

Dr. Paul W. Percival
Senior Supervisor
Professor, Department of Chemistry

Dr. Byron D. Gates
Supervisor
Assistant Professor, Department of Chemistry

Dr. Vance E. Williams
Supervisor
Assistant Professor, Department of Chemistry

Dr. Colin H. Jones
Internal Examiner
Professor, Department of Chemistry

Date Defended/Approved: **March 29, 2007**

ABSTRACT

(1,1,1-trifluoroacetylacetonato)silver(I) was synthesized from silver(I) oxide and 1,1,1-trifluoroacetylacetone in dichloromethane. The crystal structure of the silver complex was determined to be of the orthorhombic space group *Fddd*, with *a*: 11.442 Å, *b*: 15.276 Å, *c:* 31.069 Å, and *Z*=32. The compound was characterized by FT-IR and ^{1}H and ^{13}C NMR spectroscopy. Photolysis of a solid-state film of this complex at 254 nm leads to a crystalline silver and silver oxide film, composing of 94 mol% silver and 6 mol% oxygen. The resistivity of a film of 250 nm thick was found to be 2.1 μΩ cm. Multiple intermediates were observed in the FT-IR spectra during irradiating a solid-state film of this complex. Different photolithographic patterning methods are presented. The thermal decomposition of solid-state films in different environments was investigated. The decomposition rate increased with increasing relative humidity and showed no change with or without oxygen present.

DEDICATION

For though the fig-tree shall not flourish,

Neither shall fruit be in the vines;

The labor of the olive shall fail,

And the fields shall yield no food;

The flock shall be cut off from the fold,

And there shall be no herd in the stalls:

Yet I will rejoice in Jehovah,

I will joy in the God of my salvation.

To my God, Jesus Christ

who loves me and died for me.

献给深爱我的神，耶稣基督。

To my beloved wife XiaoYe Sheng,
who loves me faithfully during calm and storms.

献给深爱我的妻子盛晓叶，我的忠贞的伴侣，

无论在和平还是在风暴中。

ACKNOWLEDGEMENTS

Special thanks go

To Dr. Ross Hill, who taught me photochemical metal organic deposition and gave me the opportunities of learning some advanced material analytical technologies;

To Dr. Raymond J. Batchelor for single-crystal structure determination;

To my new committee members for their valuable time and help during my thesis writing;

To Dr. Bret Heinrich, a kind emeritus professor, who offered great help on the composition analysis as well as his valuable discussions;

To Dr. Karen Kavanagh, who taught me to operate high-resolution transmission electron microscopic systems and exposed me to the mysterious green screen; and Dr. Fink and Dr. Li Yang for HRTEM images acquisition.

To Mr. Ken Myrtle, who helped me on the Auger electron spectroscopic analysis of thin films;

To Mr. Owen for help on mass spectroscopic analysis, Mrs. Tracey for NMR spectral acquisition, and Mr. Yang for elemental analysis.

To the colleagues in Dr. Hill's group for their friendship;

To NSERC Canada and the Department of Chemistry of SFU for their generous financial support.

TABLE OF CONTENTS

LIST OF FIGURES

LIST OF TABLES

LIST OF SCHEMES

LIST OF ABBREVIATIONS AND SYMBOLS

ε	extinction coefficient
θ	Incident angle
λ	wavelength in nm
α,β,γ	angles between vectors in a unit cell
χ^2	the reduced chi-square
δ_i	the propagated error
ρ_r	rocking
A, (A_t, A_0)	the absorbance (at time t or time zero)
a, b, c,	vectors of a unit cell
Abs.	absorption
acac	acetylacetonate
AES	Auger electron spectroscopy
Ag(I)tfa	(1,1,1-trifluoroacetylacetonato)silver(I)
Ag_2L_2	represents the silver complex in an amorphous film
AgO_x	silver oxide(s)
C	concentration
Coeff.	coefficient
CVD	chemical vapour deposition
C_x	the atomic concentration
D_{hkl}, d	d-spacing between lattice plan (h k l)
d_i	the scale factor
Expt. (expt)	experiment
FT-IR	Fourier transform Infrared
h, k, l	lattice indices
H_2O_a	the water in air
H_2O_i	the water molecules in the film of Ag(I)tfa
hfa	1,1,1,5,5,5-hexafluoroacetylacetonate
Htfa	1,1,1-trifluoroacetylacetone

I	the intensity of the transmitted light
I_0	the intensity of the incident light
I_f	the current between two probes not crossed
I_x	the peak-to-peak Auger amplitude
K	crystallite shape constant
k_d, k_{-d}, k_2, k	the rate constants
L	length
l	path length of light
MOCVD	metal organic chemical vapour deposition
No.	the quantity of
Ph_3P	triphenylphosphine
R	circular radius
RH	relative humidity level
R_s	sheet resistance
s	the error associated with the measured data
SEM	Scanning electron spectroscopy
S_x	the relative elemental sensitivity factor
TEM	transmission electron spectroscopy
tfa	1,1,1-trifluoroacetylacetonate
TGA	thermogravimetric analysis
UV	Ultra-violet
V_f	the voltage applied between two probes on a film
V_{film}	volume of the measured area of the film
XRD	X-ray powder diffraction
δ	bending mode
δ_d	degenerate bend
δ_s	symmetric bend
ν	stretching vibration

CHAPTER 1: INTRODUCTION

1.1. Introduction

Many methods have been developed to prepare metal and/or metal oxide composite films. The photochemical metal organic deposition method developed in Hill's laboratory[1-3] can be used to convert solid-state films of metal organic complexes under light irradiation to metal and/or metal oxide films. At the same time as the development of this deposition method, many metal organic complexes have been synthesized. Among these complexes, some organic adducts of (1,1,1-trifluoroacetylacetonato)silver(I) were synthesized.[4-8] However, converting a solid-state film of (1,1,1-trifluoroacetylacetonato)silver(I) directly to a silver and silver oxide composite film by photochemical or thermal method has not been previously reported. Although some spectroscopic data on (1,1,1-trifluoroacetylacetonato)silver(I) have been published in the literature[9], the assignments of some absorption bands were ambiguous due to the lack of the single-crystal structure of this compound. Therefore, a detailed study of its structure and spectroscopic properties would be valuable. As reported in the literature, this silver complex is photolytically and thermally sensitive. Understanding the photolytic and thermal reactions of a solid-state film of this precursor is important in order to know how a silver film could be deposited.

1.1.1. A brief introduction to photochemical metal organic deposition

Photochemical metal organic deposition has been developed in Hill's laboratory since the early 1990's. This method uses photosensitive metal organic complexes that are prepared as thin films on substrates and converted to metal and/or metal oxide films by light irradiation (Scheme 1.1).

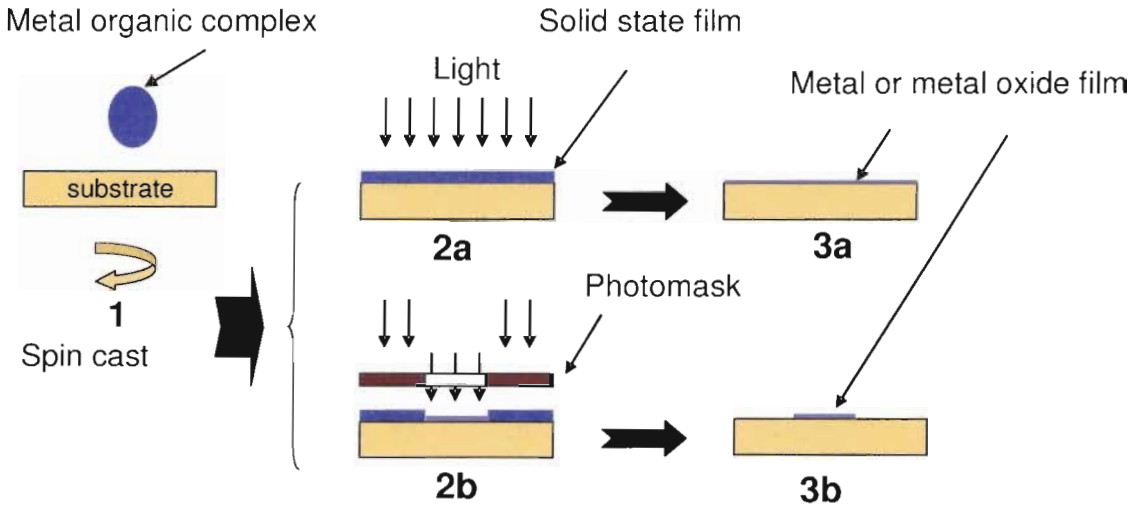

Scheme 1.1 Schematic diagram of the photochemical metal organic deposition process

A certain amount of metal organic solution (blue drop) is spin-coated onto a planar substrate to form a solid-state film (step 2a). Upon light irradiation, the film is converted to a metal and/or metal oxide film (step 3a). If a photomask is employed during irradiation (step 2b), the exposed area is converted to a metal and/or metal oxide film (step 3b). After developing the film with an appropriate solvent, a patterned film remains on the substrate.

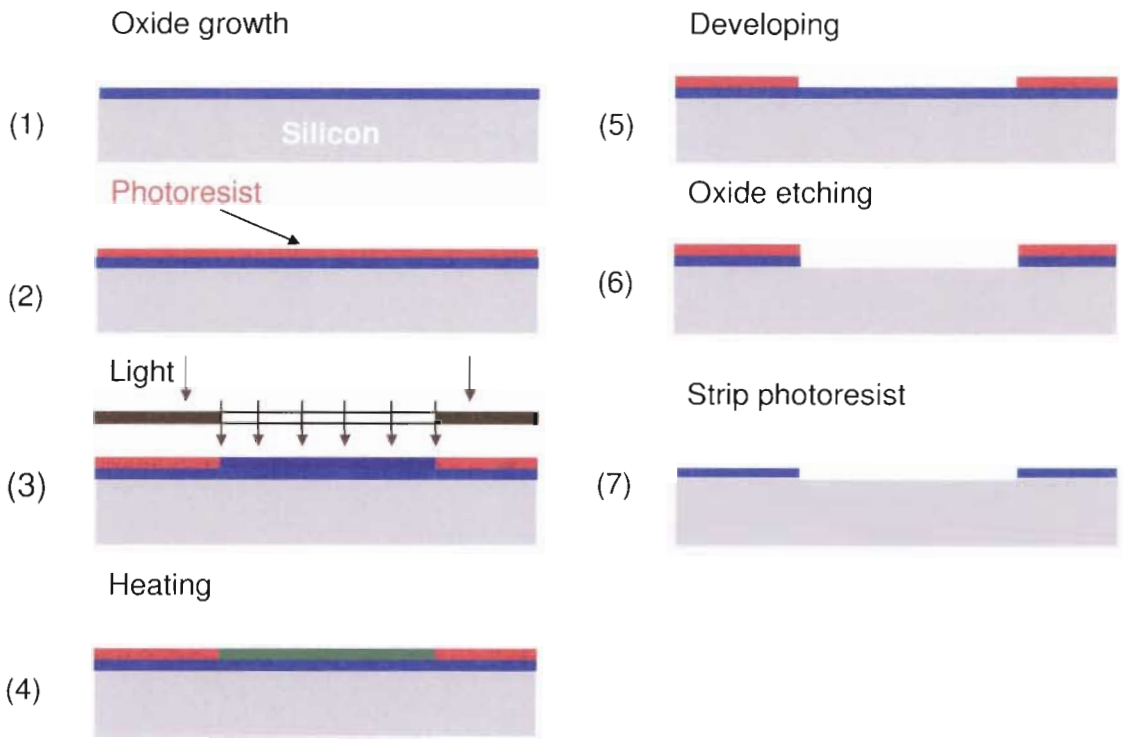

Scheme 1.2 A photolithographic procedure with a positive photoresist.

A conventional photolithographic process of patterning a silicon dioxide layer with a positive photoresist is depicted in Scheme 1.2. An oxide layer (blue layer) is grown on the silicon substrate (step 1). Then a positive photoresist (red layer) is spin coated on top of the oxide. Photolithographic exposure is selectively applied through a photomask in step 3. The film is then heated for the conversion of the exposed area (step 4) and developed with a solvent to remove the exposed area (step 5). Then the exposed oxide layer is etched in step 6. A patterned oxide film on the silicon substrate is obtained after the photoresist is removed in step 7.

Comparing these two methods, the photochemical metal organic deposition eliminates four steps from the photolithographic process with a photoresist, and reduces processing chemicals such as photoresist and chemical etchants. Less

processing steps and fewer chemicals used in the process could greatly reduce production costs and waste.

1.2. The research goals

A more detailed study of (1,1,1-trifluoroacetylacetonato)silver(I) including its crystal structure and spectroscopic properties is needed in order to explore its possible application for deposition of silver films. Such a deposition would be of great interest since no silver has been prepared by photochemical metal organic deposition. Although the mixed copper and copper oxide films have been prepared from some copper(II) organic complexes,[3] these films are nonconductive. A conductive silver film could fill the need for a photochemical metal organic deposition approach to potential microelectronic application. Therefore, three major research goals are intended for this thesis work and are listed in sections 1.2.1, 1.2.2, and 1.2.3.

1.2.1. Spectroscopic study of the structure and properties of (1,1,1-trifluoroacetylacetonato)silver(I)

1.2.1.1. Background of enol and keto forms of β-diketone

Given the tautomeric structure of many metal doctorates, it is important to understand the structures of the ligand complexes. The tautomeric structure of β-carbonyls (shown in Scheme 1.3) has been well studied by many researchers using NMR spectroscopy.[10-13]

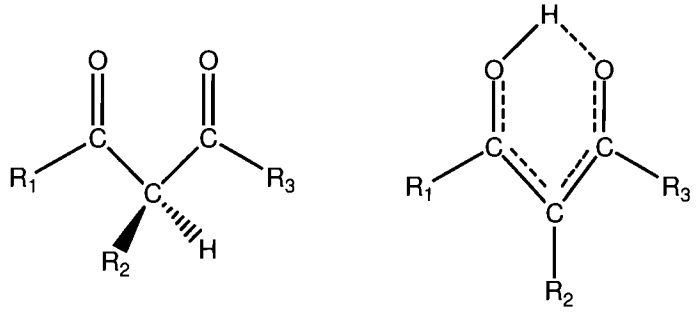

(a) Keto (b) Enol

Scheme 1.3 The tautomer structure of β-diketone complexes.

Many factors can affect the molecular structures of the chelating product. Substituent effects, solvent effects, and related equilibration constants are well documented in the literature.[14-18] In particular, it has been found that fluorination of β-diketones shifts the keto-enol equilibrium towards the enol. The enol content of 1,1,1-trifluoropentane-2,4-dione was found to be 97% in dichloromethane by Rogers in 1964.[10] This value was confirmed at 96% by Wallen in 1997.[18] In the research described in this thesis, in order to produce a highly selective product, dichloromethane was chosen as a solvent for synthesis because it favours the enol form of the ligand.

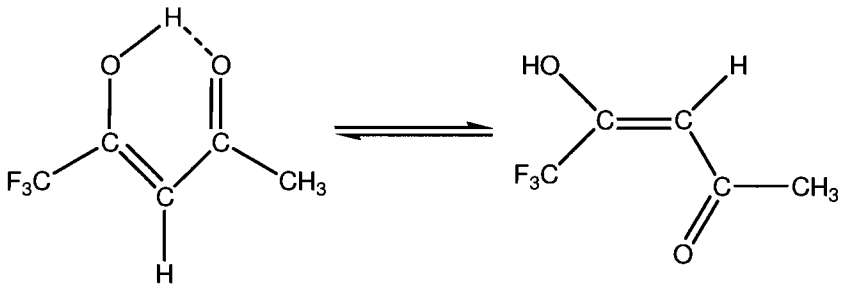

cis form trans form

Scheme 1.4 The stereoisomers of 1,1,1-trifluoroacetylacetone.

In addition, the enol structure of 1,1,1-trifluoropentane-2,4-dione has two stereoisomeric structures as shown in Scheme 1.4, suggested by Park.[16] He suggested that two types of hydrogen bonding, H-F and H-O bonding could occur in the structure in order to stabilize the enolic form. Tayyari provided spectroscopic evidence to support hydrogen bonding in the enol form of β-diketones by observing shifts in the stretching vibration of C=O and C=C in FT-IR and Raman spectra.[13] Both authors concluded that hydrogen bonding plays an important role in stabilizing the enol form of β-diketones. The different positions of the acidic proton could affect the reaction with silver(I) oxide to form different bonding structures between the metal ions and ligand, which can lead to different complexes.

1.2.1.2. The metal-ligand bonding structures of metal β-diketonates

Metal ions can chelate with β-diketone ligands through different metal-ligand bonds. Two types of metal-ligand bonds, metal-oxygen bond (type **A**) and metal-carbon bond (type **B**) shown in Scheme 1.5, have been reported for many metal β-diketonates.[9,19,20] In addition, the type **A** compounds have two resonance

structures. A delocalized ring structure has been commonly used to illustrate the structure of type **A** compounds.

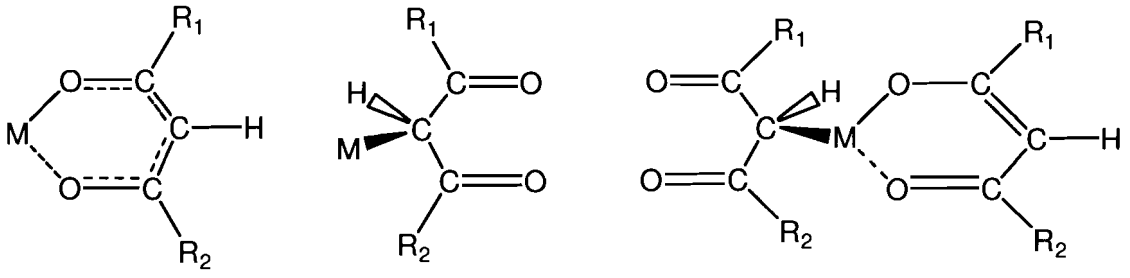

Type A Type B Type AB

Scheme 1.5 Different chelating structures of metal β-diketone compounds.

Some compounds have been reported to have both types of metal-ligand bonding (type **AB**).[20] However, few silver β-diketonates with type AB bonding have been reported in the literature[9]. Lewis pointed out that the possibility of a metal-carbon bonded structure should be considered in $(Ph_3P)Ag(tfa)$ and $(Ph_3P)Ag(hfa)$ complexes.[9] In his report, the broadening of the absorption bands from this type of bonding made the assignment of some bands ambiguous. However, in addition to the crystal structure information of the complex $K[Pt(acac)_2Cl]$, Nakamoto used deuterium substitution of the ligand to help identify the absorption bands of $K[Pt(acac)_2Cl]$, $K[Pt(acac)_3]$, and other metal β-diketonates complexes.[21] In his paper the bands corresponding to complexes with different metal-ligand bonds were distinguished. Whether (1,1,1-trifluoro-acetylacetonato)silver(I) has simple Ag-O bonds or also has Ag-C bonds is of much interest. A single-crystal structure of Ag(I)tfa can provide useful information. At the same time, the infrared spectra of this complex in the crystalline state and

amorphous film state would provide useful structural information for understanding the reaction mechanism.

1.2.2. Investigation of photochemical decomposition of a solid-state film of (1,1,1-trifluoroacetylacetonato)silver(I)

The solid-state film of (1,1,1-trifluoroacetylacetonato)silver(I) was found to be photosensitive. To explore whether this photoreaction leads to deposition of a silver film is important. To understand the general physical properties of the deposited film such as conductivity, film structure, and composition has potential value for potential interconnection metallization applications. Many metal and metal oxide films have been prepared by the photochemical metal organic deposition method in the literature.[1-3] However, all of these metal oxide films were amorphous. Metallic silver is normally crystalline. Whether any deposited silver oxide is crystalline or not is of much interest. A detailed study of the deposited film may also add understanding to the reaction process.

1.2.3. Investigation of thermal decomposition of a solid-state film of (1,1,1-trifluoroacetylacetonato)silver(I)

A solid-state film of (1,1,1-trifluoroacetylacetonato)silver(I) was found to be heat and moisture sensitive. To explore whether thermal reaction leads to the same silver or silver oxide film as a photochemical reaction is of great interest. To investigate how water is involved in the decomposition of the film may help

explain the kinetics of the reaction. An investigation of the reaction kinetics could be useful to understand the deposition of silver and silver oxide films.

1.3. The structure of the thesis

This thesis consists of five chapters. A general introduction and the research goals are given in the first chapter. Each following chapter has an independent introduction.

In **Chapter 2** the synthesis of crystalline (1,1,1-trifluoroacetylacetonato)silver(I) is presented. Then, this silver complex is characterized by various techniques, including elemental analysis, single-crystal X-ray diffraction, FT-IR spectroscopy, proton and ^{13}C NMR spectroscopy, and thermogravimetric analysis. Two types of silver atoms with different coordination numbers as well as connectivity were found in the structure. The assignment of the infrared absorption bands of a crystalline film as well as an amorphous film of this complex is presented. The infrared bands attributed to the stretching vibration of Ag-C and Ag-O bonds are assigned. The thermal stability of the complex is also discussed.

In **Chapter 3** a mechanistic investigation of the deposition of silver and silver(I,III) oxide from a solid-state film of (1,1,1-trifluoroacetylacetonato)silver(I) is presented. The electronic absorption spectrum of an amorphous film of (1,1,1-trifluoroacetylacetonato)silver(I) is presented first. Then, the changes of a film under light irradiation is monitored by FT-IR spectroscopy. The competition between the photochemical and thermal reactions of the films of Ag(I)tfa is also

discussed and the products are identified. The sheet resistance of the deposited film are measured on both single and multiple sequential deposition of the photolyzed film on silicon substrate. A proposal for a photochemical mechanism would be premature because of the unverified complex structure and unidentified multiple intermediates.

In **Chapter 4** an investigation of thermal decomposition of a solid-state film of (1,1,1-trifluoroacetylacetonato)silver(I) is presented. The volatile thermal products from this film are analyzed by mass spectrometry. The solid products are analyzed by AES and XRD measurements. Then, infrared spectra of the films under different relative humidity levels are presented. The possibility of the involvement of water and oxygen in the decomposition of this film is discussed. A kinetic model for the reaction between the film and water is unavailable due to the complex and heterogeneity of the reaction system. Suggestions for possible future work are given at the end of this chapter.

The last chapter, **Chapter 5**, contains an overall summary of the thesis work.

1.4. Reference list

(1) Hill, R. H.; Becalska, A.; Chiem, N. *Organometallics* **1991**, *10*, 2104-2109.

(2) Hill, R. H. *Photonics Science News* **1996**, *2*, 12-14.

(3) Avey, A. A.; Hill, R. H. *Journal of the American Chemical Society* **1996**, *118*, 237-238.

(4) Darr, J. A.; Poliakoff, M.; Blake, A. J.; Li, W.S. *Inorganic Chemistry* **1998**, *37*, 5491-5496.

(5) Darr, J. A.; Poliakoff, M.; Li, W.S.; Blake, A. J. *Journal of the Chemical Society, Dalton Transactions: Inorganic Chemistry* **1997**, 2869-2874.

(6) Fragala, M. E.; Malandrino, G.; Puglisi, O.; Benelli, C. *Chemistry of Materials* **2000**, *12*, 290-293.

(7) Xu, C.; Corbitt, T. S.; Hampden-Smith, M. J.; Kodas, T. T.; Duesler, E. N. *Journal of the Chemical Society, Dalton Transactions: Inorganic Chemistry* **1994**, 2841-2849.

(8) Xu, C.; Baum, T, H.; Rheingold, A. L. *Inorganic Chemistry* **2004,** *43*, 1568-1573.

(9) Gibson, D.; Lewis, J.; Oldham, C. *Journal of the Chemical Society [Section] A: Inorganic, Physical, Theoretical* **1966**, 1453-1456.

(10) Rogers, M. T.; Burdett, J. L. *Canadian Journal of Chemistry* **1965**, *43*, 1516-1526.

(11) Belford, R. L.; Martell, A. E.; and Calvin, M. *Journal of Inorganic and Nuclear Chemistry* **1956**, *2*, 11-31.

(12) Burdett, J. L.; Rogers, M. T. *Journal of Physical Chemistry* **1966**, *70*, 939-941.

(13) Tayyari, S. F.; Zeegers-Huyskens, T.; Wood, J. L. *Spectrochimica Acta, Part A: Molecular and Biomolecular Spectroscopy* **1979**, *35A*, 1265-1276.

(14) Andreassen, A. L.; Bauer, S. H. *Journal of Molecular Structure* **1972**, *12*, 381-403.

(15) Bassetti, M.; Cerichelli, G.; Floris, B. *Journal of Chemical Research, Synopses* **1988**, 236-237.

(16) Park, J. D.; Brown, H. A.; Lacher, J. R. *Journal of the American Chemical Society* **1953**, *75*, 4753-4756.

(17) Ng, G.; Goldberg, D. E. *Journal of Inorganic and Nuclear Chemistry* **1967**, *29*, 707-781.

(18) Wallen, S. L.; Yonker, C.R.; Phelps, C. L.; Wai, C. M. *Journal of the Chemical Society, Faraday Trans.* **1997**, *93*, 2391-2394.

(19) Nakamoto, K.; Martell, A. E. *Journal of Chemical Physics* **1960**, *32*, 588-597.

(20) Gibson, D. *Coordination Chemistry Reviews* **1969**, *4*, 225-240.

(21) Behnke, G. T.; Nakamoto, K. *Inorganic Chemistry* **1968**, *7*, 330-335.

CHAPTER 2:
SYNTHESIS AND CHARACTERIZATION OF (1,1,1-TRIFLUOROACETYLACETONATO) SILVER(I)

2.1. Introduction to transition metal β-diketonates

Metal β-diketonates and their derivatives have been well studied by FT-IR and NMR spectroscopy for their coordination versatility of metal-C (M-C) and/or metal-O (M-O) bonded structures.[1-3] For example, the infrared spectra of divalent and trivalent transition metal complexes with M-O or M-C bonded structure were well studied by Nakamoto.[4,5] Some substituted or addition compounds of metal β-diketonates were studied by Nakamoto and others,[3,6,7] and the influence of fluorine in substituted metal β-diketonates was reported by Belford.[8] The infrared spectra of platinum compounds containing two types of metal-ligand bonding showed the versatility of coordination compounds with β-diketone ligands.[9,10] In the case of silver(I) β-diketonates, the hydrated silver(I) hexafluoroacetylacetonate $[\{Ag(hfa)\}_2](H_2O)]$ contains only Ag-O bonds in its crystal structure.[11] No detailed assignment of the infrared spectrum was reported in the literature. Many organic adducts of silver(I) hexafluoroacetylacetonate or silver(I) trifluoroacetylacetonate (Ag(I)tfa) were reported in the literature to have good thermal stability.[11-15] However, few of them contain both Ag-C and Ag-O bonds in their reported crystal structures. The detailed assignments of their corresponding stretching frequencies have not been reported previously. In the

case of (1,1,1-trifluoroacetylacetonato)silver(I), Wenzel and others reported a synthesis route from silver(I) oxide and Htfa in aqueous solution.[16] They identified this complex as containing an oxygen-bonded structure based on the carbonyl stretching frequency observed at 1650 cm^{-1}. They also suggested that silver π bonding to a C=C bond could be possible. No single crystal structure determination of (1,1,1-trifluoroacetylacetonato)silver(I) has been reported in the literature to support this type of bonding. This silver complex was reported as unstable in air but no particular reasons for this property were reported. The cause of this instability could be due to the amorphous state of the product and possible water content, since the product was prepared from aqueous solution. The reason for the instability of Ag(I)tfa is examined in this thesis.

In this chapter of the thesis, a single-step synthesis of Ag(I)tfa in a selected organic solvent is reported by modification of a synthesis routine reported in the literature.[11] The product was characterized by single-crystal structure analysis, FT-IR spectroscopy, ^{1}H- and ^{13}C-NMR spectroscopy, and thermogravimetric analysis. The infrared absorption bands of Ag(I)tfa complex containing both Ag-O and Ag-C bonds are assigned. The difference in the FT-IR spectra of Ag(I)tfa in crystalline and amorphous states is presented for the first time. Finally, the thermal stability of Ag(I)tfa is reported.

2.2. Synthesis of (1,1,1-trifluoroacetylacetonato)silver(I)

Ag(I)tfa has previously been synthesized in aqueous media or by other methods in the literature.[16] However, in order to eliminate possible contamination of other metal ions or other chemical residues in the deposition of a high purity silver and/or silver oxide film, a single-step acid-base reaction between silver(I) oxide and 1,1,1-trifluoroacetylacetone (Htfa) in dichloromethane was employed to synthesize this complex. The chemical reaction can be expressed by the following equation:

$$Ag_2O + 2Htfa \xrightarrow{CH_2Cl_2} 2Agtfa_{(s)} + H_2O$$

The silvery product precipitated from the solution and the byproduct water and solvent were removed from the solid product by vacuum filtration and air flowing. Some black solids were found on the bottom of the container after dissolving this product in ethanol or other organic solvent. This material could be unreacted silver(I) oxide.[2,17] After storing the filtrate in a freezer overnight, white crystals precipitated on the bottom of the container and were collected by vacuum filtration and dried by air flow. The final product was white or silvery needle-like crystals. The product was kept in a light-proof container and stored in a freezer. No change in appearance or infrared spectrum of the product were observed after it was stored over two months. This stability could be mainly due to the crystalline nature of the product since the noncrystalline product was reported as unstable in air in the literature. The negligible water content in the dried product could contribute to this stability since the amorphous film of the product reacts

with water in air quickly under ambient conditions. The reaction between the amorphous form of the silver complex and water will be presented in Chapter 4.

Elemental Analysis: Calculated for $C_5H_4O_2F_3Ag$: C: 23.0%, H: 1.55%. Found: C: 22.7±0.4 %, H: 1.7±0.4%.

2.3. Characterization

2.3.1. Crystal Structure

Crystallographic data for Ag(I)tfa are shown in Table 2.1. A tetramer structure of Ag(I)tfa ($[Ag_2(CF_3COCHCOCH_3)_2]_2$) is shown in Figure 2.1. A packing diagram of the unit cell is shown in Figure 2.2. Selected bond distances and angles are listed in Table 2.2.

During the crystal structure analysis, the $CF_3COCHCOCH_3$ group was found to be disordered (end-to-end) so that a complementary partial F/H relative occupancy was required for the two distinct terminal CF_3/CH_3 groups. In Figure 2.1, the hydrogen and fluorine atoms in two end groups are superimposed.

Table 2.1 Crystallographic data for Ag(I)tfa.

Formula weight	259.92
Crystal system	Orthorhombic
Space group	*Fddd*
a, Å	11.442(3)
b, Å	15.276(6)
c, Å	31.069(8)
α, β, γ, degrees	90, 90, 107
V, $Å^3$	5524.87(30)
Z	32
d_{expt}, g/cm^3	2.510
Abs. coeff, mm^{-1}	2.89
Crystal size (mm)	$0.11 \times 0.13 \times 0.43$
No. of reflections collected	1783
No. of unique reflections (merging R)	920 (0.025)
No. of observed reflections ($I0>2.5\sigma(I0)$)	658
2θ range, degrees	4 - 45
No. of parameters	130
RF	0.05
Goodness of fit	2.9

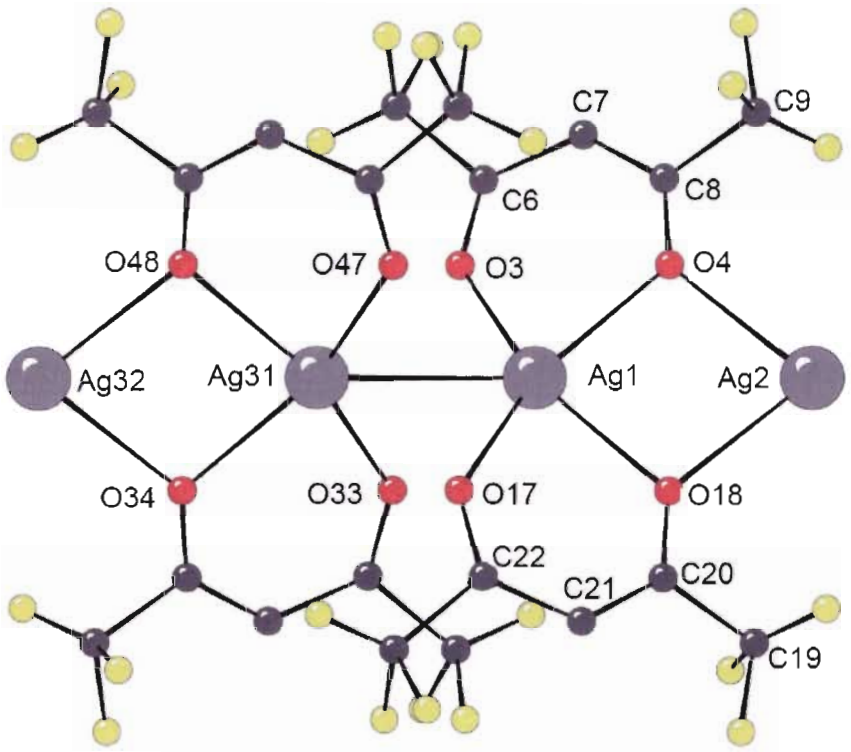

Figure 2.1 A tetramer structure of Ag(I)tfa viewed along the *a*-axis. The superposition of fluorine and hydrogen atoms is not resolved.

Table 2.2 Selected interatomic distances (Å) and bond angles (degrees).

Interatomic distances (Å)			
Ag(1) - Ag(31)	2.877(3)	Ag(2b) -C(21)	2.339(2)
Ag(1) - O(4)	2.384(2)	Ag(2) - O(18)	2.488(3)
Ag(1) - O(17)	2.384(4)		
Bond angles (°)			
Ag(31)-Ag(1)-O(3)	64.7(3)	C(3d)-Ag(32)-C(3e)	143.7(7)
Ag(31)-Ag(1)-O(17)	137.8(3)	O(4)-Ag(1)-O(18)	84.3(5)
O(3)-Ag(1)-O(4)	149.8(4)	Ag(2b)-C(21)-C(22)	98.94(3)
O(3)-Ag(1)-O(17)	129.4(5)	O(18)-Ag(2)-O(4)	80.2(4)
O(17)-Ag(1)-O(18)	76.7(3)	O(34)-Ag(32)-C(3e)	109.3(4)
O(34)-Ag(32)-(3d)	98.3(4)	Ag(2b)-C(21)-C(20)	98.78(3)

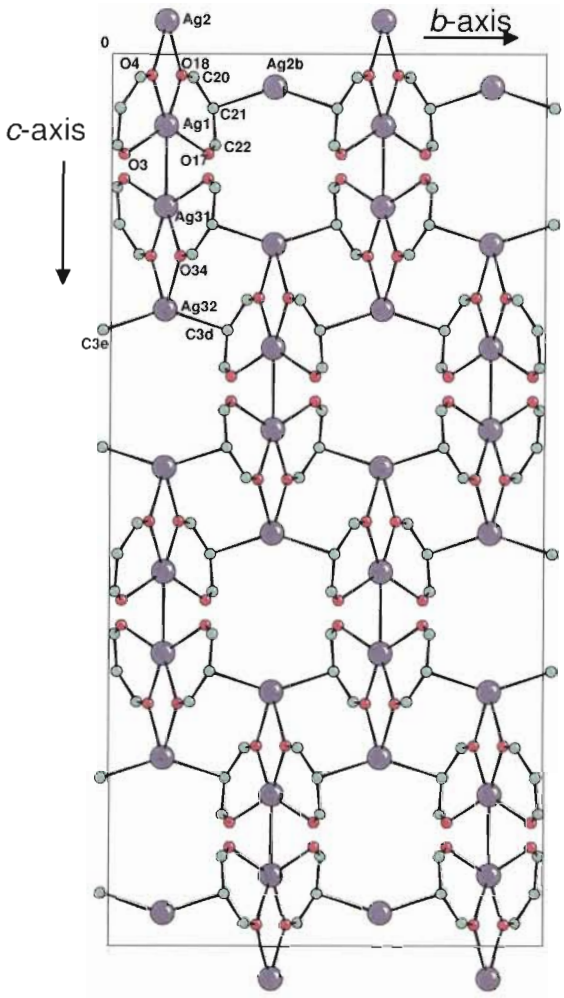

Figure 2.2 A packing diagram of the unit cell of Ag(I)tfa viewed along the *a*-axis.

In the crystal structure of Ag(I)tfa, two types of coordinated silver atoms were found. The coordination number of the Ag(1) and Ag(31) atoms (defined as type-1) is five. Each type-1 Ag atom coordinates with two ligands asymmetrically through four oxygen atoms and connects to another same type Ag atom with a Ag-Ag interaction. The bond lengths of the C(20)–O(18) and C(21)–O(17) bonds are 1.236(3) Å and 1.216(2) Å, which are close to the C=O bond length (1.230 Å). These values are very close to those (1.27 and 1.31 Å) of the β-diketone complex of trimethylplatinum(IV) reported by Swallow.[18] The two bond

lengths between three ring carbon atoms (C(20)–C(21), C(21)–C(22)) are 1.405(2) Å and 1.441(3) Å. These values are shorter than the standard single bond length of C–C (1.540 Å) and longer than the standard double bond length of C=C (1.340 Å). These data suggest a ring structure for the ligand. In addition, the bond lengths of the Ag(1)-O(3) and Ag(1)–O(4) bonds are 2.336 (2) and 2.384 (1) Å. These values are greater than the sum of the covalent radii (2.270 Å) and shorter than the sum of van der Waals radii (3.240 Å). These two bond lengths are in the range from 2.135(2) Å to 2.634(12) Å of the reported values for silver complexes in the literature.[19-22] These data suggest that the silver atom is chelated with the ligand through oxygen atoms.

The coordination and connectivity of the Ag(2), Ag(32), and Ag(2b) atoms (defined as type-2) differs from that of the type-1 silver atoms. The coordination number of these type-2 silver atoms is four. Each type-2 silver atom coordinates with two oxygen atoms – one from each of the two ligands coordinating with the adjacent type-silver atom. The bond lengths of the Ag(2)–O(4) and Ag(2)–O(18) bonds both are 2.488(1) Å, which is longer than that of the type-1 Ag-O bond. On the other hand, each Ag(31) atom coordinates with two middle carbon (C3) atoms of the rings – one from each of the two ligands in two adjacent units. The bond lengths of the Ag(32)–C(3e) and Ag(32)–C(3d) are 2.339(2) Å, which is greater than the sum of the covalent radii of Ag-C (2.270 Å) and shorter than that of the van der Waals radii (3.420 Å). This value is in the range from 2.060 Å to 2.634 Å of silver complexes in the literature.[21,23] Therefore, it is believed that the type-2 silver atoms are bonded to two C3 atoms from two adjacent ligands.

In brief, two types of bonding between silver and ligand in the crystal structure are revealed, namely Ag–O and Ag–C bonding. This information is important for further spectroscopic characterization and mechanistic study on the photodegredation of this silver complex.

The other important information obtained from the crystal structure of Ag(I)tfa is the short distance between two silver atoms. It is worth noting that four silver atoms in each tetramer unit align linearly along the *c*-axis while the identical tetramer units connect with each other through four Ag-C bonds. Among these four linear silver atoms, the distance (3.667 Å) between the Ag1 and Ag2 atoms is far greater than the sum of the covalent radii (2.68 Å) and considered as non-bonding. However, the distance between Ag(1)-Ag(31) was found to be 2.876(3) Å, the shortest distance of Ag-Ag interaction without ligand support among the known silver(I) complexes listed in the Cambridge crystal structure database[a] (Table 2.3). The Ag-Ag distance of some ligand support silver complexes are listed in the same table as well. Some distances are shorter than that of Ag(I)tfa.

A negative value of magnetic susceptibility of the crystalline product indicates that the product is diamagnetic. Therefore, it is believed that Ag(I)tfa is a silver(1+) organic ligand coordinated complex.

[a] Accessed the website http://www.ccdc.cam.ac.uk/products/csd/ through licensed terminal software in the library of Simon Fraser University in May 2006.

Table 2.3 Selected Ag-Ag interactions without and with ligand support from the compounds listed in the Cambridge structure database.[b]

Complex formula without ligand support	Bond Length (Å)
$(C_{20}H_{16}Ag_2Cl_2N_4O_8)_n$	3.153(4)
$(C_8H_{16}Ag_2CdN_8)_n$	3.175(3)
$C_{24}H_{24}Ag_2N_6O_6$	3.087(6)
$(C_{42}H_{72}Ag_{10}Cd_4N_{34})n$	3.172(4)
$C_{38}H_{22}Ag_2F_{10}N_2$	3.067(8)
$(C_6H_6Ag_2N_4)_n$	3.160(4)
$C_{48}H_{36}Ag_6N_{18,}\ 2(C_5H_5N)$	3.227(9)
$C_{66}H_{114}Ag_6N_{12}S_{12}$	3.041(7)
$(C_{60}H_{92}Ag_4S_4)_n$, $n(CHCl_3)$	2.987(12)
$(C_{28}H_{22}Ag_6N_4O_{20})_n$	3.090(1)
$(C_{20}H_{20}Ag_2N_4O_8P_2)_n$ $2n(H_3O_4P)$	3.286(6)
$(C_{12}H_{16}AgN_8Ni)_n$, $n(H_2O)$	3.037(7)
$C_{14}H_{16}Ag_2N_2O_6$	3.069(2)
$C_{30}H_{26}Ag_2F_6N_{10}O_4$, $2(CHCl_3)$	3.068(3)
$C_{40}H_{66}O_4Ag_2F_6P_2$	3.095(1)
$Tl[Ag(CN)_2]$	3.110(3)
Bulk silver	2.890(3)
Complex formula with ligand support	**Bond Length (Å)**
$C_{14}H_{14}Ag_2N_2Si_4$	2.669(1)
$C_{10}H_{30}Ag_2N_4$	2.705(1)
$C_{18}H_{42}Ag_2B_2F_8N_8$	2.814(1)
$C_4H_6F_6S_2O_7Ag_2$	3.060(1)

[b] Database was accessed in May 2006.

2.3.2. ^{1}H and ^{13}C NMR spectra

Ag(I)tfa was studied in solution by ^{1}H and ^{13}C nuclear magnetic resonance spectroscopy. Benzene-d6 was used as the solvent to avoid possible reactions between the solutes (Ag(I)tfa or Htfa) and solvents like chloroform-d and methanol-d4. The ^{1}H NMR spectra of Ag(I)tfa and Htfa in benzene-d6 are shown in Figure 2.3 and Figure 2.4.

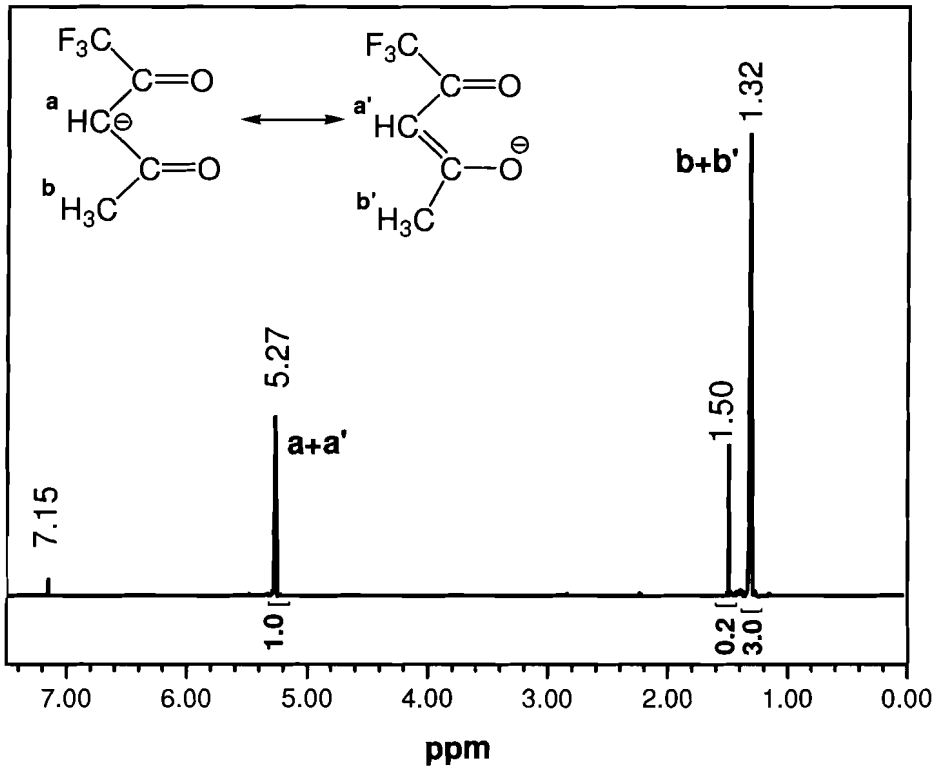

Figure 2.3 1H NMR spectrum of Ag(I)tfa in benzene-d6.

The ^{1}H NMR spectrum of Ag(I)tfa in benzene-d6 consists of four singlets. The chemical shifts associated with these peaks are 1.32, 1.50, 5.27, and 7.15 ppm (Figure 2.3). The singlet at 7.15 ppm is assigned to the residual proton of benzene-d6. The chemical shifts at 5.27 am 1.32 ppm are believed to be contributed from the protons (a and b, a' and b') of ligand ion of Htfa in two

resonance structures.[24] The ratio of the integrals of the peaks at 5.27 and 1.32 ppm is 3, which is consistent with the ratio between the protons of the ligand ion.

The chemical shift at 1.50 ppm could be contributed from a contamination in the solvent. It should not be contributed from the residual water in benzene, which normally is observed at 0.5 ppm. A similar signal was also observed at 1.54 ppm with a large quantity in the NMR spectrum of Htfa in benzene-d6. One possible source could be the residual of washing acetone used for washing the dropping pipettes.

These chemical shifts from Ag(I)tfa in solution are similar to that of the ligand in benzene-d6 (Figure 2.4), observed at 5.47 and 1.74 ppm. The chemical shift observed at 5.47 ppm could be attributed to the vinyl proton (-CH=) and 1.74 ppm to the allylic protons ($C=C-CH_3$) in the enol form of Htfa. The ratio of the integral of these two peaks was 3.0, which is consistent with the ratio between the protons of the ligand in the enol form. No chemical shifts from the protons (a' and b') of the ligand in a keto form were observed. The proton labeled as ^{c}H should have a very broad band close to 10 ppm for the enolic proton. However, it was not observed in the spectrum. The reason of that may be due to the residue of water that interacts with this proton.

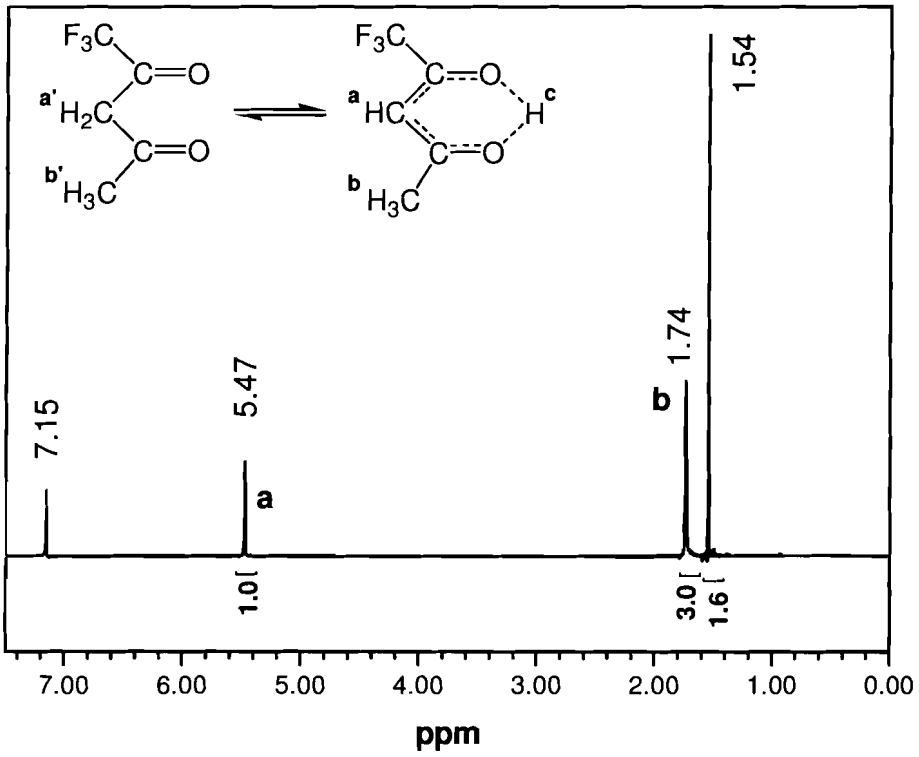

Figure 2.4 ^{1}H NMR spectrum of 1,1,1-trifluoroacetylacetone in benzene-d6.

The difference of the chemical shifts between these two spectra could be due to the structure and charge difference between the ligand and ligand ion. The different electron density around the atoms can affect the chemical shifts of the adjacent hydrogen atoms.

The possibility of Ag^{+} chelating with the ligand in solution is unlikely since the solvation energy of solvents is normally greater than the bonding energy between a silver ion and the ligand. In addition, silver has a relatively low affinity for oxygen donors,[26] so most silver(I) organic compounds dissociate to form ion pairs in organic solvents, including silver ions and complexed silver ions, free and complexed ligand ions. Therefore, it is believed the same situation is true for Ag(I)tfa in most organic solvents.

^{13}C NMR spectrum A proton-decoupled ^{13}C NMR spectrum of Ag(I)tfa in methanol-d4 is shown in Figure 2.5. Methanol-d4 was used as the solvent instead of benzene-d6 because Ag(I)tfa shows a greater solubility in methanol-d4. A high solubility in a solvent is essential for a high quality ^{13}C NMR spectrum.

This spectrum consists of three singlets, two quartets, and one septet. Their associated chemical shifts were observed at 29.3, 84.7, 199.2, 118.8, 172.6, and 47.7 ppm, respectively. Apart from the septet, which is attributed to the solvent CD_3OD, all the other five peaks are attributed to the ligand ions of Ag(I)tfa. Among them, the singlet at 29.3 ppm is attributed to the alkyl carbon **1** (**C**-C(O)-R). The singlet at 199.2 ppm is attributed to the ketone carbon **2** (C-**C**(O)-R). The singlet at 84.7 ppm is assigned to the carbon **3** (R-H**C**=C(O)-R"). The quartet at 172.6 ppm is attributed to the carbon **4** (R-**C**(O)-CF_3) coupled with three adjacent fluorine atoms. The quartet at 118.8 ppm is attributed to the carbon **5** (R-C(O)-**C**F_3) coupled directly with three fluorine atoms.

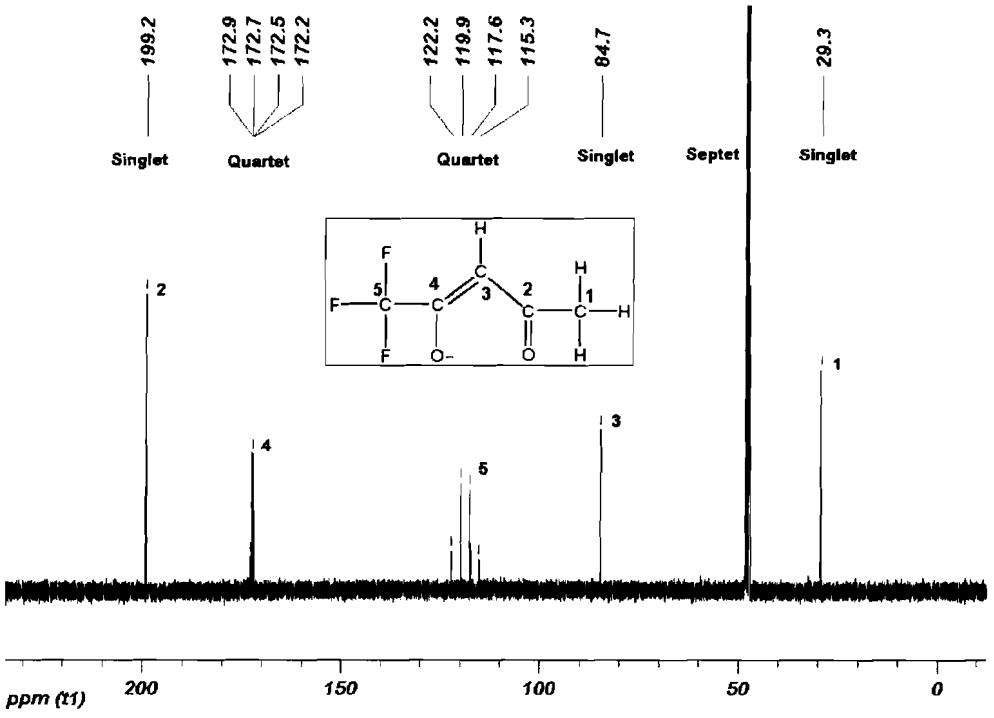

Figure 2.5 ^{13}C NMR spectrum of Ag(I)tfa in methanol-d4.

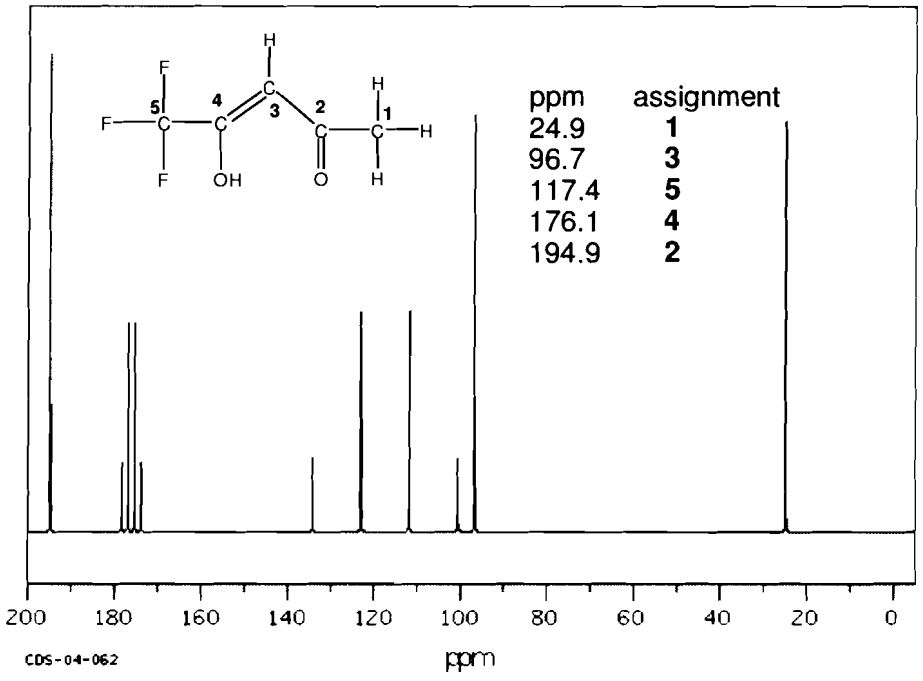

Figure 2.6 ^{13}C NMR spectrum of the ligand (Htfa) in $CDCl_3$ from the literature[25], reproduced with permission.

These chemical shifts are in good agreement with those of the ligand (Htfa) in the literature[25] (Figure 2.6) except that the chemical shift of carbon **3** differs by 12 ppm. The negative charge located on the middle carbon could be the reason for this difference.

2.3.3. FT-IR spectrum of (1,1,1-trifluoroacetylacetonato)silver(I)

2.3.3.1. FT-IR spectrum of crystalline Ag(I)tfa

Because Ag-O and Ag-C bonds were found in the crystal structure of Ag(I)tfa, the absorption bands of these bonds are of interest. A KBr pellet mixed with crystalline Ag(I)tfa was prepared by standard procedure as well as a KBr pellet mixed with crystalline (1,1,1-trifluoroacetylacetonato)Cu(II).[26] The FT-IR spectrum of the crystalline Ag(I)tfa was recorded from a KBr pellet and it is shown in Figure 2.7 (a). A FT-IR spectrum of crystalline (1,1,1-trifluoroacetyl-acetonato)Cu(II) was recorded by the same method as a reference. The spectrum is shown in Figure 2.7 (b).

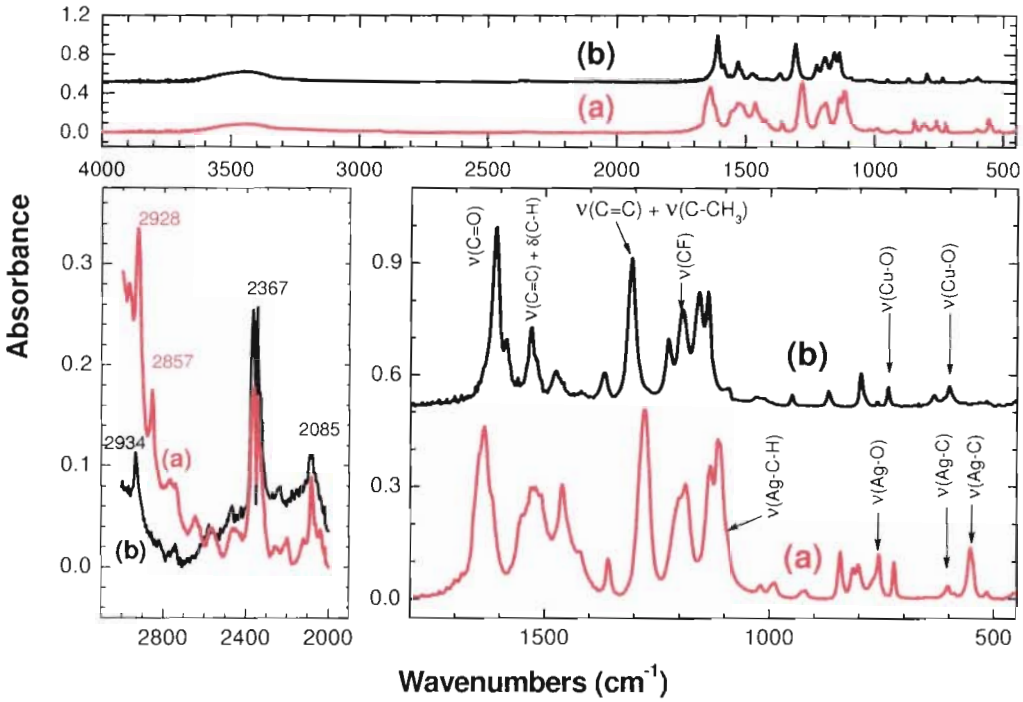

Figure 2.7 FT-IR spectra of (a) Ag(I)tfa (red solid curves) and (b) $Cu(tfa)_2$ (black solid curves) in KBr pellets.

FT-IR spectral assignments In order to assign the stretching vibration of Ag-O and Ag-C bonds more correctly, the absorption bands of three other related metal β-diketonates with distinct metal-ligand bonding are compared with that of Ag(I)tfa. Two of them are $K[Pt(acac)_3]$ (**1**) and $Na_2[Pt(acac)_2Cl_2]$ (**2**) cited from Nakamoto's work in the literature.[9] Among them, compound **1** contains both Pt-C and Pt–O bonds as revealed by its crystal structure, and compound **2** has only Pt–C bonds.[27] Although crystal structures of some silver β-diketonates are reported in the literature, none of them has Ag-O and Ag-C bonds connecting the same silver atom. The lack of similar silver complex in the literature was the other reason for choosing these complexes for reference. The effect of the different metal ions on the absorption bands will be considered as well. Furthermore, the deuterium substitutions used in these cited compounds by

Nakamoto added much clarity for the assignment of M-C and M-O bonds. No deuterium substituted silver complex of Ag(I)tfa was prepared.

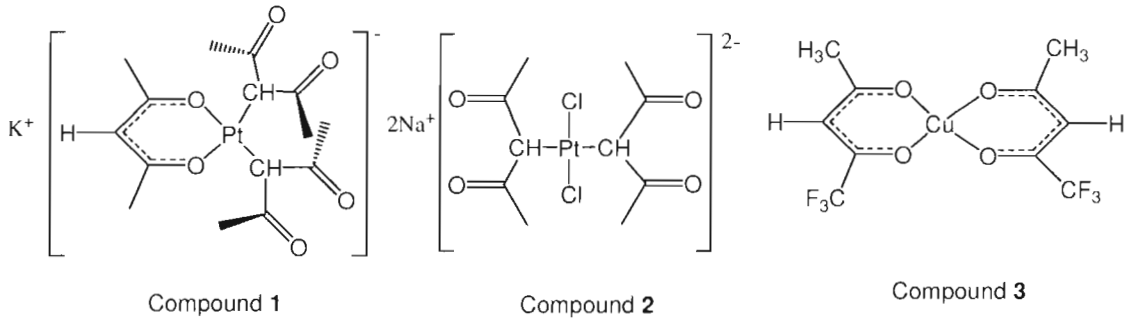

Compound **1** Compound **2** Compound **3**

Figure 2.8 Molecular structures of the cited compounds of (**1**) $K[Pt(acac)_3]$, (**2**) $Na_2[Pt(acac)_2Cl_2]$,[9] and $Cu(tfa)_2$.[26]

Because these two compounds have different end-groups (two CH_3 groups) of β-diketonate ligand from that (one CF_3 and one CH_3) of Ag(I)tfa, a transition metal complex chelated with the identical ligand to that of Ag(I)tfa can add much clarity to the assignment of the related absorption bands. Hence, (1,1,1-trifluoro-acetylacetonato)Cu(II) (compound **3**) which contains only Cu-O bonds in its crystal structure[26] was chosen. Its FT-IR spectrum is shown in Figure 2.7 labeled as (b).

In both infrared spectra shown in Figure 2.7, some broad absorption bands in the infrared spectra of Ag(I)tfa and compound **3** were deconvoluted to multiple peaks with a peak-fit program in order to identify the best positions of the peaks. The program used for peak fitting was Origin software[c], in which a Gaussian function was used for the peak shape. In addition, the assignment of some absorption bands (1020, 997, 989, 928, 920, and 843 cm^{-1}) was inferred from the literature data[9] listed in Table 2.4.

[c] A student version of OriginPro7.5SV purchased from OriginLab Corporation in October 2005.

4000-1700 cm^{-1} region Five absorption bands were observed in the FT-IR spectra in Figure 2.7. A broad absorption band observed around 3500 cm^{-1} in both spectra was attributed to the stretching vibration of O-H bonds. This could be due to some water absorbed on the surface of the KBr pellets or water absorbed in the compounds. The absorption peaks observed above 2900 cm^{-1} were attributed to the stretching vibration of C-H bonds. The assignment of the band observed at 2857 cm^{-1} from Ag(I)tfa is unclear and it was absent in the copper complex. The absorption bands around 2400 cm^{-1} in both spectra are believed to be due to the stretching of the O=C=O molecule. A weak absorption band was observed at 2085 cm^{-1}, which could be attributed to isothiocyanate (-N=C=S). It should not be attributed to immonium ($C=N^{+}$-H) bands due to the lack of broad ammonium band (2500-2300 cm^{-1}). However, no sulphur or nitrogen atom is present in the molecule of Ag(I)tfa. A possible reason for this band could be air contamination.

1700-1500 cm^{-1} Region This region contains major functional groups of the metal chelated organic ligands. Many characteristic absorption bands were observed in both spectra. The absorption bands attributed to the carbonyl are found at 1636 cm^{-1} and 1620 cm^{-1} in Ag(I)tfa; 1609 cm^{-1} and 1586 cm^{-1} in $Cu(tfa)_2$ (compound **3**). The differences of the carbonyl absorption bands between the two complexes are mainly due to structural differences. Yaqub pointed out that the electron density of the carbonyl bond in metal-oxygen bonded compounds should decrease as the electronegativity of the metal increases.[27] However, the difference is insignificant between the electronegativity of silver(1.93) and that of

copper (1.90). In fact, the observed frequency of carbonyl in the silver compound is actually higher than for the copper compound. Nakamoto also found that the frequencies of carbonyl bonds (1681 and 1652 cm^{-1}) in compound **1** were higher than in compound **2** (1652 and 1626 cm^{-1})[10] and he stated that these are most characteristic of the presence of uncomplexed carbonyl oxygen atoms and the attendant higher bond order. In Ag(I)tfa, this could be due to two types of coordinated silver atoms. The type-1 silver atoms coordinate with four oxygen atoms from two chelated ligands, and the type-2 silver coordinate with two oxygen and two carbon atoms from four adjacent ligands.

The band observed at 1532 cm^{-1} in Ag(I)tfa was attributed to C=C bonding coupled with C-H bending. The same stretching vibration was observed at 1519 cm^{-1} in compound **1** and 1530 cm^{-1} in compound **3**. This stretching was not observed in compound **2**, as expected, because it is a C-bonded structure with no C=C bond character.

1500-1100 cm^{-1} Region This region contains the bands from many functional groups, including the M-C-H group. The absorption band at 1462 cm^{-1} in Ag(I)tfa was attributed to a perturbed stretching of the C=O bond, which suggested a ring structure in the compound. This same stretching vibration is observed at 1478 cm^{-1} in compound **3**. This band is absent in compound **2**, a C-bonded structure.

The vibration of the perturbed C=C stretch coupled to C-CH_3 in-plane bending was observed at 1281 cm^{-1} in Ag(I)tfa, at 1308 cm^{-1}in compound **3**, 1275 cm^{-1} in compound **1**, and is absent from compound **2**. The absorption band observed at

1188 cm^{-1} in Ag(I)tfa was attributed to C-F stretching[29] coupled to C-C stretching. The same band was observed at 1196 cm^{-1} in compound **3**. The C-C bond stretch was observed at 1157 cm^{-1} in compound **3** and 1134 cm^{-1} in Ag(I)tfa.

The bands observed at 1182 cm^{-1} in compound **1**, and 1198 cm^{-1} in compound **2** were assigned to the stretching of the Pt-C-H bond coupled with C-CH_3 stretching by Nakamoto using deuterium substitution at different hydrogen positions. Based on these reliable data, the bands less than 1200 cm^{-1} in Ag(I)tfa are assumed to be analogous to those of compound **1**. Due to the similar M-C3 connectivity between compound **1** and Ag(I)tfa, the band at 1096 cm^{-1} in Ag(I)tfa could be assigned to the bending of Ag-C-H coupled with C-CH_3 stretching. The noticeable difference between the stretching of Ag-C-H and Pt-C-H could be due to the connectivity between Ag and other atoms. From the crystal structure, silver atoms of this type share two oxygen atoms from two different ligands and two middle carbon atoms from another two different ligands. In compound 1, platinum is chelated with one acac ligand through two oxygen atoms and coordinated with two C3 atoms from two uncomplexed ligands. The connectivity difference could play a major role for different absorption. This absorption was absent in compound **3**, an O-bonded structure.

1100-400 cm^{-1} Region The absorption bands in this region are assigned mainly to the metal-oxygen bonds or metal-carbon bonds. As the bands at 677 cm^{-1} in compound **1** and 652 cm^{-1} in compound **2** were attributed to the stretching of the Pt-O coupled with C-CH_3 stretching and ring deformation, so is the band at 724 cm^{-1} in Ag(I)tfa attributed to Ag-O coupled with C-CH_3 stretching

and ring deformation. As the bands at 633 and 453 cm^{-1} in compound **1** were attributed to the stretching of the Pt-O bond, the bands at 604 and 451 cm^{-1} in Ag(I)tfa were attributed to the Ag-O bond by analogy. As the bands observed at 565 and 542 cm^{-1} in compound **1** and 567 cm^{-1} in compound **2** were attributed to the stretching of the Pt-C bonds, the bands at 554 and 517 cm^{-1} were attributed to the Ag-C bonds by analogy. These bands are not observed in compound **3** because compound **3** does not have metal-carbon bonds. All these absorption bands support the existence of metal-C and metal-O bonds in Ag(I)tfa, consistent with the crystal structure data of this complex.

The possible assignments of other absorption bands in this region are listed along with the above discussed bands in Table 2.4.

Table 2.4 Assignment of IR bands for Ag(I)tfa and $Cu(tfa)_2$.

1. Pt(III)	2. Pt(IV)	Assignment	3. Cu(II)	4. Ag(I)	Differences
1681s	1652s	ν_{as}(C=O)	1609vs	1636vs	
1652m	1626s	ν_{as}(C=O)	1586s	1620sh	
1568s		ν_s(C=O)		1550sh	
1519s		ν(C=C) + δ(C-H)	1530s	1532	
		ν(C=O)+ δ(C=C)	1518m	1522s	
		ν_s(C=O)	1478m	1462s	
1417sh	1465sh	$\delta_d(CH_3)$	1456sh	1422sh	
1388		ν_s(C=O)	1368m	1360m	
1353s	1433s	$\delta_s(CH_3)$			
1334s	1350s	δ(C-C) + ν(C-CH_3)			
1275m		ν(C=C) + ν(C-CH_3)	1308vs	1281vs	
1236m		δ(C-H)	1227s	1202sh	
			1196s	1188s	ν(CF)[29]
1194sh	1193s	ν(C-C)	1157s	1134s	
			1138 s	1117s	$\delta_s(CF_3)$[29]
1182s	1193s	ν(Pt-C-H) + ν(C-CH_3)		1096sh	**ν(M-C-H)** + ν(C-CH_3)
1038m		$\rho_r(CH_3)$of 1		1020w	
1020m	1024m	$\rho_r(CH_3)$of 1		997w	
1008m	1007m	$\rho_r(CH_3)$of 1		989w	
965m		ν(C-CH_3) of 1	951w	928w	
928m	948m	ν(C-CH_3) of 1		920w	
877m	901m	ν(C-CH_3) of 1	872w	843m	
862m	852s	δ(C-C-C) + ν(C-C) + ν(C-CH_3)		814m	
772s		π (C-H)	799m	803m	
677w		ν(Pt-O) + ν(C-CH_3) + ring def.	736w	758m	**ν(M-O)**+ν(C-CH_3)+ ring def.
657sh	652s	δ(C-C) + ν(Pt-C) + ν(C-CH_3)		724m	δ(C-O)+**ν(Ag-C)** +ν(C-CH_3)
633s		ν(Pt-O)	602w	604w	**ν(M-O)**
565m	567w	ν(Pt-C)		554m	**ν(Ag-C)**
542m		ν(Pt-C)		517w	ν(Ag-C)
523s	537s	δ(C-CH_3)			
453s		ν(Pt-O)	444w	451w	**ν(M-O)**

Key: ν, stretching; δ, bending; δ_d, degenerated bending, δ_s, symmetric bending; ρ_r, rocking.
Intensity designations: s, strong; m, medium; sh, shoulder; w, weak.

2.3.3.2. X-ray powder diffraction of a solid-state film of Ag(I)tfa

Although the FT-IR spectrum of the crystalline silver complex was discussed above, most of the research work described in this thesis was conducted on solid-state films of Ag(I)tfa. It is, therefore, important to understand the possible structure(s) of Ag(I)tfa in the solid-state film.

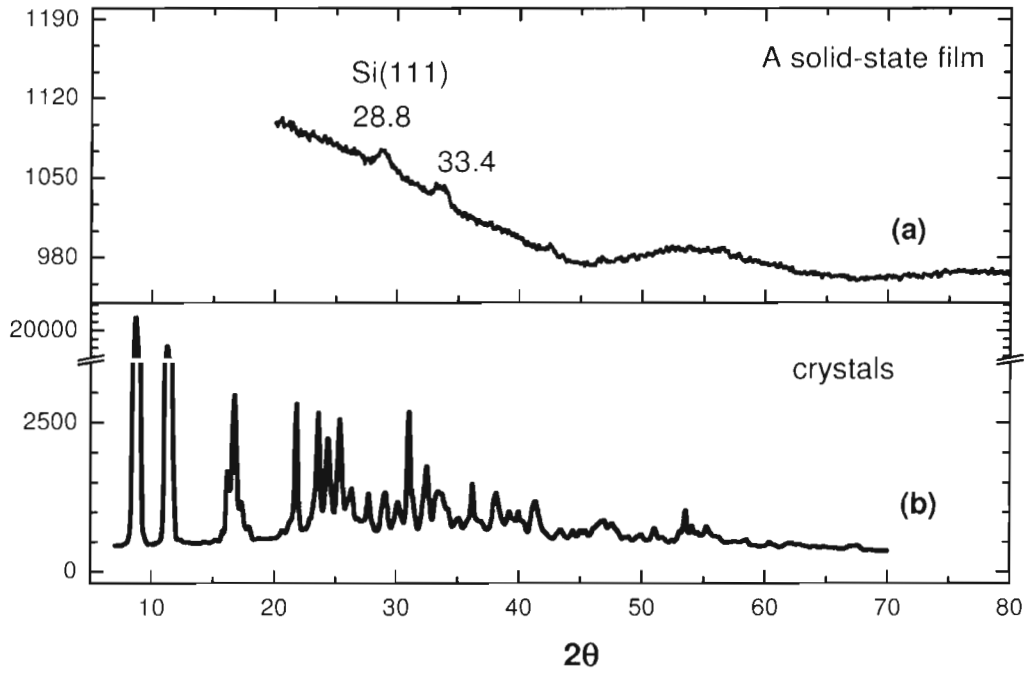

Figure 2.9 X-ray powder diffraction pattern of (a) a solid-state film of Ag(I)tfa on a silicon substrate and (b) crystals of Ag(I)tfa in a glass tube.

An X-ray diffraction pattern of a solid-state film of Ag(I)tfa is shown in Figure 2.9 (a) together with an X-ray diffraction pattern of crystals of Ag(I)tfa as (b) in the same figure. Many diffraction peaks are observed in the spectrum (b) while only two weak peaks are observed at 28.8° and 33.4° in spectrum (a). It is unlikely that the solid-state film is crystalline in a comparison between these two XRD patterns. The peak at 28.8° in spectrum (a) could be attributed to the substrate Si(111) (28.4°). The other peak could be attributed to silver oxide, $Ag_2O_2(10\underline{2})$

(33.1°) or Ag_3O_4 (33.5°). No peaks from silicon or silicon oxide match this peak as closely as the AgO possibilities. However, without additional data, the assignment of this peak is ambiguous. Based on the diffraction patterns, it is believed that the solid-state film of Ag(I)tfa is amorphous.

2.3.3.3. FT-IR spectrum of an amorphous film of Ag(I)tfa

The molecular structure of the crystalline Ag(I)tfa could differ much from that of the amorphous Ag(I)tfa. Understanding of the amorphous film from the spectroscopic data is very important. Therefore, a FT-IR spectrum of an amorphous solid-state film of Ag(I)tfa on a sodium chloride single-crystal substrate was obtained (Figure 2.10, spectrum in black). The FT-IR spectrum of crystalline Ag(I)tfa is shown in the same figure as red.

In the FT-IR spectra, the bands attributed to ν(C=O) differed in profiles and positions while the remaining bands agreed within five wavenumbers (see labels in Figure 2.10). The changes of the bands of ν(C=O) could be mainly due to the geometry changes of Ag(I)tfa because the order of packing of Ag(I)tfa molecules in the crystal structure no longer existed in the amorphous film. In addition to this geometry change, the broken Ag-Ag interaction (Figure 2.1) could change the electron density around the rings as well. The other absorption bands with small changes could be considered as attributed to similar connectivity between atoms.

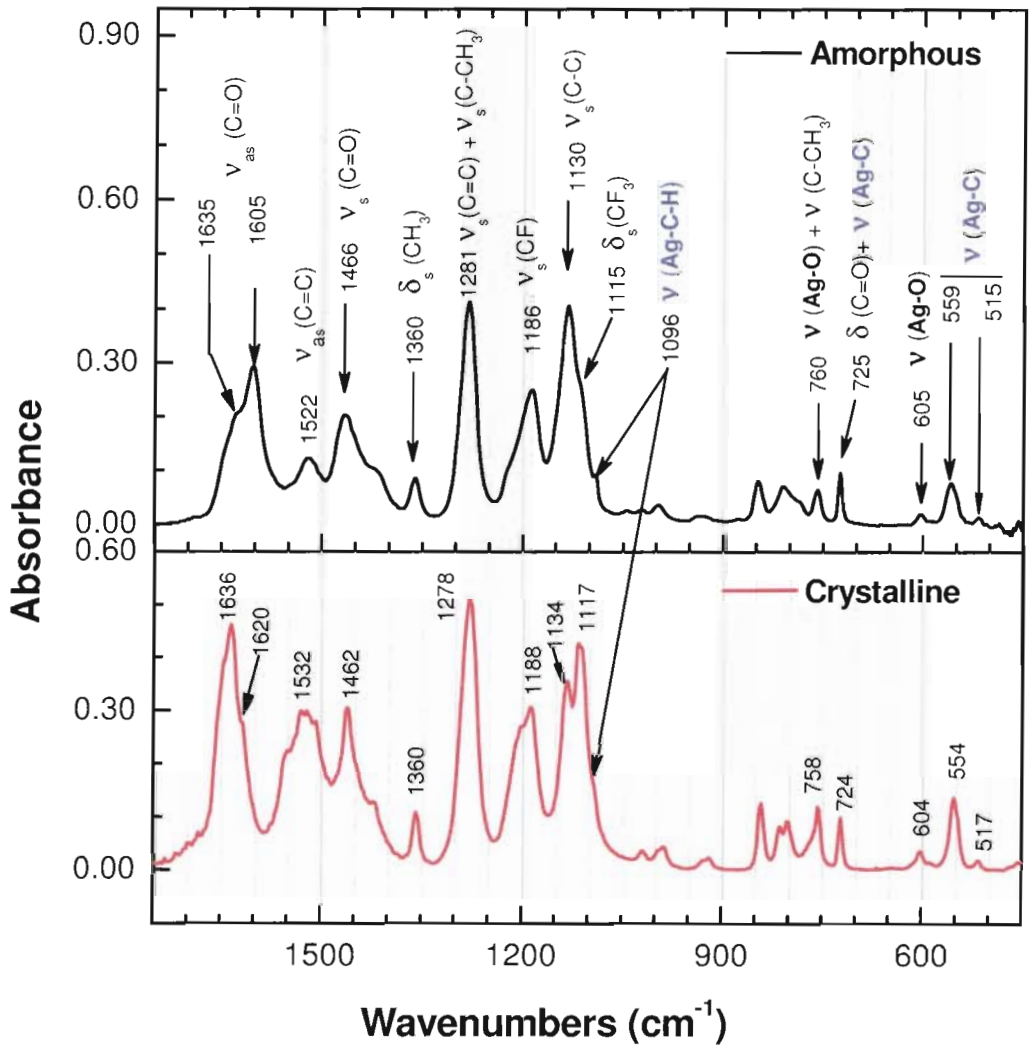

Figure 2.10 FT-IR spectra of Ag(I)tfa obtained from (top) an amorphous film on a NaCl disc in the dark (RT 24 °C, RH: 26 %) and (bottom) from a KBr pellet.

If the assignments of the IR bands for crystalline Ag(I)tfa are reliable, then it is important to notice that the stretching of Ag-C-H and two Ag-C bonds are observed at 1096, 554, and 517 cm^{-1}. As these bonds in crystalline Ag(I)tfa build up the network among Ag(I)tfa, these bonds in the amorphous complex should have the same connectivities. Since the differences of these bands are so small, a completely different structure or connectivity between silver and ligand given

identical absorption bands is unlikely. Therefore, it is believed that the amorphous film could have a polymeric network like that in the crystalline structure as shown in Figure 2.11.

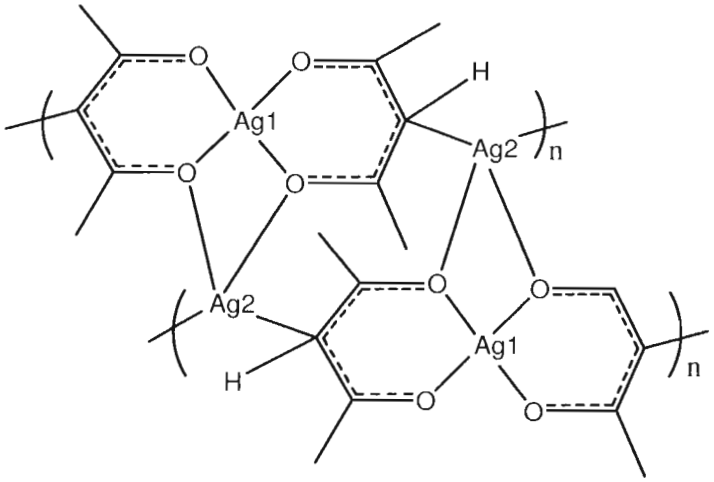

Figure 2.11 A tetrameric unit of polymeric structure of Ag(I)tfa in an amorphous film.

2.3.4. Thermogravimetric Analysis of Ag(I)tfa

The crystalline product of Ag(I)tfa showed an excellent stability in a light-proof container under ambient conditions. The decomposition temperature of this crystalline complex becomes very interesting since the amorphous complex was reported as air sensitive in the literature.[9] The crystals of Ag(I)tfa were subjected to thermogravimetric analysis with a heating rate at 10 degrees per minute in air. A plot of weight percentage versus the temperature is shown in Figure 2.12.

Three weight loss steps were observed in the decomposition curve. Two major decomposition steps occurred at 120 °C and 325 °C. A small step started from

40 ℃ and showed a weight loss at 91 ℃, which could be due to the loss of the water absorbed in the compound.

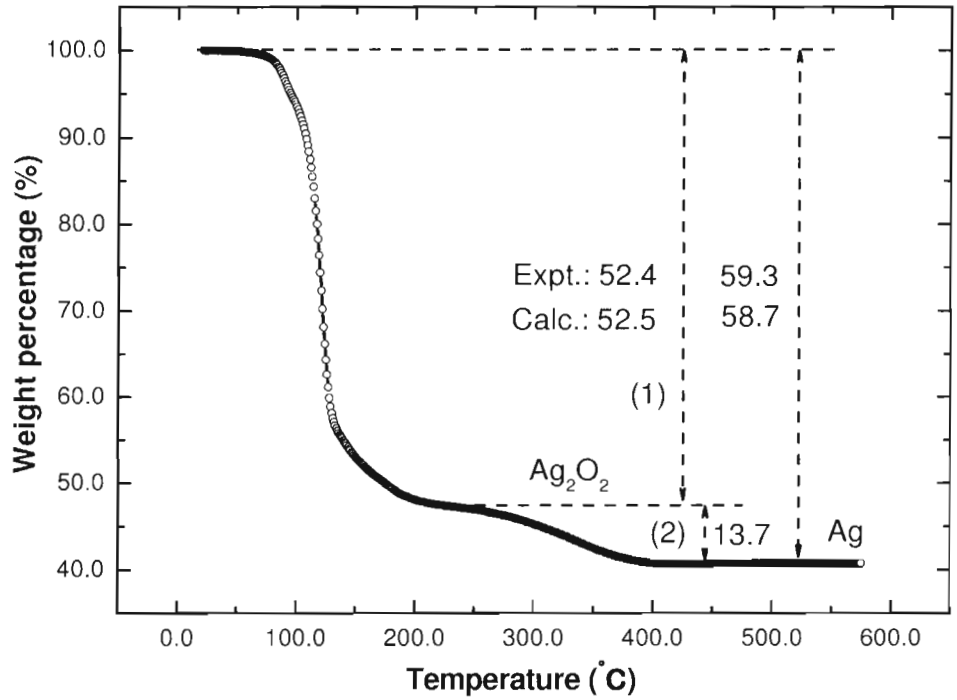

Figure 2.12 TGA curve of (1,1,1-trifluoroacetylacetonato)silver(I) polycrystals.

The weight losses of the two steps 1 and 2 in Figure 2.12 suggest at least two reaction steps. The total weight loss in step 1 is calculated to be 52.4(±0.7) wt%, and the one including step 2 59.3(±0.6) wt%. The weight loss percentage between 1 and 2 is 13.7(±0.9) wt%. The deposited product in the sample crucible was silvery and suspected to be silver. The theoretical weight loss percentage from Ag(I)tfa to silver(I,III) oxide (Ag_2O_2) is 52.5 wt%, from Ag(I)tfa to Ag 58.7 wt%, from Ag_2O_2 to Ag 12.9 wt%. These calculated data matched well with the experimental results within error. If this is true, then the decrease of weight at 91 ℃ should be due to the formation of silver(I,III) oxide from silver during heating instead of the loss of surface water.

On the other hand, it could be argued that silver oxide may be produced directly from Ag(I)tfa. If the weight loss at 91 °C (3.9 (±0.4) wt%) was due to the water loss, then the weight loss of step 1 corresponding to the decomposition of Ag(I)tfa is 50.4(±0.6) wt%. This weight loss matches the weight loss (50.5 wt%) from Ag(I)tfa to Ag_3O_4 (Ag(II,III) oxide). However, Ag_3O_4 decomposes above 60 °C as reported in the literature.[30] The intermediate appeared to be stable before 200 °C, which is much higher than the decomposition temperature of Ag_3O_4. This suggests that the intermediate at 200 °C could not be Ag_3O_4.

Therefore, it is believed that silver (I,III) is the intermediate and silver is the final product.

2.4. Experimental

2.4.1. Materials and instruments

Material Silver(I) oxide (>99 %), and 1,1,1-trifluoro-2,4-pentanedione (98.0 %), were purchased from Aldrich and used as received without further purification. Bis(1,1,1-trifluoroacetylacetonato)copper(II) was purchased from Aldrich and used as received. Deuterated benzene and methanol were purchased from Cambridge-Isotopes Company and used as received. The substrates of Si(100) and Si(111) were purchased from Wafernet Company.

Instruments The infrared spectra of the samples were recorded on a Bomen Michelson 120 FT-IR spectrophotometer at a resolution of 4 cm^{-1}. The ^{1}H and ^{13}C nuclear magnetic resonance spectra were recorded on a Bruker AMX-500 NMR spectrometer. Elemental analysis was carried out with an EA-1110 elemental analyzer. The single-crystal structure was determined on an ENRAF Nonius CAD-40F single-crystal X-ray diffractometer with monochromatic Mo-Kα radiation (λ =0.7101 Å). The thermogravimetric analysis was conducted on a SHIMADZU TGA-50 thermogravimetric analyzer. The magnetic susceptibility was measured on a Johnson Matthey's product model MSB #5632.

2.4.2. Synthesis of (1,1,1-trifluoroacetylacetonato)silver(I)

1,1,1-trifluoro-2,4-pentanedione (1.3489 g) was added to dichloromethane (25.0 mL) in a 50.0 mL round flask. Silver(I) oxide (1.0148 g) was added slowly into this solution with vigorous magnetic stirring. The solution was kept stirring for three hours in the flask wrapped entirely with aluminum foil. A silver-grey

solid precipitated in the flask. The precipitate was filtered under vacuum through a funnel with a frit and dried by air flow for ten minutes. The precipitate was transferred into a 50.0 mL beaker. Absolute ethanol (30.0 mL) was added to the beaker and stirred. A grey colloidal solution was observed with some black solid at the bottom of the beaker. This grey colloidal solution was filtered into a round glass dish using a Millex syringe pump. This solution was then kept in a freezer overnight. White needle-like crystals were observed to precipitate from the solution. The white crystals were collected in a funnel with a frit under vacuum and dried by air flow for ten minutes. All the operations were conducted under yellow ambient light. The crystals were transferred to a glass vial. The vial was inserted into a Schlenk tube wrapped with aluminum foil. The tube was evacuated for two hours with a roughing pump. The yield of the final product was 1.63 g (72.5%).

The magnetic susceptibility of the crystalline products was measured on a Johnson Matthey's product model MSB #5632 by the author. The reading of 60 mg Ag(I)tfa crystals filled in a glass tube at 2.0 cm was -24 c.g.s. units, which indicated the complex is diamagnetic.

It was noticed that some white powders precipitated in the ethanol solution in the fridge (three times during three years). These solids are insoluble in available organic solvents in our laboratory. The formation of these solids were unpredictable. No characterization was performed due to low light sensitivity and low solubility of these powders.

2.4.3. Preparation of single crystals

Single crystals of the product were obtained by the following procedure. White crystalline product (0.0425 g) was dissolved in absolute ethanol (0.2502 g) in a vial. An aliquot was transferred into a NMR tube. Ten drops of hexanes were added slowly to the top of the solution without disturbing the existing solution. This tube was capped with a lid and stored in a fridge overnight. Colorless single crystals grew on the inner wall of the tube and were collected.

A single crystal mounted on a glass fiber using epoxy adhesive was analyzed with an Enraf-Nonius CAD-4F diffractometer with monochromatic Mo K_α radiation. The diffractometer was covered entirely by thick black plastic films to avoid light irradiation. The data was acquired by the program DIFRAC.[31] It was found that the intensities of the standard reflections reduced 30% during the progress of data acquisition. Absorption corrections (by integration) were performed using programs from the NRCVAX crystallographic suite,[32] as well as data reduction (including corrections for polarization and Lorentz effects).

The space group *F2dd* was derived from the systematic absences. However, only 16 of the measured *0kl* reflections were observed ($14.8 > I_o/\sigma(I_o) > 2.5$). The structure with a centrosymmetric space group *Fddd* was solved using SIR92.[33] and refined using CRYSTALS.[34] Complex scattering factors for neutral atoms[35] were used in the calculation of structure factors. All the above crystallographic work was conducted by Dr. Raymond Bachelor in Simon Fraser University.

2.4.4. FT-IR spectra acquisition

FT-IR spectra of Ag(I)tfa and bis(1,1,1-trifluoroacetylacetono)copper(II) were obtained by a KBr-disc method. In each case, the single crystals were ground with potassium bromide and the mixture was pressed into a transparent pellet. FT-IR spectra of the pellets were recorded in air.

The FT-IR spectra of a solid-state film of Ag(I)tfa were obtained by the following procedure. First, a solution was prepared by dissolving white crystals of Ag(I)tfa 0.1024 g in 1.134 g of absolute ethanol in a vial. Then a film was prepared by spin-coating a substrate (sodium chloride single-crystal disc) with this solution at 5000 rpm for 30 seconds. A FT-IR spectrum of this film was recorded in air.

2.4.5. X-ray powder diffraction

A solution was prepared by dissolving 0.0723 g (1,1,1-trifluoroacetylacetonato)-silver(I) in 0.7289 g absolute ethanol. A solid-state film was prepared by spin coating this solution on a silicon substrate at a speed of 5000 rpm. The film was subjected to X-ray powder diffraction. An XRD pattern was recorded. The X-ray exposure time was five minutes.

A glass tube filled with white (1,1,1-trifluoroacetylacetonato)silver(I) crystals was sealed with epoxy on the open end and subjected to X-ray powder diffraction. An XRD pattern under identical conditions was recorded.

2.5. Reference list

(1) Chi, K.-M.; Lin, C.-T.; Peng, S.-M.; Lee, G.-H., *Organometallics* **1996**, *15*, 2660-2663.

(2) Darr, J. A.; Poliakoff, M.; Blake, A. J.; Li, W.-S. *Inorganic Chemistry* **1998**, *37*, 5491-5496.

(3) Nakamoto, K.; Behnke, G.T. *Inorganic Chemistry* **1967**, *6*, 433.

(4) Nakamoto, K.; McCarthy, P. J.; Ruby, A.; Martell, A. E. *Journal of the American Chemical Society* **1961**, *83*, 1066-1069.

(5) Nakamoto, K.; Martell, A. E. *Journal of Chemical Physics* **1960**, *32*, 588-597.

(6) Gibson, D.; Lewis, J.; Oldham, C. *Journal of the Chemical Society [Section] A: Inorganic, Physical, Theoretical* **1966**, 1453-1456.

(7) Holtzclaw, H. F. Jr.; Collman, J. P. *Journal of the American Chemical Society* **1957**, *79*, 3318-3322.

(8) Belford, R. L.; Martell, A. E. *Journal of Inorganic and Nuclear Chemistry* **1956**, *2*, 11-31.

(9) Behnke, G. T.; Nakamoto, K. *Inorganic Chemistry* **1968**, *7*, 330-335.

(10) Nakamoto, K. M.; Martell, A. R. *Inorganic Chemistry* **1968**, *7*, 330.

(11) Xu, C.; Corbitt, T. S.; Hampden-Smith, M. J.; Kodas, T. T.; Duesler, E. N. *Journal of the Chemical Society, Dalton Transactions: Inorganic Chemistry* **1994**, 2841-2849.

(12) Evans, W. J.; Giarikos, D. G.; Josell, D.; and Ziller, J. W. *Inorganic Chemistry* **2003**, *42*, 8255-8261.

(13) Bailey, A.; Corbitt, T. S.; Hampden-Smith, M. J.; Duesler, E. N.; Kodas, T. T. *Polyhedron* **1993**, *12*, 1785-1792.

(14) Zanotto, L.; Benetollo, F.; Natali, M.; Rossetto, G.; Zanella, P.; Kaciulis, S.; Mezzi, A. *Chemical Vapor Deposition* **2004**, *10*, 207-213.

(15) Southward, R. E.; Chisholm-Brause, C.; Dean, C. J.; Stoakley, D. M.; Thompson, D. W. *Polymer Preprints (American Chemical Society, Division of Polymer Chemistry)* **2000**, *41*, 38-39.

(16) Wenzel, T. J.; Sievers, R. E. *Analytical Chemistry* **1981**, *53*, 393-399.

(17) Fragala, M. E.; Malandrino, G.; Puglisi, O.; Benelli, C. *Chemistry of Materials* **2000**, *12*, 290-293.

(18) Swallow, A. C.; Truter, Mary, R. *Proceedings of the Royal Society (London)* **1960**, *251*, 205-217.

(19) Wang, Q.-M.; Mak, T. C. W. *Journal of the American Chemical Society* **2001**, *123*, 1501-1502.

(20) Cote, A. P.; Ferguson, M. J.; Khan, K. A.; Enright, G. D.; Kulynych, A. D.; Dalrymple, S. A.; Shimizu, G. K. H. *Inorganic Chemistry* **2002**, *41*, 287-292.

(21) Ladd, J. A.; Hope, H.; Balch, A. L. *Organometallics* **1984**, *3*, 1838-1846.

(22) Ho, D. M.; Bau, R. *Inorganic Chemistry* **1983**, *22*, 4073-4079.

(23) Omary, M. A.; Webb, T. R.; Assefa, Z.; Shankle, G. E.; Patterson, H. H. *Inorganic Chemistry* **1998**, *37*, 1380-1386.

(24) Burdett, J. L.; Rogers, M. T. *Journal of the American Chemical Society* **1964**, *86*, 2105-2109.

(25) Retrieved on February 1, 2007 from http://*www.aist.go.jp/RIODB/SDBS* SDBS #3965

(26) Che, C.-M. *Advances in Transition Metal Coordination Chemistry* Greenwich, JAI Press, **1996**.

(27) Yaqub, M.; Koob, R. D.; Morris, M. I. *Journal of Inorganic and Nuclear Chemistry* **1971**, *33*, 1944-1946. (27)

(28) Kidd, M. R.; Sager, W. H. *Inorganic Chemistry* **1967**, *6*, 946.

(29) Behnke, G. T.; Nakamoto, K. *Inorganic Chemistry* **1967**, *6*, 433-440.

(30) Standke, B.; Jansen, M. *Journal of Solid State Chemistry* **1988**, *67*, 278-284.

(31) Gabe, E. J.; White, P.S.; Enright, G.D. *DIFRAC A Fortran 77 Control Routine for 4-Circle Diffractometers* N.R.C., Ottawa, **1995**.

(32) Gabe, E. J.; Page, Le, Y.; Charland, J.P.; Lee, F. L.; and White, P. S. *Journal of Applied Crystallography* **1989**, *22*, 384.

(33) Altomare, A. C.; Giacovazzo G.; Guagliardi A.; Burla M.C.; Polidori, G. C. *Journal of Applied Crystallography* **1994**, *27*, 435.

(34) Watkin, D. J.; Prout, C.K.; Carruthers, J.R.; Betteridge, P.W.; Cooper, R.I. *CRYSTALS Issue 11* Chemical Crystallography Laboratory, University of Oxford: Oxford, England, **1999**.

(35) International Union of Crystallography, *International Tables for X-ray Crystallography* Kynoch Press, Birmingham, England, **1975**; Vol. IV. (37)

CHAPTER 3:
PHOTOCHEMICAL DEPOSITION OF SILVER AND SILVER OXIDE FILM FROM A SOLID-STATE FILM OF (1,1,1-TRIFLUOROACETYLACETONATO)SILVER(I)

3.1. Introduction

Silver nanoparticles and thin films have attracted a lot of interest in various research areas. For example, Roucox reported that silver nanoparticles have remarkable catalytic activity.[1] In ultra large-scale integrated circuits, silver is a promising candidate as a material for interconnection metallization because elemental silver has the highest electrical conductivity among all known metals.[2] The properties of silver films, micro-structured lines, and the growth of diffusion barriers have been widely studied for the metallization schemes with a small feature size.[3-5] The relationship between the conductivity of thin silver films and the roughness of the surface was reported in the literature.[6] All this research work discovered many important properties of silver nanoparticle films and their potential applications. Many deposition methods have been developed to prepare silver nanoparticles or films, such as PVD, CVD, MOCVD, sol-gel and others. In addition, many silver complexes have been developed for use with these deposition methods. However, these methods could not be used to create films with desired patterns in a single step. With the exception of the sol-gel method, all other deposition processes require expensive capital investment and

high operation costs. For example, a typical commercial CVD system for laboratory scale costs over several hundred thousand dollars.

In the research described in this chapter, a silver and silver oxide composite film was prepared from (1,1,1-trifluoroacetylacetonato)silver(I) (Ag(I)tfa) by a photochemical metal organic deposition method. Thin film deposition by this method requires an investment as little as that of a few UV lamps. This method converts thin solid-state metal organic films to metal and/or metal oxide films upon irradiation with ultraviolet light.[7-8] The process has several advantages over other current thin film deposition technologies described previously. The key component of this process is the photosensitive metal organic precursor, which directly affects the conversion rate and quality of the resultant film. In Chapter 2, a photosensitive compound, (1,1,1-trifluoroacetylacetonato)silver(I), was synthesized for this purpose. A silver and silver oxide film prepared from this complex by photochemical metal organic deposition is presented in this Chapter.

In addition, most metal oxides prepared by photochemical metal organic deposition are amorphous. Crystalline metal oxides prepared under ambient conditions have not been previously reported. High purity metallic films have also not been previously prepared by this method. The deposition of crystalline silver and silver oxide created interest in the mechanism of photochemical degradation of the metal organic precursor, as well as the physical properties of the deposited film. Both the characterization of the silver nanoparticles within the film and investigation of the photochemical mechanism are reported in the following chapter.

In this Chapter, AES, SEM and HRTEM technique were used to analyze the photoproduced films. AES was used to analyze the film compositions for all elements except hydrogen. AES is normally a surface characterization technique and does not give bulk composition if the film is inhomogeneous. A surface cleaning by argon ion sputtering can eliminate surface contaminations from the real composition of the film. SEM is employed to use secondary back scattered electron to image the surface morphology, mostly the topology of the surface. The size and shape of the nanoparticles can be easily imaged and the surface roughness can be revealed. HRTEM can investigate the crystalline nanostructure of individual nanoparticles. The electron diffraction obtained from the HRTEM system can provide information on lattice parameters. Given that electrons diffract more than X-rays, electron diffraction can give more information on the material being investigated than the X-ray diffraction technique.

3.2. Results

3.2.1. Ultraviolet spectrum of a solid-state film of Ag(I)tfa

A UV-vis spectrum was recorded from a solid-state film prepared by spin coating with a solution of Ag(I)tfa in ethanol onto a calcium fluoride disc (Figure 3.1, panel A), in which the bare substrate was the background. Another spectrum was recorded from a solution in a quartz cell (Figure 3.1, panel B), in which absolute ethanol was the background. The spectrum of the ligand in ethanol is shown in Figure 3.1 panel C, in which absolute ethanol was the background.

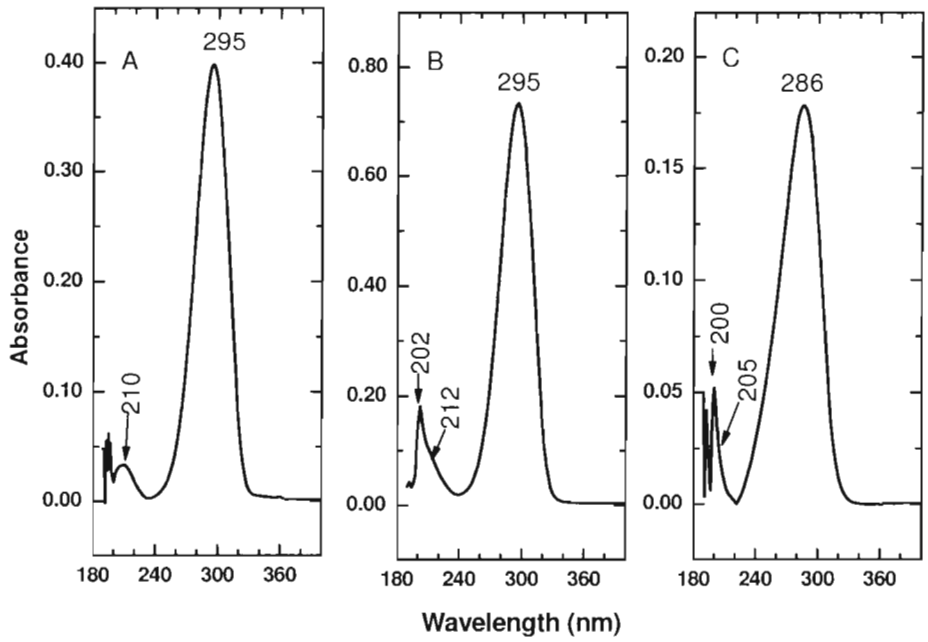

Figure 3.1 UV-vis absorption spectra of (A) Ag(I)tfa in a solid-state film, (B) Ag(I)tfa in ethanol, (C) Htfa in ethanol.

A strong absorption band at 295nm was observed in both panels A and B. The weak band at 210 nm in panel A is believed to be due to the residual solvent ethanol, which has an absorbance at 210 nm[9]. A similar weak absorption band at 202 nm with a shoulder peak at 212 is observed in panel B of Figure 3.1.

The strong absorption band at 295 nm in panels A and B is close to that of $Cu(tfa)_2$ (298 nm) in chloroform in the literature.[10] However, no assignments of the electronic transitions were given. This strong absorption could be attributed to the transitions from the ligand ions since the absorption band of enolic anions of Htfa was observed at 292 nm in a carbonate-bicarbonate buffer[11] instead of from Htfa, which has a strong absorption at 286 nm (Figure 3.1 C).

It is important to understand the electronic transitions associated with this strong absorption. A detailed review of the types of electronic transitions of transition metal complexes is given by Buono-Core.[12] He stated, for metal organic complexes there are three basic types of electronic transitions: i) *d-d* transitions; ii) intraligand transitions; and iii) charge-transfer transitions. Buono-Core assigned the excitation of *d-d* transitions of $Cu(acac)_2$ and $Cu(hfac)_2$ (in solution) in the visible region from 542-680 nm. No absorption was observed in this region of the UV-vis absorption spectrum of Ag(I)tfa. In addition, for the d^5 and d^{10} complexes, their spin transitions are forbidden.[13] Hence, this absorption of Ag(I)tfa should not be due to the d-d transitions. Secondly, Buono-Core assigned the excitation of $Cu(acac)_2$ at $\lambda \approx 290$ nm to the intra-ligand singlet–singlet transitions, $\pi \rightarrow \pi^*$ transitions between the molecular orbitals localized on the ligands. He also pointed out that the ligand-to-metal charge-transfer (LMCT) or metal-to-ligand charge-transfer (MLCT) transitions in metal β-diketonates can be excited at $\lambda \approx 250$ nm. No absorption band was observed around 250 nm in the spectrum of Ag(I)tfa, which could be solely due to the different chelating ligands. However, from the experimental results presented in the following sections, it has

been found that a solid-state film of Ag(I)tfa was photoreduced to elemental silver under light irradiation. The photoreduction of transition metal diketonates under irradiation is ascribed to LMCT transitions. For example, $Cu(acac)_2$ having a maximum excitation wavelength at 241 nm was photoreduced under irradiation at 254 nm in a deoxygenated ethanolic solution.[12] Buono-Core assigned this excitation to LMCT transitions unambiguously. By considering the difference between acac and tfa chelating ligands, the photoreduction from Ag(I)tfa to silver should be assigned to charge transfer transitions (LMCT) rather than intraligand transitions based on the photoreduction product, silver.

It is worth noting that the electronic absorption spectrum (Figure 3.1 B) of Ag(I)tfa in solution showed two major peaks (202 and 295 nm) and a shoulder at 212 nm, which could be deconvoluted to at least two peaks at 207 and 210 nm with a Gaussian function. The formation of those shoulder bands could be due to the complexed ions formed in solution. The strong peak at 295 nm is identical to that from the amorphous film. This suggested that the silver complex in the solution could be photolyzed under light irradiation at same wavelength. It would be expected that the complex structure of Ag(I)tfa in solution should be different than that in an amorphous film. The different molecular structure or symmetry would affect the molecular orbital energies, which would lead to different excitation energy if the same transitions between silver and the ligand ions occur. However, the observed experimental data do not agree with this.

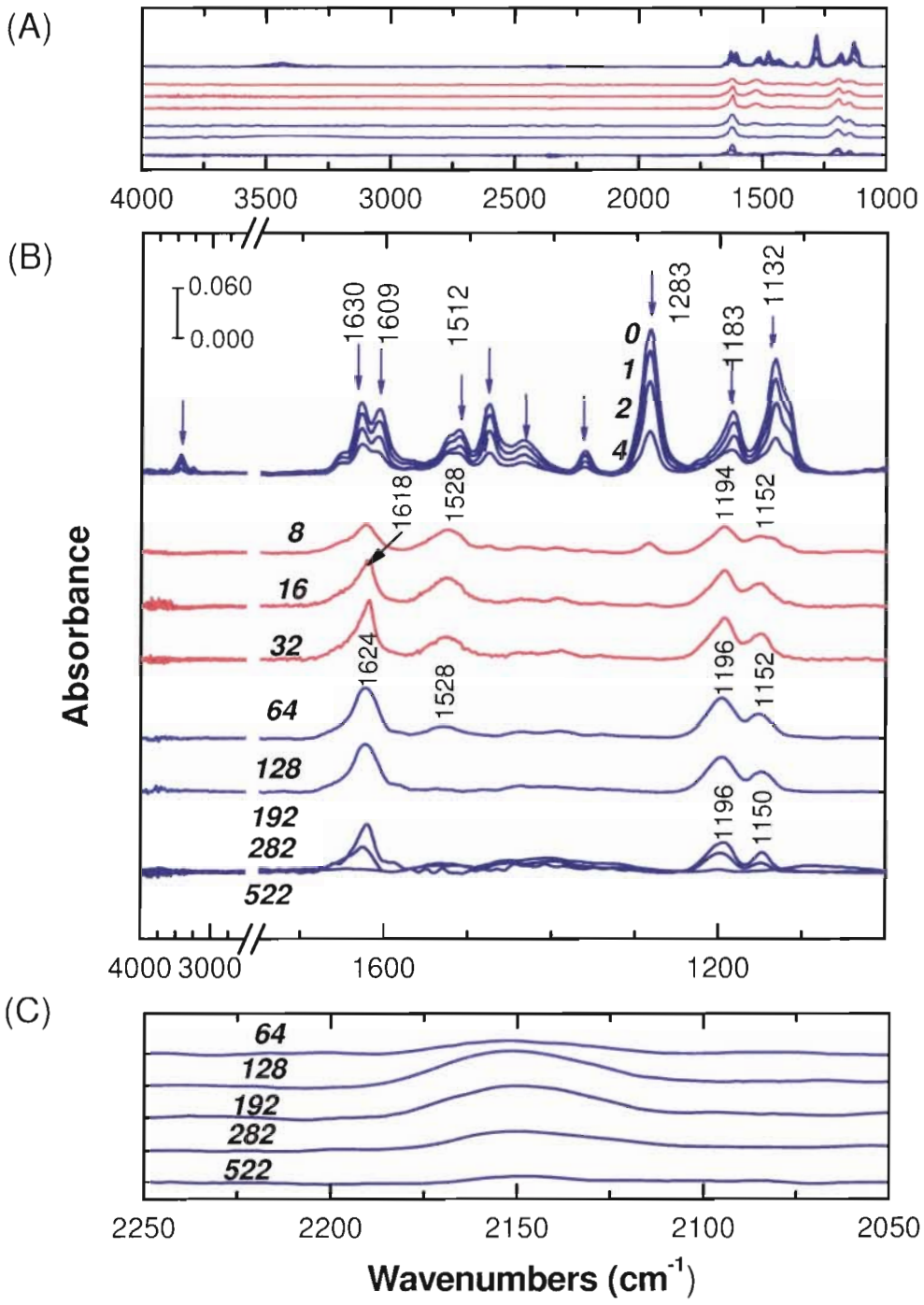

Figure 3.2 FT-IR spectra of a film of Ag(I)tfa under light irradiation at 254 nm in the dark (RT: 24 °C, RH: 22 %) for different times. Panel A is the spectra in a range from 4000 to 1000 cm^{-1}, panel B the detailed spectra in the same range with same time scale, panel C the detailed spectra in a range from 2250 to 1050 cm^{-1} (the italic numbers are photolysis times in minutes)..

3.2.2. FT-IR spectra of a solid-state film of Ag(I)tfa under irradiation

The photochemical reaction of an amorphous film of Ag(I)tfa was monitored by FT-IR spectroscopy. The changes of the infrared absorption spectra of the film with increasing irradiation time were recorded in the dark at 24 ℃ and 22 % humidity (Figure 3.2). Panel A shows the full range spectrum from 4000 to 1000 cm^{-1}. Panel B shows how the spectra of the film in the region of interest changed with photolysis time. Panel C shows a portion of the spectrum from 2100 to 2250 cm^{-1}. No absorption bands were observed in the region between 2100 to 1750 cm^{-1}. Intensities are plotted in Figure 3.3 in order to reveal the existence of multiple intermediates.

As shown In Figure 3.2, after the film was irradiated for eight minutes, four new absorption bands were observed at 1618, 1528, 1192, and 1152 cm^{-1} (Figure 3.3 E) while all initial absorption bands disappeared (Figure 3.3 D). The growth of new absorption bands indicated the formation of an intermediate (I2). The band at 1618 cm^{-1} was mainly attributed to ν(C=O), 1528 cm^{-1} to ν(C=C) bond, 1194 cm^{-1} to δ(C-H), and 1152 cm^{-1} to ν(C-C) bond. After the film was irradiated for 16 minutes, the most intense absorption band at 1283 cm^{-1} in the initial spectrum of Ag(I)tfa decreased 98.8% in intensity. If the intermediate I2 were indeed a direct product of the film under irradiation, it is expected that the new absorption bands would reach a maximum at the same time. However, the absorbance of the band at 1618 cm^{-1} continued growing about 31% after UV irradiation for an additional 16 minutes (Figure 3.3 E). The other two bands at

1194 $cm^{-1}$and 1152 cm^{-1} increased in intensity over 13 % except the one at 1528 cm^{-1} decreased in intensity. These continuing increases of absorbance could not be due to the 2% residue of the initial silver complex, but must be due to a different intermediate I1. In addition, it is expected that this intermediate I1 is expected to have similar functional groups to those of Ag(I)tfa because no new absorption bands were observed corresponding to this intermediate.

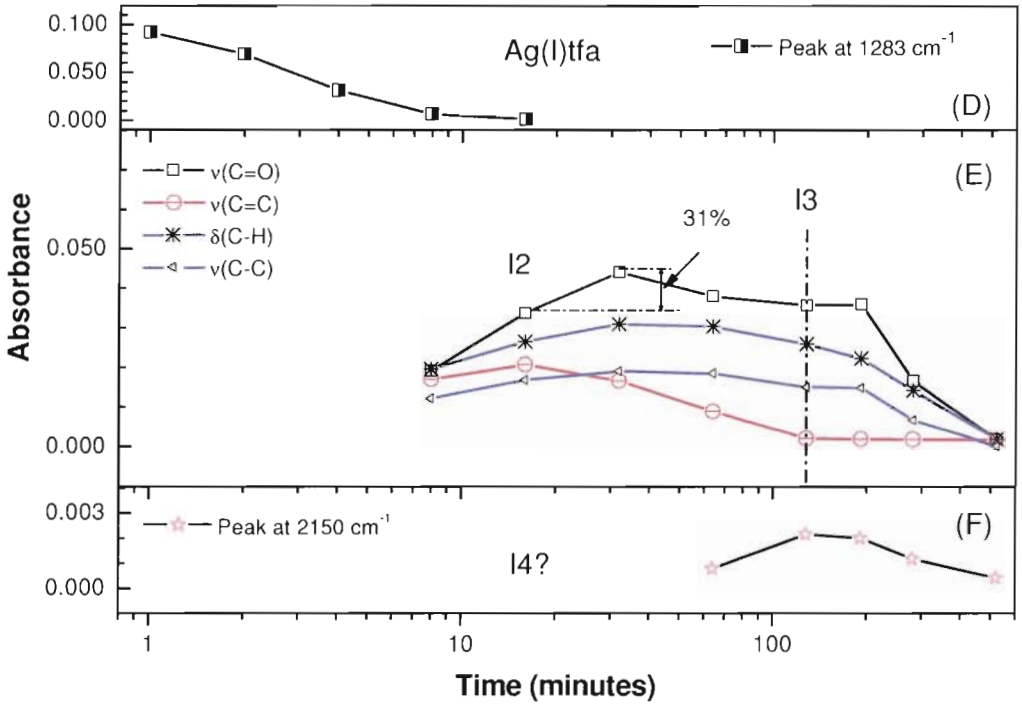

Figure 3.3 The changes of absorbance of the characteristic bands and the possible intermediates, (D) Ag(I)tfa in the film, (E) the intermediate I2 and the intermediate I3, (F) the possible intermediate I4.

With continuing irradiation the changes of FT-IR spectra of the film revealed another intermediate I3 produced during photolysis (Figure 3.3 E). After the film was irradiated for an accumulated time of 64 minutes, the absorbance of the band at 1528 cm^{-1} decreased over 50 % (red open circles) while the band at 1618 cm^{-1} decreased about 13 % and the other two at 1192 and 1152 cm^{-1}

showed almost no changes. These spectral changes indicate that the intermediate underwent a reaction. After the film was irradiated for an accumulated time of 128 minutes, the band at 1528 cm^{-1} decreased to the baseline while the other three bands decreased to less than 10 %. These spectral changes indicate the formation of a different intermediate I3. The remaining absorption bands decreased to the baseline over more than six hours. This low photosensitivity also supports the existence of the new intermediate I3. In addition, the remaining bands are believed to be attributed to the same functional groups as those of the intermediate I2.

Beside these three intermediates observed in the film during photolysis, a very weak band at 2150 cm^{-1} (Figure 3.2 C) appeared in the spectrum after the film was irradiated for an accumulated time of 64 minutes. This band maximized at 128 minutes of irradiation and then decreased to near background after 522 minutes of irradiation (Figure 3.3 F). This band could be attributed to the stretching vibration of the C≡C bonds. Based on its extremely low absorbance, this band could be attributed to a by-product absorbed on the surface of the film.

3.2.3. Mass spectrum of the volatile products

A sample of volatile products generated from the UV irradiation of a film of Ag(I)tfa was collected in a quartz cell. The volatile products were analyzed by mass spectrometry. The mass spectrum (Figure 3.4) showed the absence of any species with a mass/charge greater than 120.

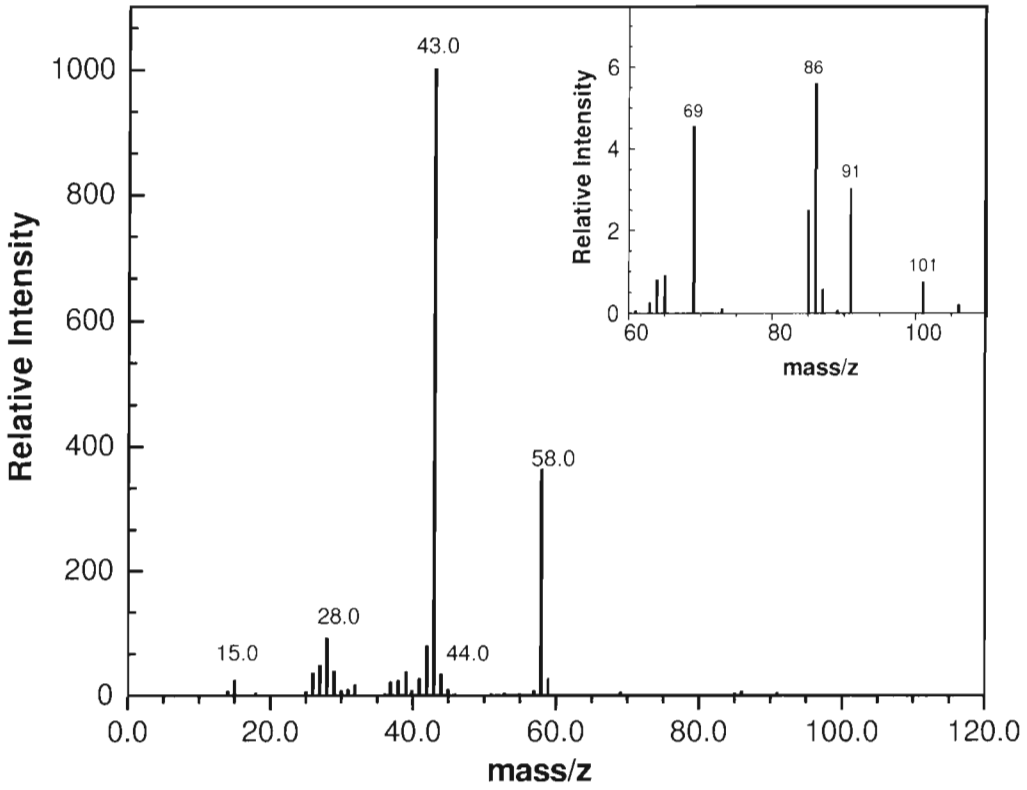

Figure 3.4 Mass spectrum of the volatile products in a quartz cell produced from a solid-state film of Ag(I)tfa under light irradiation at 254 nm for two hours (24 ℃).

Neither molecular ions of Ag(I)tfa (MM: 260.95 g/mol) nor that of the pure ligand (Htfa, MM: 154.0 g/mol) were detected in the spectrum. The peaks at mass/z 101, 91, 86, 85, 69, and 43 match well with the ones found in the mass spectrum of the ligand (Htfa)[14] (Figure 3.5). The very low quantities of the species of mass/z 101 and 91 suggest that there could be a very small amount of the ligand molecules (Htfa) in the volatile gases.

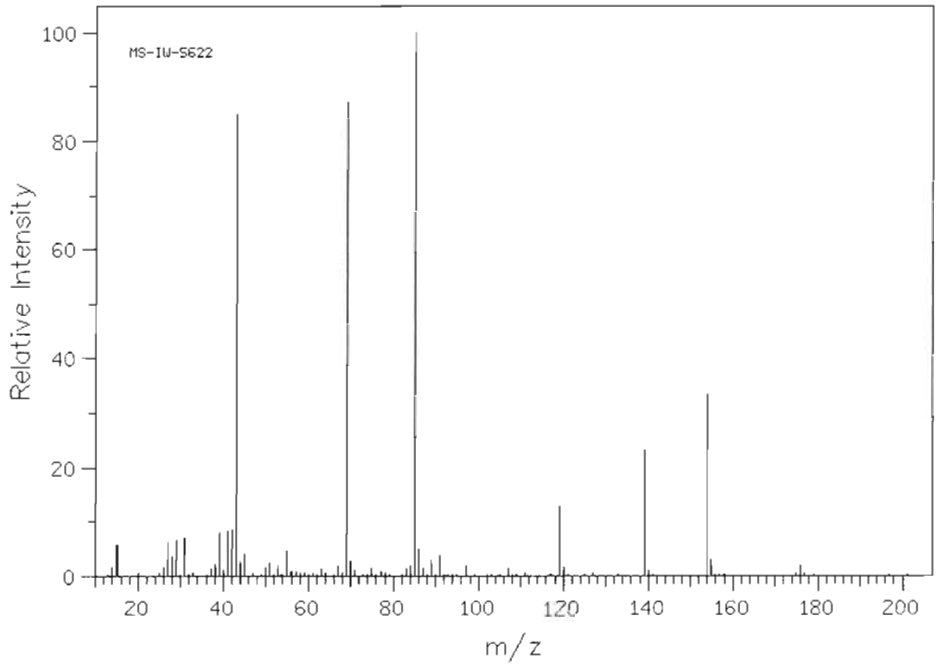

Figure 3.5 Mass spectrum of 1,1,1-trifluoro-2,4-pentanedione in the literature,[14] reproduced with permission.

In the mass spectrum of the volatile gases, the most abundant fragment of mass/z 43 was predominately assigned to $[CH_3C(O)]^+$, which has been detected in the mass spectra of many other metal chelated β-diketone complexes[15-17]. The next most abundant species of mass/z 58 could have a formula of $[CH_3C(O)CH_3]^+$. However, it could also be formed by a rearrangement of other fragments (43 and 15) or dissociation of others. The peak at mass/z 69 could have contributions from both $[CF_3]^+$ and $[COCHCO]^+$. The ligand eliminates a CF_3 group via homolytic cleavage, as is evident from the stability of the residual ion [17]. The species of mass/z 85 may have a formula of $[CH_3C(O)CH_2C(O)]^+$, which is one hydrogen atom less than the species of mass/z 86, having a possible formula of $[CH_3C(O)CH_2C(O)H]^+$. The major fragments detected in the volatile gases of the sample are listed in Table 3.1.

Table 3.1 The assignment of major fragments in the volatile gases produced from decomposition of a film of Ag(I)tfa under light irradiation at 254 nm (RT: 24 ℃).

ions (mass/z)	Abundance	Assignments
91	66	$[CF_2CC(O)H]^+$
86	122	$[CH_3C(O)CH_2C(O)H]^+$
85	54	$[CH_3C(O)CHC(O)H]^+$
69	99	$[CF_3, COCHCO]^+$
59	562	$[CH_3CH(O)CH_3]^+$
58	7932	$[CH_3C(O)CH_3]^+$
45	186	$[CH_3CH_2O]^+$
44	721	$[CO_2]^+$
43	21872	$[CH_3CO]^+$
42	1716	$[H_2C=C=O]^+$
28	1963	$[CO]^+$
27	1037	$[CH_2=CH]^+$
15	514	$[CH_3]^+$

3.2.4. The thermal and photochemical reactions

As the thermal decomposition of the film in air is explored in Chapter 4, it is important to understand the relationship between thermal decomposition and the photochemical reaction. A film of Ag(I)tfa similar to that used in photolysis was prepared on a silicon substrate by spin coating. The changes of the films kept in a dark room without irradiation were monitored by FT-IR spectroscopy (Figure 3.6). A plot of the absorbance at the 1283 cm^{-1} peak versus time for the films with and without UV irradiation is shown in Figure 3.7.

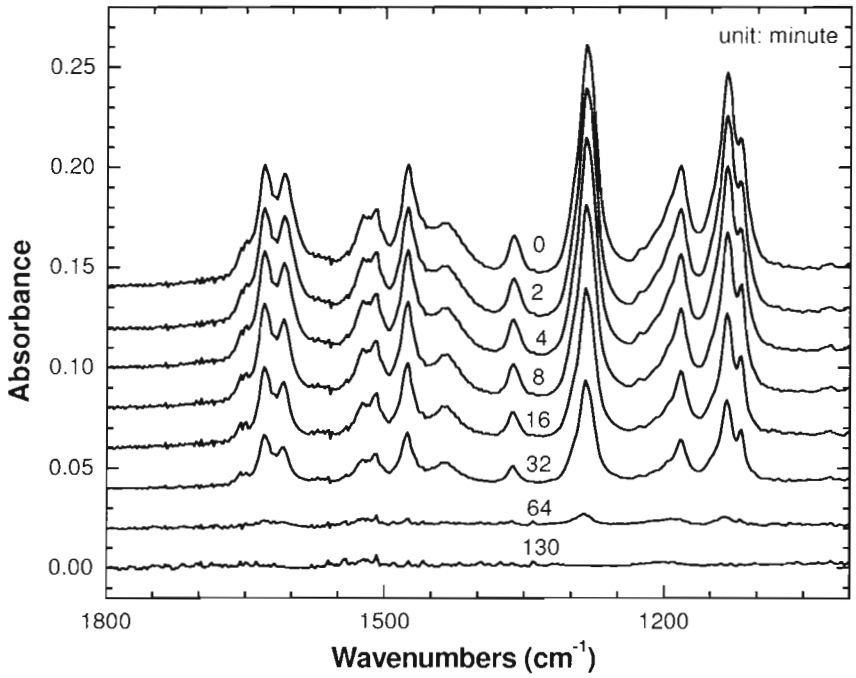

Figure 3.6 The changes of the FT-IR spectra of a solid-state film of Ag(I)tfa on a calcium fluoride disc while kept in the dark without irradiation and under ambient conditions (RT: 22 ℃, RH: 22 %).

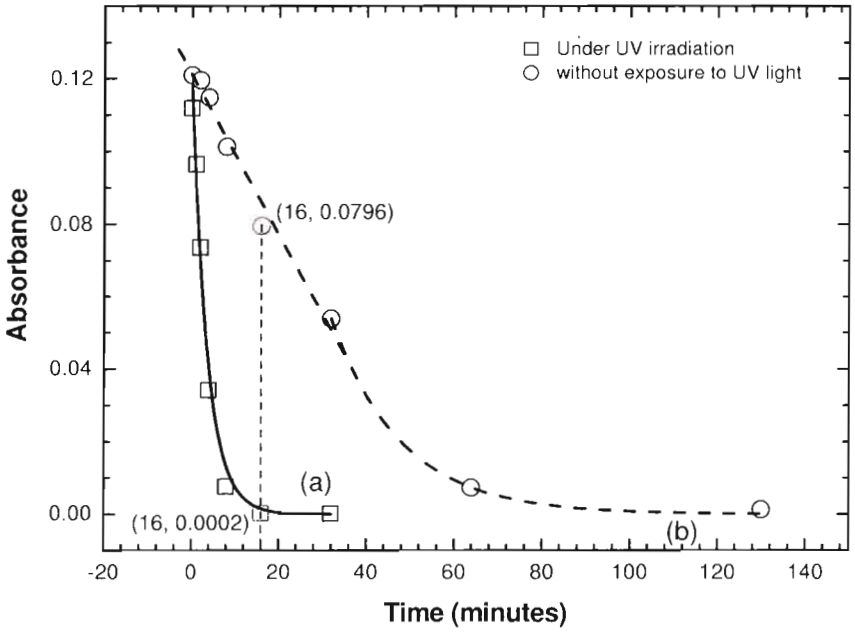

Figure 3.7 Absorbance at 1283 cm^{-1} as a function of time for two identical films of Ag(I)tfa either (a) under UV irradiation (open squares) or (b) kept in the dark without exposure to UV light (open circles).

In Figure 3.7, the experimental data were fitted by different functions. The data from the film exposed to UV light were fitted with a first-order exponential decay function. The data from the film kept in the dark without exposure to UV light did not fit with a simple first-order decay function but required both of zero-order (a linear line) and first-order decay function. More detailed analysis is presented in Chapter 4. From the graph, the absorbance at 1283 cm^{-1} of the film under irradiation decreased by 99.8% after16 minutes. The same conversion of the film without UV irradiation would need over 130 minutes in total. It is apparent that the rate of photochemical reaction is much greater than the overall rate of thermal decomposition.

3.2.5. Analysis of the chemical composition of the deposited film

3.2.5.1. Surface contaminations and the film composition

The chemical composition of a photolyzed film of Ag(I)tfa was analyzed by Auger electron spectroscopy (AES). Because pollutants from air have been found in many metal or metal oxide thin film surfaces in the literature after they were exposed to air, the composition of the film before and after argon surface cleaning was investigated by AES. An Auger electron spectrum of the film before sputtering is shown in Figure 3.8.

The atomic concentration of any constituent in the film is calculated from the following equation.

$$C_x = \frac{I_x/(S_x d_x)}{\sum_i I_i/(S_i d_i)} \qquad (1)$$

where C_x is the atomic concentration, I_x and I_i the peak-to-peak Auger amplitudes, S_x the relative elemental sensitivity factor,[18] and d_i the relative scale factor, which is same for all the elements in this case.

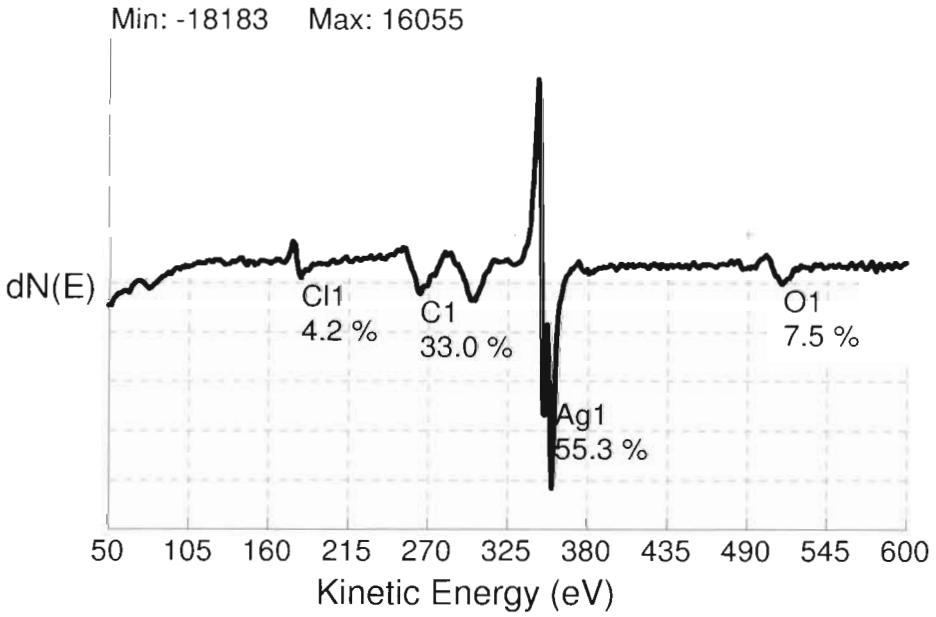

Figure 3.8 Auger electron spectrum of a film deposited on a silicon substrate before cleaning. The film was prepared from a solid-state film of Ag(I)tfa under light irradiation at 254 nm in air and in the dark (RT: 24 ℃, RH: 22%).

From the Auger spectrum in Figure 3.8 the composition of the film comprised chlorine, carbon, silver, and oxygen, and their characteristic kinetic energies were observed at Cl: 183.0, C: 272.0, Ag: 351.0, and O: 513.0 eV,[18] respectively. The corresponding atomic concentrations were calculated to be Cl: 4.2 mol%, C: 33.0 mol%, Ag: 55.3 mol%, and O: 7.5 mol%. Due to the overlap of the peaks of carbon and silver at 272.0 eV, the atomic concentrations of these elements are not accurate.

In order to determine whether carbon found in the film was surface contamination or a residue throughout the entire film, more Auger spectra of the film were recorded after sputtering for 18, 30, and 90 seconds in Figure 3.9, Figure 3.10 and Figure 3.11 respectively. Based on the experimental conditions, the sputtering rate of silicon is estimated to be 1.0 nm/min, silicon dioxide is 0.85 nm/min, and Ag to be 20.0 nm/min.[19] The etching depth of argon sputtering of the film for 90 seconds is estimated to be 30 nm, which is less than the thickness of the original film, 70 nm measured by a profilometer. Therefore, the data should represent the compositions of the films.

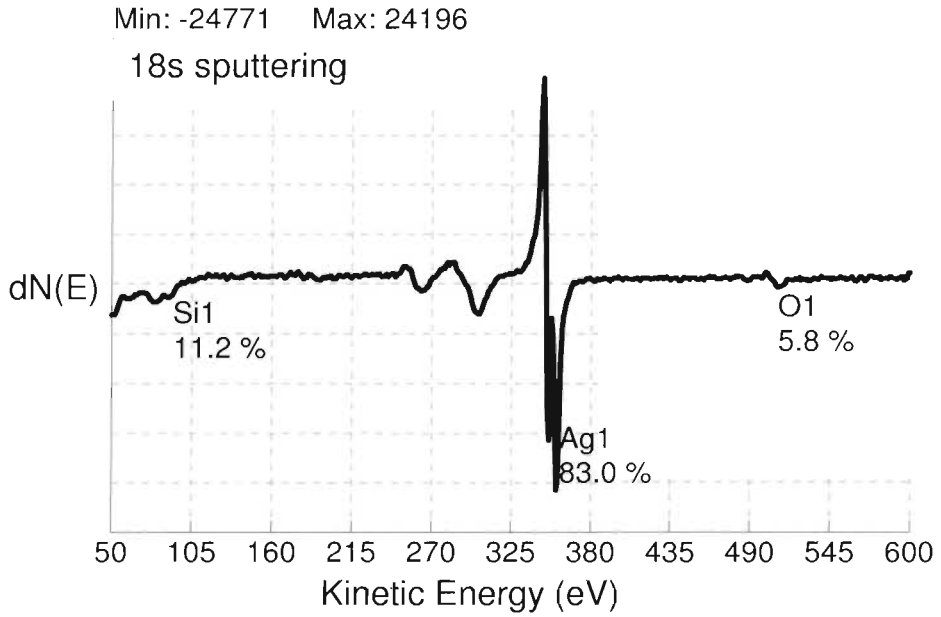

Figure 3.9 Auger electron spectrum of the photoproduced film after sputtering for 18 seconds.

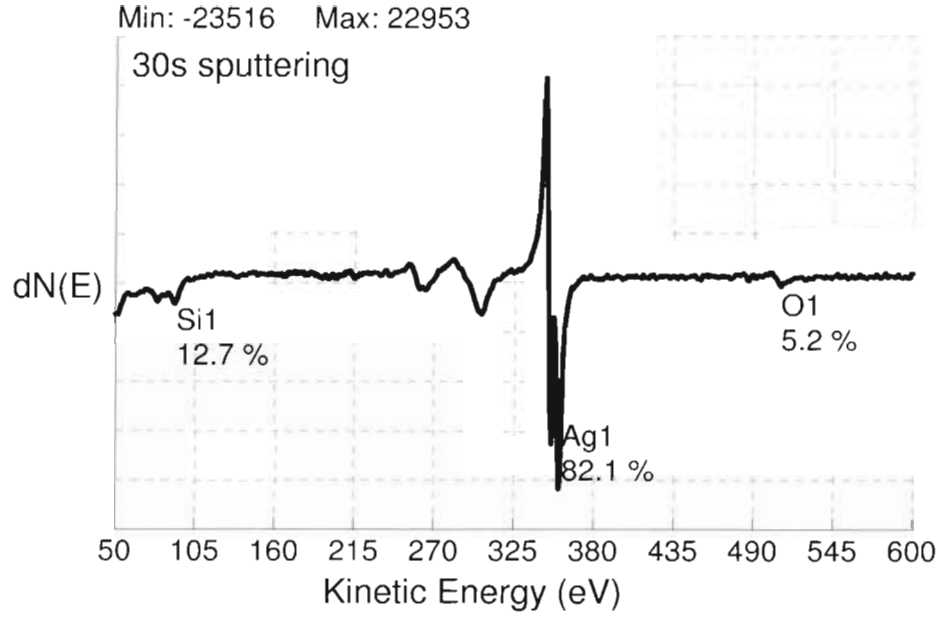

Figure 3.10 Auger electron spectrum of the photoproduced film after sputtering for 30 seconds.

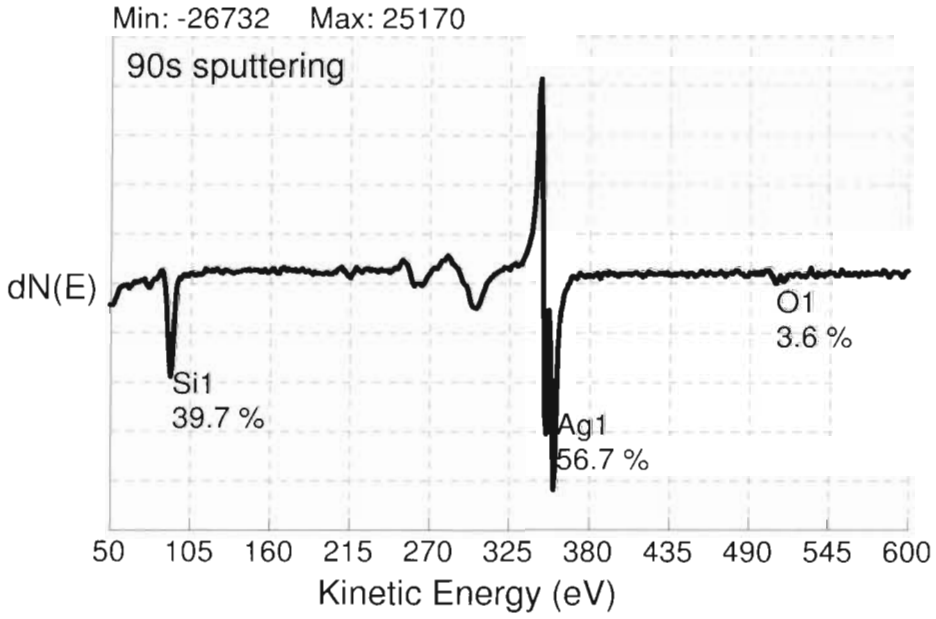

Figure 3.11 Auger electron spectrum of the photoproduced film after sputtering for 90 seconds.

The atomic concentrations of the elements of the film were calculated by three different methods from these three spectra. The first calculation method (1) included all elements except silicon. The second calculation method (2) included

all elements except carbon. The third calculation method (3) included only silver and oxygen elements. The calculated atomic compositions of the elements detected in the resultant film are summarized in Table 3.2.

Table 3.2 The calculated atomic concentrations of the elements of the photoproduced film after sputtering by argon for different periods.

Composition (mol%)		Ag	O	C	Cl	Si
As deposited	1	55.3(±0.8)	7.5(±3.0)	33(±19)	4.2(±1.8)	0
	2	55.3(±0.8)	7.5(±3.0)	33(±19)	4.2(±1.8)	0
	3	88.0(±1.3)	12.0(±4.0)	-	-	-
Sputtered for 18 s	1	72.3(±1.1)	5.1(±1.8)	23(±13)	0	-
	2	83.0(±1.2)	5.8(±2.0)	-	0	11.2(±1.7)
	3	**93.4(±1.4)**	**6.6(±2.0)**			
Sputtered for 30 s	1	71.6(±1.1)	4.5(±1.6)	24(±14)	0	-
	2	82.1(±1.2)	5.2(±1.9)	-	0	12.7(±1.9)
	3	**94.0(±1.4)**	**6.0(±2.0)**			
Sputtered for 90 s	1	71.6(±1.1)	4.5(±1.6)	24(±14)	0	-
	2	56.7(±0.9)	3.6(±1.3)	-	0	40(±6)
	3	**94.0(±1.4)**	**6.0(±2.0)**			

Based on these calculations, the surface contamination and the composition of the film were determined. Two contaminants were determined. First, the chlorine content was deemed a surface contamination due to its disappearance after sputtering. The source of chlorine could be some residual dichloromethane absorbed on the surface or sodium chloride in human sweat or others. Second, the carbon content was deemed a surface contamination. The ratio between the peak at 266 eV and 351 eV is unchanged at 0.041(±0.002) after the film was sputtered for 30 seconds. This ratio matches well that (0.042(±0.002)) of metallic

silver in the literature.[18] This suggests that there are no carbon signals. Otherwise, the ratio would be greater than the literature value.

It is worth noting that the atomic concentrations of silver and oxygen calculated by method (3) were unchanged after the film was sputtered for 30 seconds to 90 seconds although the silicon content increased significantly. This increasing indicates that the silicon was a contribution from the silicon substrate. In addition, based on the high content of silver (94.0±1.4 mol%) in the film and relatively small content of oxygen, metallic silver was deemed a predominant component in the film while oxygen could be mainly associated with silver oxide.

3.2.5.2. The oxygen effects

Due to concern about the oxygen content found in the film prepared in air, it was of interest to know whether a pure silver film could be obtained if the Ag(I)tfa film was kept in an oxygen-free environment during preparation. Therefore, two identical solid-state films of Ag(I)tfa were prepared on two identical silicon substrates. Both Ag(I)tfa films were photolyzed with UV light at 254 nm at 22 ℃, and one film was kept in a glove bag purged by ultra-pure grade nitrogen gas (minimum purity of N_2 : 99.998%, O_2 : 8.0 ppm, and H_2O : 5.0 ppm) at a flow rate 5.0 liters per hour and the other in air. Both resultant films were analyzed by AES following a sputtering clean (Figure 3.12 and Figure 3.13).

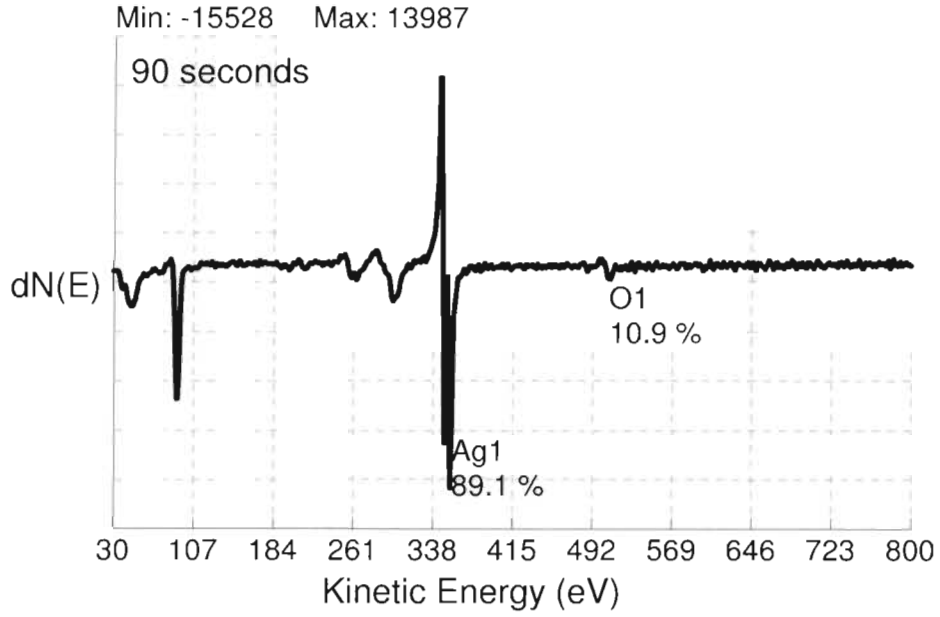

Figure 3.12 Auger electron spectrum of a sputtered film prepared from Ag(I)tfa by UV irradiation at 254 nm for eighty minutes in air and in the dark and under ambient conditions (ambient conditions: RT: 24 ℃, RH: 22 %).

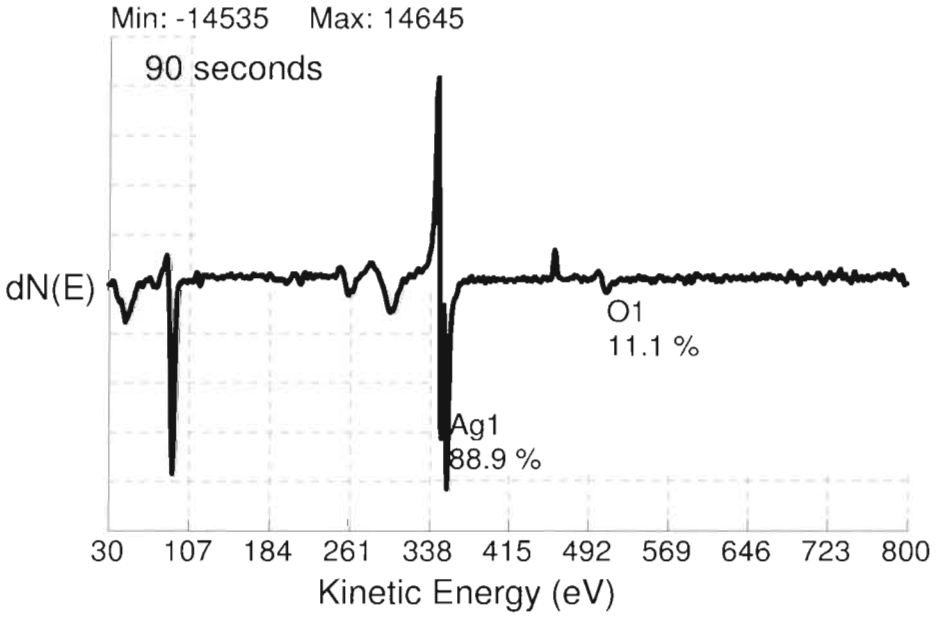

Figure 3.13 Auger electron spectrum of a film after sputtered for 90 seconds, which was prepared from a solid-state film of Ag(I)tfa under UV irradiation for eighty minutes at 254 nm in a bag purged by ultra-pure grade nitrogen gas in the dark at RT: 24 ℃.

Based on the atomic concentrations of silver and oxygen, the compositions of the two films produced in different gases are in good agreement. The similar compositions suggest that different oxygen content in the environment affects the composition of the film insignificantly. These experiments provide no definitive understanding whether the formation of silver oxide was due to the residual oxygen in ultra-pure nitrogen gas or the exposure in air before the Auger measurement. However, the X-ray data in section 3.2.8 suggest that the silver oxide is silver(I,III) oxide. This oxide is not a common oxidation product of silver in air under ambient conditions. This suggests that the silver oxide could be an oxidation product of the complex film.

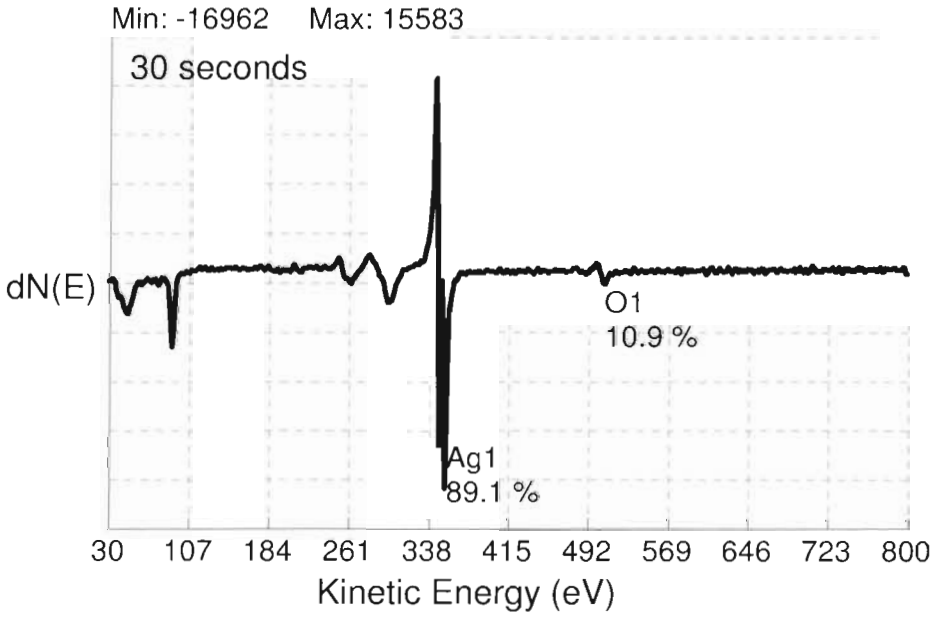

Figure 3.14 Auger electron spectrum of the film after sputtering for 30 seconds. The film was prepared in a nitrogen bag under light irradiation at 254 nm for eighty minutes in the dark at RT: 24 ℃.

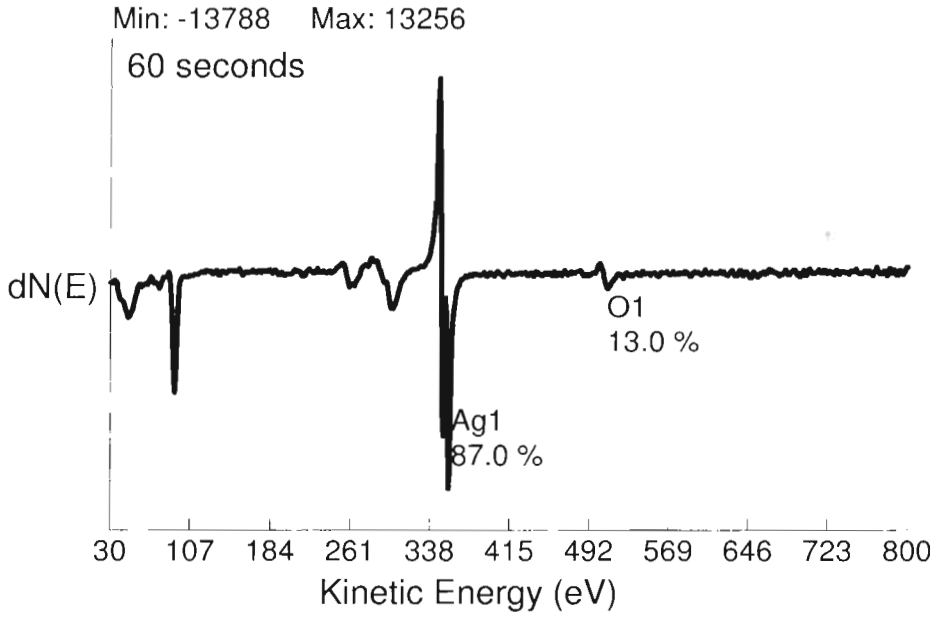

Figure 3.15 Auger electron spectrum of the film after sputtering for 60 seconds. The film was prepared in a nitrogen bag under light irradiation at 254 nm for eighty minutes in the dark at RT: 24 ℃.

Because of the observation of a silicon signal in the Auger spectra, the native oxide found on the surface of the silicon substrate could be a source of the oxygen content. Two additional Auger spectra of the same film prepared in nitrogen after sputtered for 30 and 60 seconds were recorded and are shown in Figure 3.14 and Figure 3.15. In the Auger spectra, the oxygen content first increased from 10.9 % to 13.0 % after the sputtering time of the film was increased from 30 seconds to 60 seconds, and then decreased to 11.1 % after sputtered for an additional 30 seconds. The increase of the oxygen content could be because silicon oxide on the substrate was exposed to the applied beam. The decrease of the oxygen content of the film after sputtering for more time could be due to the penetration of the native oxide layer. This was consistent with the observation of a large increase in the silicon signals.

Therefore, the oxygen content of the film in these measurements consisted of a partial contribution from the native silicon oxide. Could the oxygen content be mainly due to the native oxide? It is highly unlikely since the native oxide layer was 12-19 Å thick. The film of silver and silver oxide prepared under experimental conditions was estimated to be 600 Å thick. The etching depth of silver by argon sputtering for 90 seconds was about 400 Å. Therefore, the detected Auger signal should be attributed mainly to the film.

In addition, it is worth noting that the oxygen and silver contents (88.9 mol% and 11.1 mol%) of the film prepared in air differ from those in the previous sample (94.0 mol% and 6.0 mol%). This difference could be mainly caused by the variation of the deposition temperature, which would affect the thermal reaction of the film during irradiation. All the film were placed on a big iron plate to regulate the temperature, which was equilibrated with the room temperature. However, the room temperature varied.

3.2.6. X-ray powder diffraction of a photoproduced film

The deposited film was analyzed by X-ray powder diffraction. In order to increase the signal ratio between the film and the noise, a thicker film was prepared by repeating the photodeposition process three times with the same stock solution of Ag(I)tfa on the same silicon substrate. An X-ray power diffraction pattern recorded from this sample is shown in Figure 3.16, in which the literature data of silver and silicon[20-21] are shown in the bottom panels.

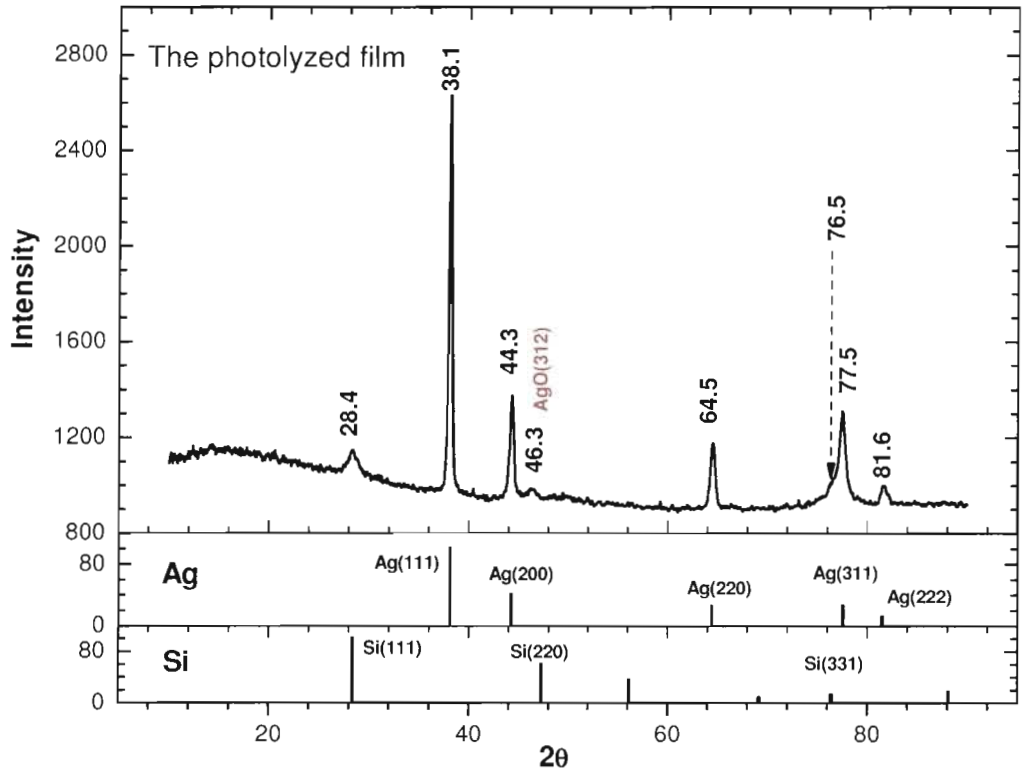

Figure 3.16 X-ray powder diffraction pattern of a film on a silicon substrate prepared from sequential processing of solid-state films of Ag(I)tfa under light irradiation at 254 nm (RT: 24 ℃, RT: 22 %).

Most diffraction peaks shown in Figure 3.16 match well with the literature values of the bulk silver. The 2θ values observed at 38.1°, 44.3°, 64.5°, 77.5°, and 81.6 were contributed by the reflections from the lattice planes of Ag(111), Ag(200), Ag(220), Ag(311), and Ag(222), respectively. Because of broadening of the peak at 77.5°, a Si(311) peak at 76.5° was resolved by Gaussian fitting[22] as a shoulder of the peak at 77.5°. Therefore, it is apparent that the film contained metallic silver.

The other diffraction peaks were contributed from the substrate and silver oxide. The peaks at 28.4° and 76.5° were contributed by the silicon substrate, Si(111) and Si(331). A weak and broad diffraction peak observed at 46.3° does not

match any peaks attributed to the silicon substrate. Although many SiO_2 structures have a diffraction peak close to this position, it is highly unlikely because the native oxide grown on the top of the silicon substrate is deemed amorphous. This peak could be contributed by the lattice plane 312 (46.2°) of the tetragonal Ag_2O_2 (space group:88).[23] For a better justification, more diffraction peaks from the Ag_2O_2 crystals are needed.

Table 3.3 Nanoparticle sizes calculated from the Scherrer equation.

2θ	FWHM (degree)	Estimated size (nm)
38.1	0.307	28.6
44.3	0.408	22.0
64.5	0.486	20.2
81.7	0.636	17.3
	Average(±SD)	22(± 5)

The size of the silver crystals was calculated to be 28.6 nm at the peak of 38.1° according to the Scherrer equation,[30]

$$D_{hkl} = K\lambda/(\beta Cos(\theta))$$

where D is the size of the crystal, $h\ k\ l$ the Miller indices, λ the wavelength of the Cu $K\alpha$ line (1.5418 Å), β the pure diffraction breadth, θ is the Bragg angle, K is crystallite shape constant. The K value is given as 0.94 in the literature[30] when β is taken as the full-width at half-maximum (FWHM) of the peak. The calculated crystal sizes associated with other peaks are listed in Table 3.3.

3.2.7. Morphology of silver nanoparticles

The XRD results showed that the deposited film was polycrystalline silver. The size, shapes, and structures of silver nanocrystals were of great interest. The film prepared photochemically from Ag(I)tfa was subjected to HRTEM and SEM investigation.

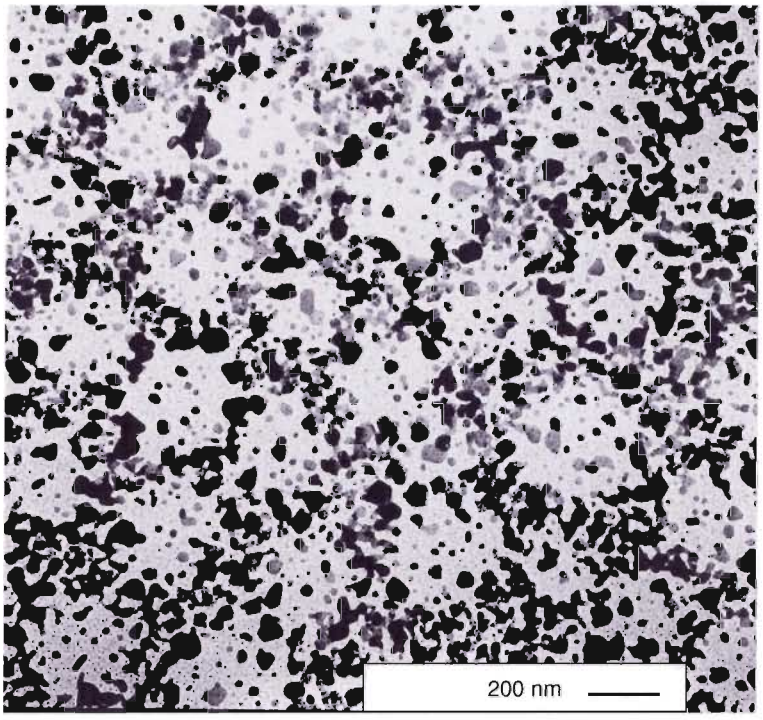

Figure 3.17 HRTEM bright field image[a] of a film on a carbon-coated copper grid prepared from a solid-state film of Ag(I)tfa under light irradiation at 254 nm (RT: 20 °C, RH: 22 %).

[a] It was taken in 2002 by Dr. Victoria Fink, a postdoctoral fellow in Dr. Kavanagh's group in the Physics Department of Simon Fraser University, Canada.

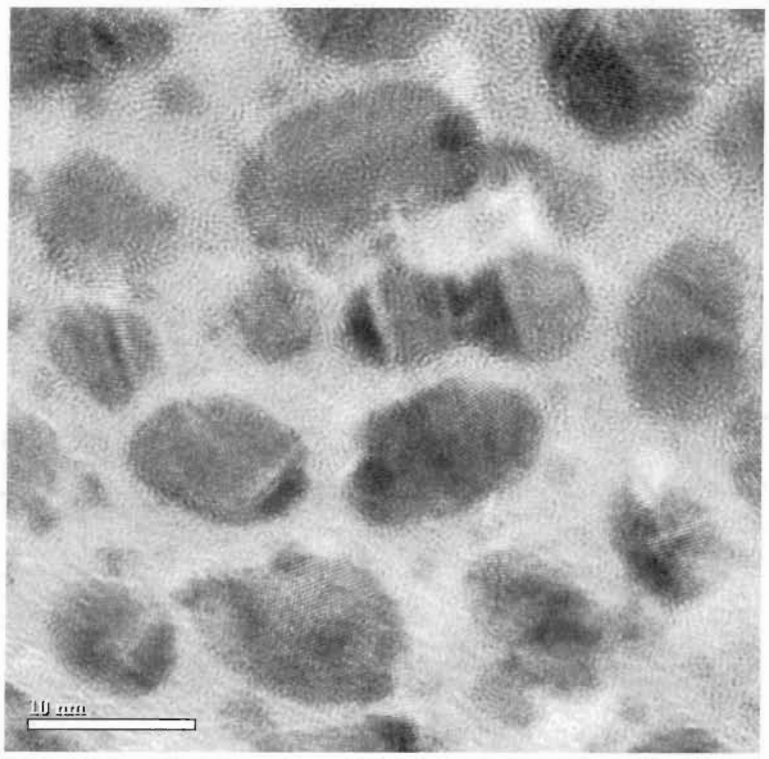

Figure 3.18 HRTEM image of a polycrystalline nanoparticle of a film on a carbon coated copper grid prepared from a solid-state film of Ag(I)tfa under light irradiation at 254 nm in the dark (RT: 24 ℃, RH: 22 %). The scale marker in the bottom left image is 10 nm.

3.2.7.1. HRTEM image and electron diffraction pattern

A bright field TEM image was obtained from a film photoproduced from Ag(I)tfa on a carbon-coated copper grid (Figure 3.18). The dark/shaded areas in the figure are where the nanoparticles were deposited on the grid. The light gray areas are where the electrons went through the bare carbon film. Separation between silver nanoparticles is clearly observed in the image and the spacing between nanoparticles is irregular. The shape of the nanoparticles is irregular as well, and the size of the nanoparticles varies from a few nanometers to over a hundred nanometers in diameter.

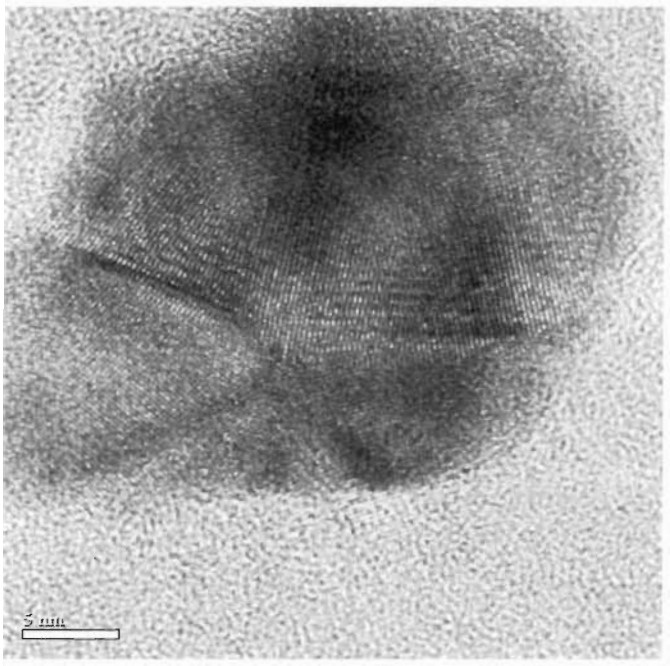

Figure 3.19 HRTEM image of a nanoparticle of a film on a carbon coated copper grid prepared from a solid-state film of Ag(I)tfa under light irradiation at 254 nm (RT: 24 ℃, RH: 22 %). The scale marker in the bottom left image is 5 nm.

Two high-resolution TEM images of a film prepared from a solid-state film of Ag(I)tfa under UV irradiation at 254 nm are shown in Figure 3.18 and Figure 3.19. Uniform lattice fringes (dark shaded lines) orientated in different directions are observed on all the nanoparticles in Figure 3.18. The lattice fridges indicate that the nanoparticles are crystalline. The different orientations indicate that these nanoparticles are polycrystalline. The other HRTEM image of single nanoparticle is shown in Figure 3.19. Different orientations of lattice fringes were observed over the whole particle. A dark line observed on the left side of the image is an indication of the twinned structure of two crystals, which could be formed by the aggregation of the photoreduced silver nanoparticles or stacking of the reduced silver on top of the others. These observations indicate the investigated

nanoparticle was a polycrystalline particle. These results are consistent with that in literature,[24] where the deposited film was polycrystalline film.

3.2.7.2. Electron diffraction

A digital image of a negative of an electron diffraction pattern[b] of a silver film is shown in Figure 3.20. The diffraction ring patterns are observed clearly. This indicates that the film is composed of a polycrystalline material. After indexing the diffraction pattern of the film, the lattice parameters of the polycrystalline materials were calculated (Table 3.4).

According to the selection rules for cubic crystal structures, the reflections are present when ($h\ k\ l$) are all odd or all even. All five reflections with all even or odd lattice indices ($h\ k\ l$) in Table 3.4 are consistent with those of a face-centred cubic structure of silver. The mean value of the calculated lattice parameters (a: 4.09±0.005 Å) is identical to the literature value for bulk silver (4.09 Å). This does not match the lattice parameter of cubic copper (3.60 Å).[25] Therefore, these indexed rings are believed to be associated with the metallic silver.

However, some other less intensive rings were detected in the diffraction pattern in Figure 3.20. These rings may be due to some crystalline silver oxide. The identity of this oxide is unable to determine at this time due to the lack of sufficient data.

[b] It was taken in 2002 by Dr. Victoria Fink, a postdoctoral fellow in Dr. Kavanagh's group in the Physics Department of Simon Fraser University, Canada.

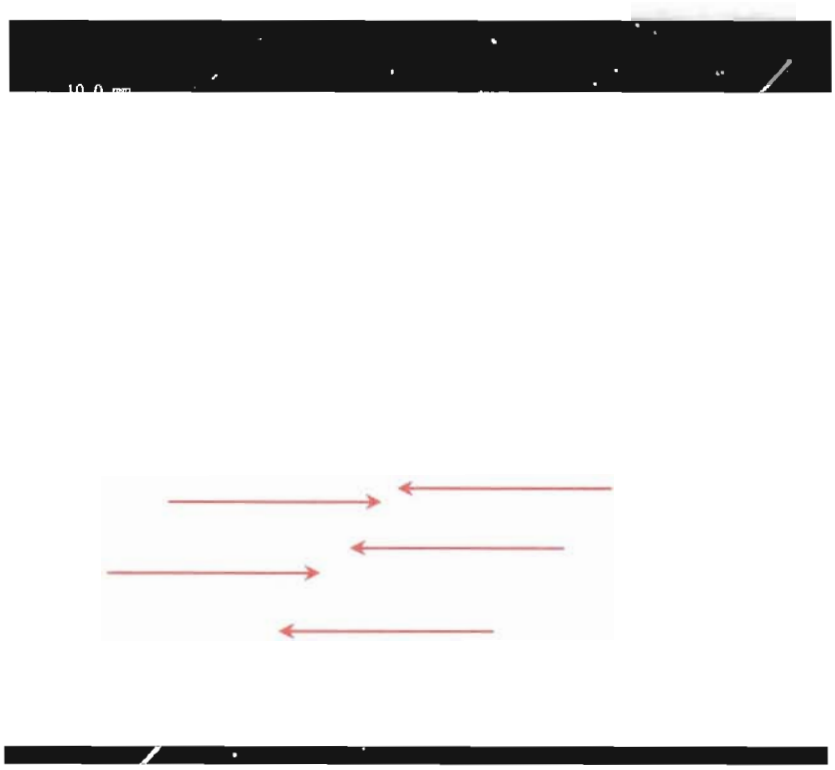

Figure 3.20 A digital image of a negative film of an electron diffraction pattern of a film deposited from Ag(I)tfa by UV irradiation at 254 nm (ambient conditions RT: 24 ℃, RH: 22%).

Table 3.4 Indexing the electron diffraction pattern.

2R (mm)	**Calib. L (m)**	**d(nm)**	$1/d^2$	$h^2+k^2+l^2$	x **3**	**h k l**	**a (nm)**
24.5	1.051	0.237	17.8	1.00	3	111	0.411
28.5	1.062	0.204	24.0	1.35	4	200	0.408
40.0	1.055	0.145	47.4	2.66	8	220	0.411
47.0	1.051	0.124	65.5	3.68	11	311	0.410
62.0	1.060	0.094	114.0	6.40	19	331	0.408
L: (m)	1.056					**Exp:**	a: 0.409 ($\pm$ 0.005)
λ: (nm)	0.00275					**Lit:**	a: 0.409

3.2.7.3. Surface morphology investigated by SEM

Although the HRTEM images of the film on a copper grid showed the porous structure of the resultant silver film, the morphology of a thick film on silicon substrate could be different. The pores in the film could be reduced or diminished by the continuing deposition of silver particles on top of each other, or increased due to a large volume of organic material escaping from the film. For this purpose scanning electron spectroscopy was employed to investigate the surface structure of the silver film deposited on the silicon substrates. At the same time, the relationship between the film structure and the substrate orientations was of great interest because the orientation of the substrates could affect the crystal growth.[26] Therefore, the SEM images of the films prepared from Ag(I)tfa were acquired on both Si(100) and Si(111) substrates (Figure 3.21).

Nanoparticles with irregular shapes were observed at various sizes and quantities in both images. No significant topological difference was observed between the two films in Figure 3.21. The nanoparticle size was in a range from 15 to 83 nm in both films.

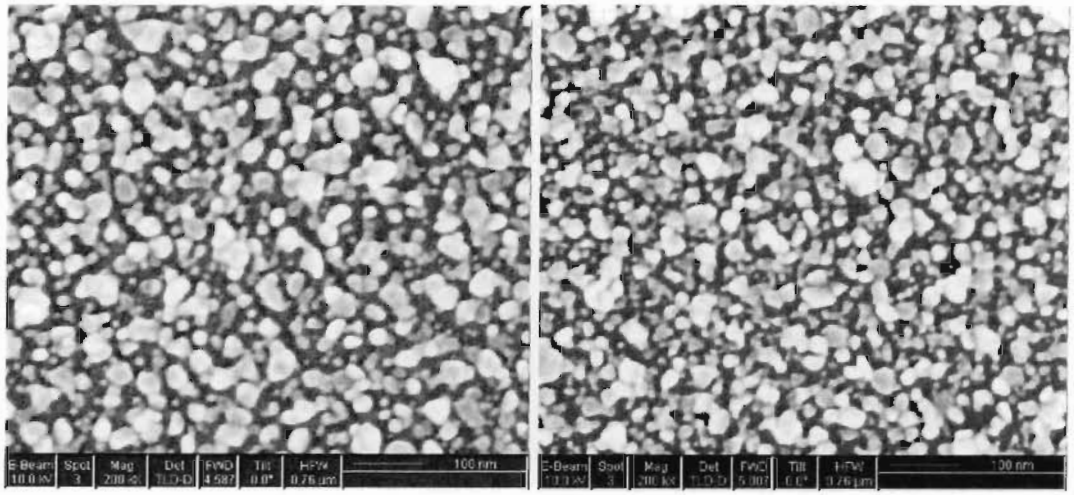

Figure 3.21 SEM images of the films on the Si(100) (left) and Si(111) (right) substrates prepared from solid-state films of Ag(I)tfa under light irradiation at 254 nm in the dark (RT: 24 ℃, RH: 22 %).

3.2.8. Determination of the early stage of silver/silver oxide formation

From the study of the changes of FT-IR spectra of a film of Ag(I)tfa during photolysis (section 3.2.2), although the entire photolysis lasted for more than eight hours, all initial absorption bands disappeared after the film was irradiated with UV light for 16 minutes. These changes could be due to the complete dissociation of the metal centres and the chelated organic ligands. If this was true, the photoredox reaction should have been complete. Then the photo-produced product, such as crystalline silver detected by other techniques, should have been formed in the film. This information is important to understand the photoreaction stages, which are vital to the photochemical reaction mechanism of the solid-state film of Ag(I)tfa. Since one photoproduct is polycrystalline silver, the formation of the product in the amorphous film could be followed by X-ray diffraction. Therefore, a solid-state film of Ag(I)tfa was investigated by X-ray

diffraction after photolysis for different periods. A plot of the absorbance of the band at 1283 cm^{-1} versus time (Figure 3.22) was used to determine the appropriate period of photolysis.

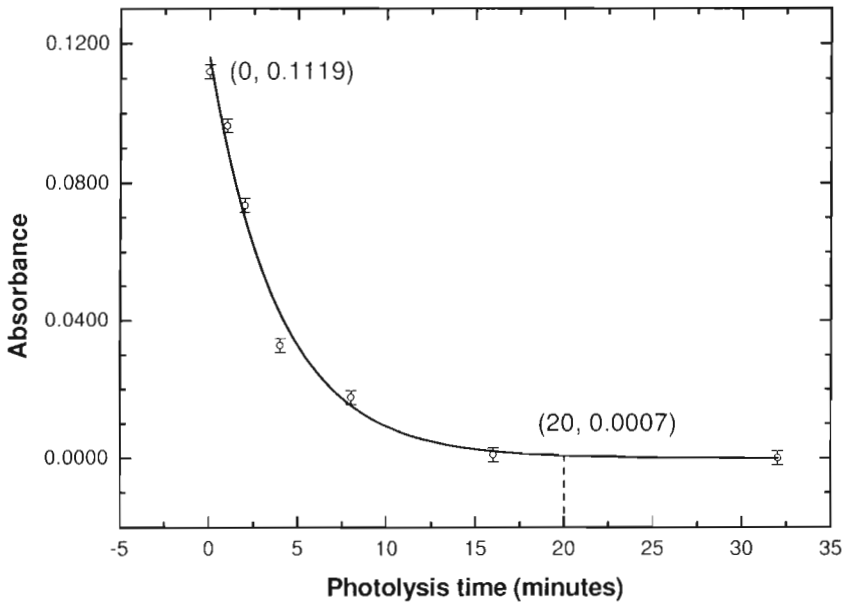

Figure 3.22 A plot of absorbance of the band at 1283 cm^{-1} versus photolysis time for a film of Ag(I)tfa under light irradiation at 254 nm (data points were obtained from the FT-IR spectra presented in Figure 3.2, the error bar is 0.5%).

The experimental data can be fit with a first-order exponential decay curve. The absorbance of the film at 20 minutes was 0.00071, a conversion greater than 99.4%. This suggests that 20 minutes is sufficient for the reaction of the film to reach completion. An XRD pattern of Ag(I)tfa film recorded after 20 minutes irradiation is shown in Figure 3.23, and for 60 minutes in Figure 3.24.

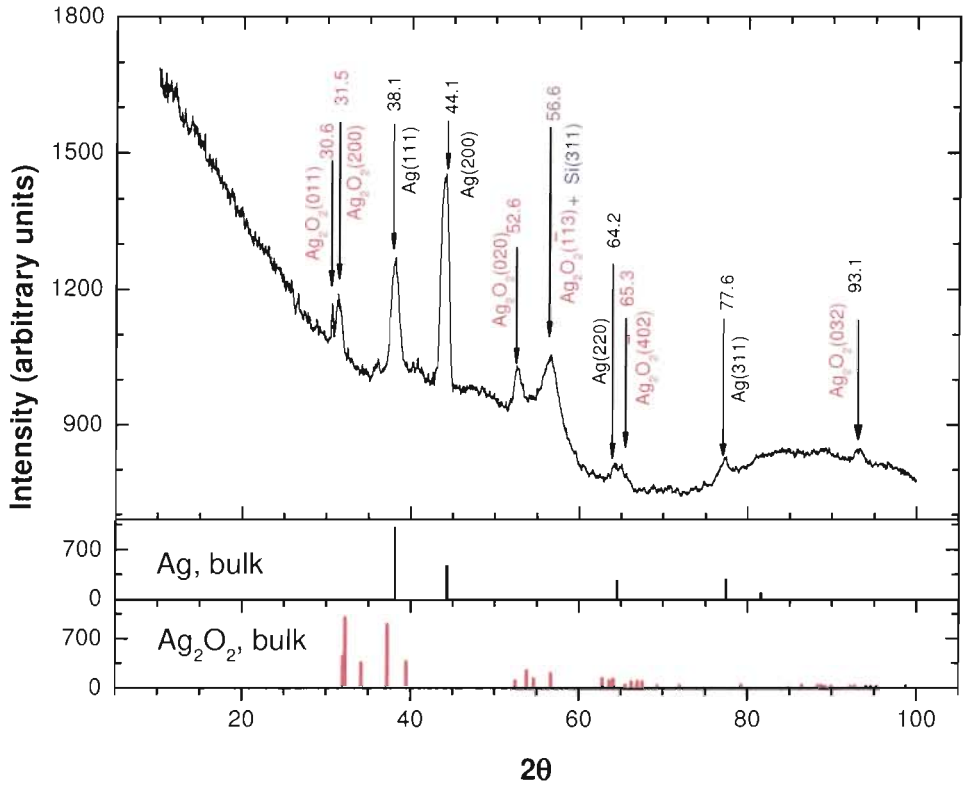

Figure 3.23 XRD pattern of a film prepared from a solid-state film of Ag(I)tfa on a silicon substrate under light irradiation at 254 nm for 20 minutes in the dark (RT: 24 ℃, RH: 22 %). The literature data of Ag[16] and Ag_2O_2[19] are plotted at the bottom of the figure.

Two sets of diffraction peaks are evident in Figure 3.23. The peaks at 38.1°, 44.1°, 64.2°, and 77.5° are consistent with those from Ag(111), Ag(200), Ag(220), and Ag(311) in the literature.[16] The other peaks at 30.6°, 31.5°, 52.6°, 56.6°, 65.3°, and 93.1° are consistent with those from Ag_2O_2(011), Ag_2O_2(200), Ag_2O_2(020), Ag_2O_2(11$\underline{3}$), Ag_2O_2(40$\underline{2}$) and Ag_2O_2(032) in the literature.[19] It is believed that the peak at 56.61° overlapped with the reflection of Si(311) from the silicon substrate, and its contribution is believed to be predominant. Therefore, these results indicates that the irradiated film is composed of polycrystalline silver and silver(I,III) oxide.

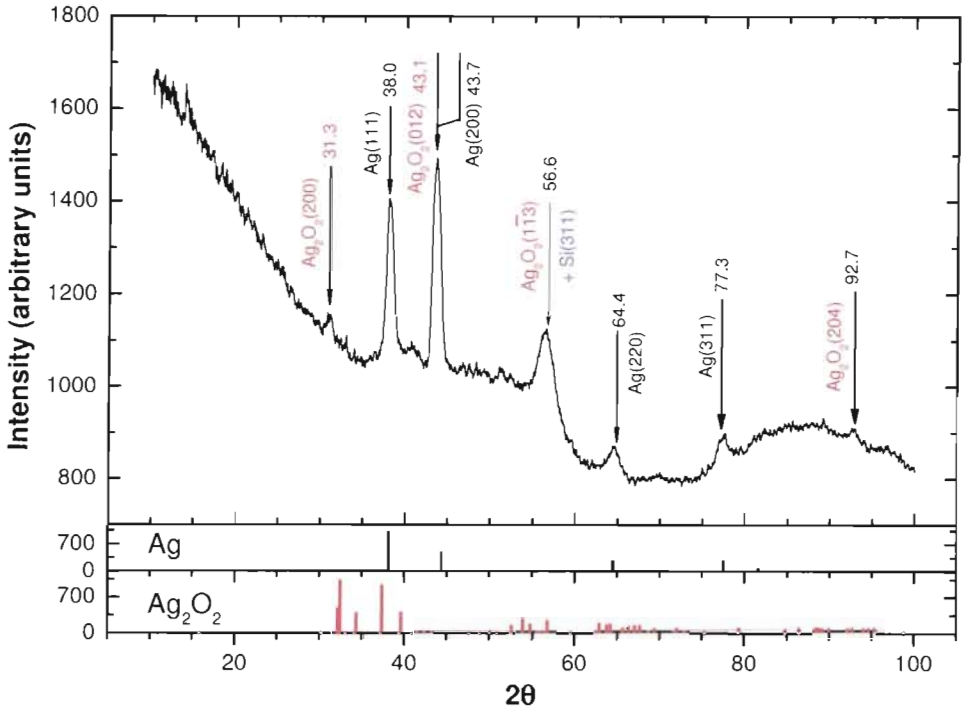

Figure 3.24 XRD pattern of a film prepared from a solid-state film of Ag(I)tfa on a silicon substrate under light irradiation at 254 nm for 60 minutes in the dark (RT: 24 ℃, RH: 22 %). The literature data of Ag[16] and Ag_2O_2[19] are plotted at the bottom of the figure.

Two sets of diffraction peaks from silver and silver(I,III) oxide are also evident in Figure 3.24. The diffraction peaks observed at 38.0°, 64.4°, and 77.5° are contributed from Ag(111), Ag(220), and Ag(311). These peaks are consistent with those found in Figure 3.23. The reflection from Ag(200) is absent and will be explained later. The other set of peaks observed at 31.3°, 43.6°, 56.6°, and 92.7° were contributed by Ag_2O_2(200), Ag_2O_2(012), Ag_2O_2(11$\underline{3}$), and Ag_2O_2(204). Comparing Figure 3.24 and Figure 3.23, two peaks attributed to Ag_2O_2(200) and Ag_2O_2(11$\underline{3}$) are almost identical in the two XRD patterns. The other two peaks were new. In addition, four peaks from Ag_2O_2(011), Ag_2O_2(020), Ag_2O_2(40$\underline{2}$), and Ag_2O_2(032) observed in Figure 3.23 were absent in Figure 3.24. At the same

time, the peak at 56.6° in Figure 3.24 should also have a predominant contribution from Si(311) of the substrate.

All the major diffraction peaks from two films and their corresponding literature values are listed in Table 3.5. Blue-highlighted peaks correspond to silver, and the yellow-highlighted peaks correspond to Ag_2O_2.

Table 3.5 The assignment of the XRD diffraction peaks of a film of Ag(I)tfa after photolysis for different periods.

Experimental Data				Cubic*		Monoclinic*		Tetragonal*	
Film-20		Film-60		Ag		Ag_2O_2		Ag_2O_2	
Peak	*I***	Peak	*I*	Peak	*I*	Peak	*I*	Peak	*I*
30.6	183	-	-	-	-	30.2 (110)	21	30.6 (211)	4
31.5	292	31.3	105	-		32.0 (200)	457	32.2 (103)	2
						32.3(11$\underline{1}$)	1000	32.6(20$\underline{2}$)	1000
-	-	-	-	-	-	37.2 (111)	908	36.9 (202)	510
38.1	542	38.0	685	38.2 (111)	1000	-	-	-	-
-	-	43.6	1000	-	-	43.4 (012)	1	43.8 (114)	1
44.1	1000			44.3 (200)	468	-	-	-	-
52.6	242	-	-	-		52.8 (115)	115	53.2(400)	156
56.6	350	56.6	334	-		56.8 (11$\underline{3}$)	213	56.9 (233)	0
64.2	100	64.4	123	64.5 (220)	256	64.2 (022)	135	64.2 (022)	0
65.3	83	-	-	-	-	65.7 (40$\underline{2}$)	57	-	-
77.5	83	77.3	105	77.5 (311)	272	77.7 (213)	0	77.5 (213)	0

*: From the literature.[16,19]; ** : Relative intensity of the diffraction peaks.

It is worth noting that silver(I,III) oxide has two different crystalline structures, monoclinic and tetragonal, listed in Table 3.5. Most of the diffraction peaks detected from the film in Figure 3.23 and Figure 3.24 were close to those in both crystal structures. However, two aspects of the experimental data support the monoclinic structure. First, the experimental peak at 52.6° is much closer to the one from the monoclinic structure (52.5°) than that from the tetragonal structure

(53.2°). Secondly, the ratios of relative intensities of diffraction peaks of the film are closer to those of the monoclinic structure in the literature. The relative intensities of the peaks at 56.6°, 64.4°, and 65.3° match well with that of monoclinic ones instead of that of the tetragonal, which are close to zero.

In addition, the result of the electron diffraction of a similar film supports the monoclinic structure as well. The estimated lattice parameters from the electron diffraction are close to those of the monoclinic structure, but differ greatly from those of the tetragonal structure (a: 6.883 Å, b: 6.883 Å, and c: 9.122 Å). Therefore, a monoclinic structure is a reasonable assignment for crystalline Ag_2O_2 produced in the film.

However, the absence of many of the major peaks associated with Ag_2O_2 may also be due to the extra peaks not being due to this oxide but to some other unidentified impurity.

3.2.9. Sheet resistance

The sheet resistance of the silver film deposited on the silicon substrate was obtained by a four-point probe with a square array method.[30] Because of possible effects of orientation of the substrate on the sheet resistance of silver film, *I/V* measurements were obtained for films prepared on both Si(111) and Si(100) substrates. Their sheet resistances were calculated from the following equation.[30]

$$R_s = \frac{9.06V_f}{I_f}$$

where R_s is the sheet resistance of the film, V_f is the voltage between two probes (not crossed), I_f is the current between the other two probes (not crossed). *I/V* measurements of the films deposited photochemically on the Si(100) and Si(111) substrates are listed in Table 3.6 and Table 3.7, respectively. It was noted that when the applied voltage was less than 12.0 mV, the readings were not constant. Consequently, the readings of voltage of the films were rejected when the applied voltages were below 12.0 mV.

Table 3.6 *I/V* measurements of the film prepared on a Si(100) substrate from a solid-state film of Ag(I)tfa under light irradiation at 254 nm in the dark (RT: 24 ℃, RH: 22%).

V_f (mv)	I_f (mA)	R_s (Ω/square)
12.84	4.9	24
12.98	6.1	19
14.31	7.1	18
21.68	11.5	17
36.2	15.7	21
	Average(± SD):	20(± 3)

Table 3.7 *I/V* measurements of the film prepared on a Si(111) substrate from a solid-state film of Ag(I)tfa under light irradiation at 254 nm in the dark (RT: 24 ℃, RH: 22%)..

V_f (mv)	I_f (mA)	R_s (Ω/square)
12.39	6.0	18.7
26.39	13.3	18.0
40.48	20.2	18.2
54.86	27.5	18.1
67.48	33.8	18.1
94.92	47.5	18.1
117.63	59.2	18.0
	Average(±SD):	18.0(± 0.3)

The average values of sheet resistance of the silver films deposited on two different substrates are in good agreement. One was 20(± 3) Ω/square and the other was 18.0(± 0.3) Ω/square. It is found that the different orientations of the silicon substrates had a negligible effect on the sheet resistance of the silver film.

Table 3.8 *I/V* measurements of a multiple-processed film on a Si(111) substrate prepared from solid-state films of Ag(I)tfa under light irradiation at 254 nm in the dark (RT: 24 ℃, RH: 22%).

V_f (mv)	I_f (mA)	R_s (Ω/square)
0.12	11.15	0.098
0.181	20.04	0.082
0.284	30.69	0.084
0.335	36.70	0.083
0.392	42.89	0.083
0.465	50.62	0.083
0.545	59.40	0.083
0.611	66.69	0.083
	Average(±SD)	0.085 (± 0.005)

In this research, a silver film was prepared by sequential deposition and UV exposure of solid-state films of Ag(I)tfa in the dark and under ambient conditions (RT: 24 ℃, RH: 22%). The film showed a reduced sheet resistance (Table 3.8). The thickness of this film was 250(±5) nm, measured by an Alpha step 100 profilometer.

The calculated sheet resistance of this multi-processed film was 0.085(± 0.005) Ω/square. It is apparent that the sheet resistance was dramatically reduced by the multiple processing of solid-state films of Ag(I)tfa on top of each other. The reason for the reduced resistivity of the films will be discussed in the following section.

3.3. Discussion

3.3.1. Sheet resistance and the film thickness

It has been found that the single processed film of Ag(I)tfa by photochemical metal organic deposition had a high resistivity about 20 Ω/square and the estimate film thickness was 70 nm. The sheet resistance of the multiple-processed film from Ag(I)tfa of a thickness of 250 nm was 0.085(±0.07)) Ω/square, which corresponds to a resistivity of 2.1 μΩ cm. This value is close to that (1.62 μΩ cm) of bulk silver in the literature.[28] The resistivity of a similar thickness silver film deposited by other techniques such as sputtering was reported to be 2.0 μΩ cm[29]. The measured value of the film prepared from Ag(I)tfa is in good agreement with that despite the additional content of silver(I,III) oxide. This indicates that the multiple-processing of photochemical metal organic deposition can produce a highly conductive silver film from solid-state films of Ag(I)tfa.

The decreased resistivity of the multiple-processed films could be due to the reduction of roughness of the film and/or condensation of the nanoparticles. Luo reported in the literature[29] that the low-temperature deposition of silver film produces rough surfaces with increasing resistivity. An annealing process smoothed the surface roughness and the decreased resistivity was observed. A single film prepared from Ag(I)tfa is composed of irregular silver and silver(I,III) oxide nanoparticles in a loosely packed structure. Rough surfaces of the films were observed from both SEM and TEM images. The decreased resistivity of the

multiple-processed film could be the reduced roughness of the film. The other possible reason could be the condensation of the nanoparticles in the loosely packed structure. As we know, the photochemical reaction ejects the organic species from the film and deposits silver and oxide on the substrate. The escaping of the organic species from the film can produce pores or holes in the film. The deposition of silver and silver oxide nanoparticles under ambient condition might result in aggregation of these nanoparticles. When a second layer of Ag(I)tfa is deposited on top of this loosely packed film, the silver organic complex molecules could fill into these pores, holes, or separations between the nanoparticles. When the organic species are ejected from the film under light irradiation, the produced silver and silver(I,III) oxide may fill in the structure to reduce the numbers and size of these pores, holes, or separations of the pre-deposited film. This condensed structure could provide a better connectivity between nanoparticles so that the conductivity of the film is increased.

It is worth noting that the presence of the insulator silver(I,III) oxide does not affect the resistivity of the multiple-processed film as expected. Based on the Auger analysis result, the high content of metallic silver in the film could be one of the reasons.

It is not possible to develop a mechanism for the photochemical deposition of silver and silver oxide film from solid-state films of Ag(I)tfa at this time for the following reasons. First, the identities of the multiple intermediates revealed by

the FTIR spectra of the solid-state film under light irradiation are unknown. Although the FT-IR spectra revealed certain functional groups of the intermediates, without additional experimental data or information, it is not possible to deduce reasonable structures or formulas for these intermediates. The second difficulty is the lack of a reliable structure of Ag(I)tfa in the amorphous state, which is a vital starting point for the mechanism. Although the FT-IR spectrum of the solid-state film indicated that the silver complex could have a similar connectivity to that of crystal structure, the real structure could be very different from the one proposed in Figure 2.11 in Chapter 2 section 2.3.3.3. With an unverified structure of Ag(I)tfa in the amorphous state and the unknown identifies of multiple intermediates, a proposal for a photochemical mechanism of decomposition of the solid-state film of Ag(I)tfa is premature.

3.4. Photolithographic patterning

3.4.1. Positive and negative photolithographic patterning

Photolithographic patterning of the metal organic films is a major advantage of photochemical metal organic deposition over other conventional thin film deposition technologies.[7-9] The positive and negative photolithographic patterning techniques have been extensively used in microelectronic patterning. Traditional photolithography with a positive photoresist gives a positive pattern, in which the material underlying the exposed areas is to be removed. Vice versa, photolithography with a negative photoresist produces a negative pattern, in

which the material underlying the unexposed areas is to be removed. In the research described in this thesis, negative photolithographic patterns of a silver and silver(I,III) oxide film were achieved from a solid-state film of Ag(I)tfa by photochemical metal organic deposition. The positive photolithographic patterns of silver and silver(I,III) oxide film were achieved by combining the photochemistry and thermal chemistry of the solid-state film of Ag(I)tfa.

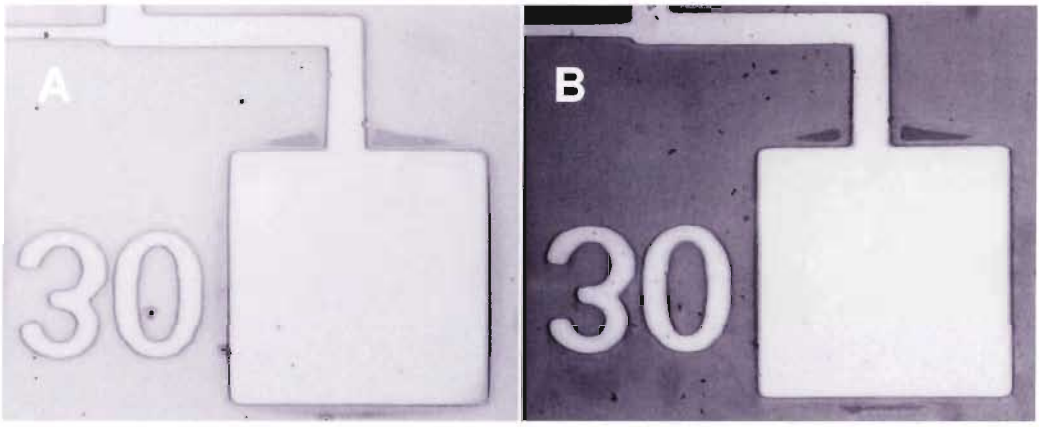

Figure 3.25 Optical microscope bright-field images of the solid-state films of Ag(I)tfa, (A) after UV irradiation through a photomask, (B) after developing. (Each edge of the square in both images is 3.0 mm)

To obtain a negative print, a solid-state film of Ag(I)tfa was deposited onto a silicon substrate by spin-coating, a photomask was then placed on the top of the film by a contact mode, and the film was irradiated by ultraviolet light through the mask. Figure 3.25 (A) shows the resulting pattern. The film was then developed by ethanol using a spin-cleaning technique. The pattern remaining on the exposed area of the film can be seen in Figure 3.25 (B). The colours are artificial and have been converted to black and white for better visualization.

As shown in the left image of Figure 3.25, the square, lines, and numbers were observed clearly on the exposed areas of the film. In the right image, these prints remained on the substrate after developing. The size of the square was 3.0 mm, which can be used as an internal scale. No distortion of the lines, curves, or straight corners was observed, although some shadow patterns around the corner of the square were observed on the substrate. The reason for these shadows could be due to defects on the photomask that transmitted light into the silver complex film. Some black dots deposited on the substrate (image 3) are deemed to be the contaminations from air or organic residues.

To generate a positive pattern, a photoprint of a silver film was first obtained by preparing a solid-state film of Ag(I)tfa on a silicon substrate. This film was exposed to UV light through a contact mask for four minutes. The exposed areas changed from blue to orange (Figure 3.26 (1)). The film was kept in the dark for 150 minutes at room temperature during which the colour of the unexposed area changed from blue to bright silver, a reflection of the deposited silver (Figure 3.26 (2)). The film was then rinsed with cyclohexanol by the spin-cleaning method (Figure 3.26 (3)). However, the reflective areas appear gray, which could be due to the light scattering by the nanoparticles of silver and/or silver oxide.

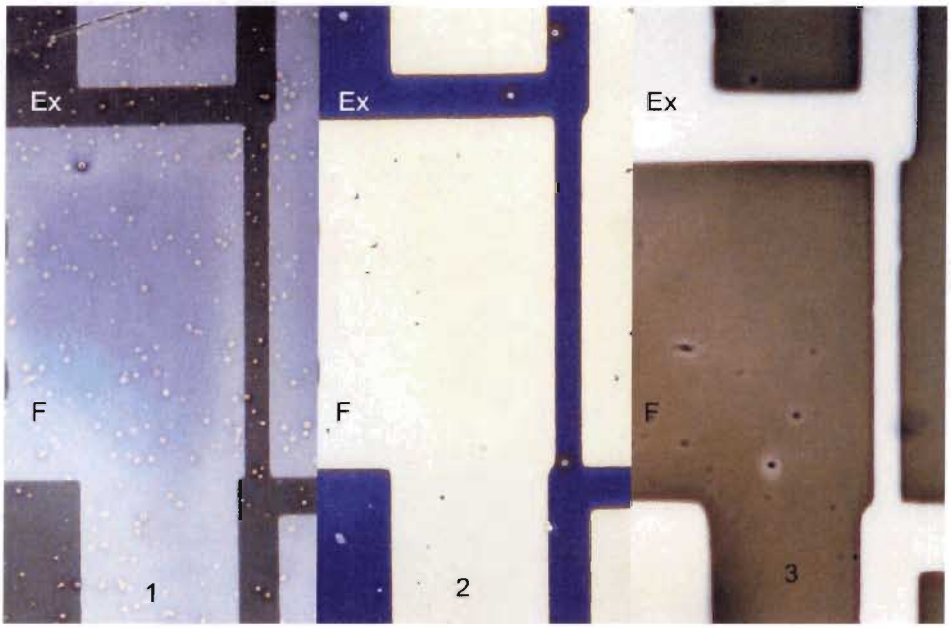

Figure 3.26 Optical microscope images of a solid-state film of Ag(I)tfa, (1) after 4 min UV irradiation through a photomask; (2) after keeping in the dark for 150 minutes; (3) after developing. (Ex: exposed area; F: film. Colors are not real due to digitization by the digital camera.).

In Figure 3.26, three stages of a positive patterning are clearly demonstrated. In the first stage, the exposed film area underwent a photochemical reaction to produce an intermediate in the film. In the second stage, the unexposed area of the film underwent thermal decomposition of Ag(I)tfa to produce silver/silver oxide on the unexposed areas of the film. Due to the different solubility between the inorganic metal/metal oxide and the organic intermediate, a negative print was developed in stage 3. The different thicknesses of lines and the corners were well reproduced on the substrate. The dots in the images could be due to contamination because most of them in image (1) were absent in image (3). Some other dots present in the final image could be the residue of film after developing or air contamination.

3.5. Experimental

3.5.1. Materials and instruments

Materials Aluminum foil was a commercially available product. The carbon-coated copper and nickel grids were purchased from SPI Supplies and Structure Probe, Inc. Ultra-pure grade nitrogen gas (minimum purity of N_2 : 99.998%, O_2 : 8.0 ppm, and H_2O : 5.0 ppm) was purchased from Praxair. Calcium fluoride discs (diameter 25 mm x thickness 20 mm) were purchased from Wilmad Lab-glass Company. (Only the new materials are listed.)

Instrumentation Electronic absorption spectra were recorded on a HP8452A UV-vis spectrometer. The mass spectra were collected on a Hewlett-Packard GCMS-5945A by DIP mode with an electron impact source. Surface analysis was performed on a scanning Auger microscope (SAM), model 595, which was made by Physical Electronics Company. All the Auger spectra were recorded under a vacuum level 10^{-9} torr, and the chamber pressure with argon was close to 10^{-7} torr with a current density 0.14 $\mu A/mm^2$.

Surface morphology of the films was investigated on an FEI dual-beam scanning electron spectroscopy (SEM). High-resolution TEM images were obtained on a Hitachi model 8100 or FEI Tecnai scanning transmission electron microscopy (STEM). X-ray powder diffraction patterns were collected on a Rigaku D/Max-Rapid X-ray powder diffractometer. The light source for film photolysis was a low-pressure mercury lamp, UVG-54 ultraviolet lamp with a 254 nm filter (power: 26.2 mW/cm^2). The light transmitted by the filter is from 240 to 300 nm. The

micron filtration for removing small pollutants in the solutions was performed with a Millex syringe-driven unit with a pore size of 0.22 micron, which was purchased from Millipore Company.

The optical images were taken on a Leitz Laborlux 12 ME-S microscope with a Nikon Coolpix 995 digital camera.

The meters used for the four-point probe measurements include an Ammeter: Keithley 197A, autoranging Microvolt DMM and dc Power supply: Hewlett Packard E3630A. Four acupuncture needles were used for the four probes.

The thickness of the film was measured with an Alpha step 100 profilometer.

3.5.2. Photolysis of a solid-state film of Ag(I)tfa

A solution was prepared in a vial by dissolving (1,1,1-trifluoroacetylacetonato)-silver(I) (0.1245 g) in absolute ethanol (1.2543 g). This solution was filtered by a Millex syringe filter unit with 0.22 micron pores. An optical smooth blue film was prepared by spin coating this solution on a silicon substrate. One FT-IR spectrum of this sample was recorded in the dark (RT: 24 °C and RH: 22 %, same as the others). This film on the substrate was placed on a large metal plate and exposed to UV light at 254 nm for one minute at a fixed distance of 1 cm. The FT-IR spectrum of the exposed sample was recorded. The same process was repeated for accumulated photolysis time of 2, 4, and 8 ... etc., up to 522 minutes.

Another solid-state film of Ag(I)tfa was prepared under identical conditions. This film was monitored by FT-IR spectrometry in the sample chamber without UV irradiation. The FT-IR spectra of the film were recorded at times 0, 2, 4, 8, 16, 32, 64, and 130 minutes.

3.5.3. Preparation of the gaseous sample for mass spectrometry

A solution was prepared by dissolving (1,1,1-trifluoroacetylacetonato)silver(I) (0.1258 g) in absolute ethanol (1.056 g) in a vial. The solution was filtered by a Millipore syringe-driven unit with a pore size of 0.22 micron before use. A film was prepared at 22 ℃ by spin coating this solution onto a silicon substrate, which had an area of 2.0 cm by 0.8 cm. The sample was inserted into a quartz cell wrapped completely with aluminium foil. The cell was pumped for one hour by a roughing pump. After the aluminium foil was removed, the film inside the quartz cell was exposed to a low-pressure mercury lamp (UVG-54) at 254 nm for two hours through the quartz windows. A mass spectrum of the volatiles in the cell was obtained immediately on an HP GCMS-5945A mass spectrometer with an electron impact source. The cell was connected to the gas inlet directly under 50 torr. The injection time of volatile gases was 4.5 minutes.

The parts of the sample cell are shown in Figure 3.27. The square cell part is made of quartz glass, in which the sample was placed. The volatile products are drawn through the glass tube (5 cm) connected to the sample chamber of the mass spectrometer.

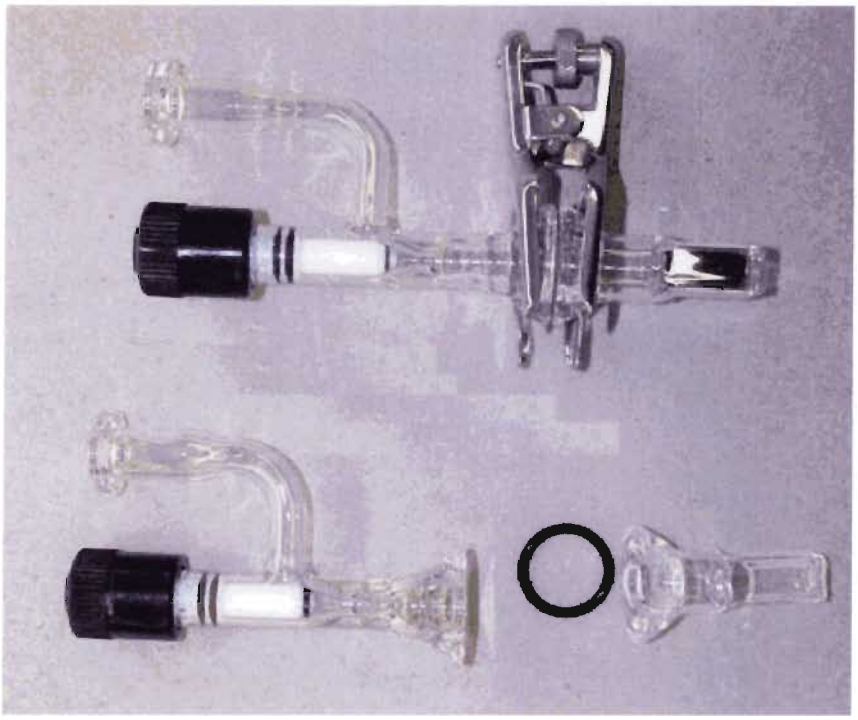

Figure 3.27 The sample cells with quartz window used for mass spectroscopic study. The top image is an assembled sample cell with a chip inside, the bottom image shows the cell parts.

3.5.4. Preparation of the films for X-ray diffraction

A solution was prepared by dissolving (1,1,1-trifluoroacetylacetonato)silver(I) (0.0315 g) in absolute ethanol (0.2892 g) in a vial. This solution was filtered by a Millipore syringe-driven unit with a pore size of 0.22 microns. This solution was used as a stock solution (C) for this part of the experiment.

A film was prepared by spin coating a Si(100) substrate at 5000 rpm from the stock solution (C). This film was exposed in air with a low-pressure mercury lamp (UVG-54) (254 nm) for eighty minutes in the dark (RT: 24 °C and RH: 22%). The process of deposition and photolysis of the precursor film was repeated

twice on the same substrate. An X-ray powder diffraction pattern was collected from this film.

A film was prepared by spin coating a calcium fluoride disc from the same stock solution (C). An FT-IR spectrum of the film was recorded. This film was exposed in air with the same mercury lamp with a filter 254 nm for eighty minutes. An FT-IR spectrum of this film was recorded. No absorption bands were observed in the spectrum of the film.

A converted film on a carbon-coated copper grid was prepared by identical procedure. A TEM image of this film was collected from a Hitachi 8100 scanning TEM system by the postdoctoral fellow in Dr. Kavanagh's group.

3.5.5. Procedure for sheet resistance measurement

Pre-treatment of the silicon substrate A diluted hydrofluoric acid solution was prepared by diluting 1.0 mL 40% HF to 10.0 mL solution in water. All the silicon chips were initially rinsed three times with acetone. Then the chips were immersed in the diluted HF solution for 30 seconds. The chips were rinsed with running distilled water for 30 minutes. The chips were dried by air and heated at 150 °C in air for one hour. All the chips were stored in a desiccator before use.

Sample Preparation A solution was prepared in a vial by dissolving Ag(I)tfa (0.0615 g) in absolute ethanol (0.8000 g). This solution was filtered by a

Millipore syringe-driven unit with a pore size of 0.22 microns. The filtered solution was used as a stock solution for all experiments in this part. All silicon substrates used in this part had an area of 1.0 cm by 1.0 cm.

Three silver films were prepared at 22 °C by spin coating silicon substrates from the same stock solution. The first film was prepared by spin coating a Si(100) substrate at 5000 rpm, followed by exposure to a low-pressure mercury lamp with a 254 nm filter for one hour. The second sample was prepared by spin coating a Si(111) substrate at 5000 rpm, followed by photolysis for one hour. The third sample was prepared similarly to the second sample on a silicon substrate with one edge covered by a 2.0 mm Scotch™ tape. The deposition of the silver film was sequentially repeated five times on the same side of the substrate. The tape was removed from the substrate and the thickness of the film was measured with an Alpha step 100 profilometer from the bare substrate to the deposited film.

A blank film was prepared by spin coating stock solution (D) onto a calcium fluoride disc. A FT-IR spectrum of this film was recorded. This film was exposed with the same UV lamp in air for one hour. A FT-IR spectrum of this film was recorded. The absorption bands disappeared completely. The first two UV irradiated samples were analyzed by scanning electron spectroscopy.

Measurement A four-point probe with a square array method was used to measure the sheet resistance of these thin silver films (Figure 3.28).

The four vertical lines positioned at the corners of a square represent the four probes and the big grey square the silver film. The bottom two probes were

connected with a voltage meter and the top two probes a current meter with a power supply.

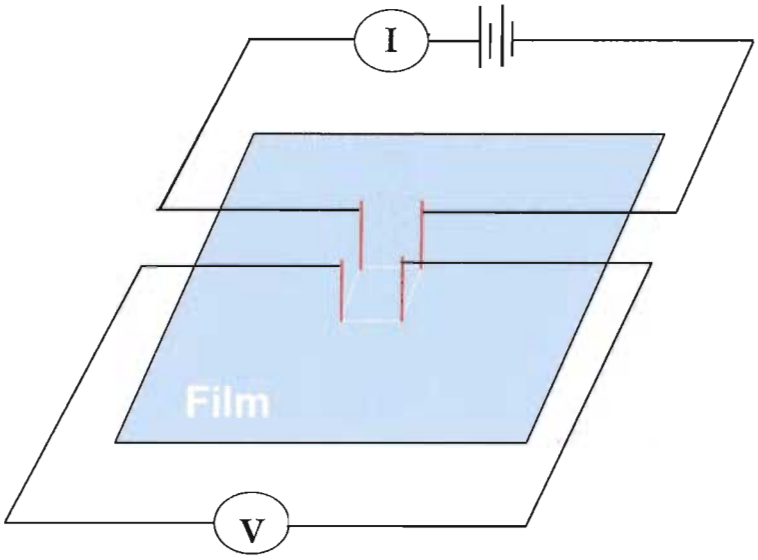

Figure 3.28 Scheme of a four-point probe with a square array used for sheet resistance measurement of thin solid films.

3.5.6. Preparation of the HRTEM sample

A solution was prepared in a vial by dissolving Ag(I)tfa (0.0615 g) in absolute ethanol (0.8000 g). This solution was filtered by a Millipore syringe-driven unit with a pore size of 0.22 microns. The filtered solution was used as a stock solution. A solid-state film was prepared on a carbon-coated copper grid. The film was exposed to UV light until no infrared absorption bands disappeared in the spectrum of an identical amorphous film, which was prepared from the same stock solution on a silicon substrate. HRTEM images were obtained from the sample deposited on the carbon coated grid.

3.5.7. Photolithographic patterning procedures

The stock solution prepared in section 3.5.6 was used to prepare a solid-state film on a silicon substrate (1.0 cm by 1.0 cm). This sample was placed on a large iron plate. A photomask was placed directly on top of the film, parallel to the plate. The film was exposed for 80 minutes under UV light at 254 nm in the dark (RT 24 ℃, RH: 26%). An optical image of this patterned film was taken. Then the film was placed onto a spin coater. Absolute ethanol was applied to the film at a speed of two drops per second for one minute while the sample was spinning at 300 rpm. After spin cleaning, an optical image was recorded of the patterns remaining on the substrate.

Another film on a silicon substrate was prepared from the same stock solution. This solid-state film was exposed to UV light for 4 minutes through a photomask in contact mode. An optical image was recorded. Then this film was wrapped with aluminium foil and keep in a drawer for 80 minutes. An optical image was recorded of the film. The film was developed by the spin cleaning method with absolute ethanol. Optical images of the patterns remaining on the substrate were recorded.

3.6. Reference list

(1) Roucoux, A.; Schulz, J.; Patin, H. *Chemical Reviews* **2002**, *102*, 3757-3778.

(2) Lide, D. R. *CRC Handbook of Chemistry and Physics* 87th Edition, **2006-2007**, 4-33.

(3) Hauder, M.; Gstouttner, J.; Hansch, W.; Schmitt-Landsiedel, D. *Applied Physics Letters* **2001**, *78(6)*, 838 – 841.

(4) Alford, T.L.; Adams, D.; Laursen, T.; Ullrich, B. M. *Applied Physics Letters* **1996**, *68(23)*, 3251- 3255.

(5) Wang, Y.; Alford, T.L. *Journal of Applied Physics* **1999**, *86*, 5407-5410.

(6) Luo, E. Z.; Heun, S.; Kennedy, M. J.; and Henzler, M. *Physical Review B* **1994**, *49*, 4858-4865.

(7) Hill, R. H. *Photonics Science News* **1996,** *2,* 12-14.

(8) Hill, R. H.; Puddephatt, R. J. *Organometallics* **1983,** *2,* 1472-1474.

(9) Rao, C. N. R. *Ultra-violet and visible spectroscopy and chemical applications* London Butterworths **1961**

(10) Bravo-Vasquez, J. P.; Hill, R. H. *Polyhedron* **2000,** *19,* 343-349.

(11) Belford, R. L.; Martell, A. E.; Calvin, M. *Journal of Inorganic and Nuclear Chemistry* **1956,** *2,* 11-31.

(12) Iglesias, E. *Langmuir* **2000,** *16,* 8438 -8446.

(13) Buono-Core, G. E.; Bronislaw, M. *Journal of Photochemistry and Photobiology, A: Chemistry* **1990,** *52*, 1-25.

(14) Fukuda, E. K.; Campana, J. E. *International Journal of Mass Spectrometry and Ion Processes* **1985,** *65*, 321-328.

(15) Retrieved on December 2006 from http://*www.aist.go.jp/RIODB/SDBS,* SDBS #3965.

(16) Reichert C.; Bancroft. G. M.; Westmore, J. B. *Canadian Journal of Chemistry* **1970,** *48,* 1362-1370.

(17) Bancroft G. M.; Reichert C.; Westmore J. B.; Gesser H. D. *Inorganic Chemistry* **1968,** *8,* 474-480.

(18) Rubesch, M.; Morris, M. L.; Koob, R. D. *Journal of Organic Mass Spectrometry* **1971,** *5,* 237-248.

(19) Wagner, C.D.; Riggs, W. M.; Moulder, J. F. *Handbook of Auger electron spectroscopy*, **1978**, Perkin-Elmer Corporation, Physical Electronics Division.

(20) Okajima, Y. *Journal of Applied Physics* **1979,** *51,* 715-717.

(21) Toebbens, D. M. S.; Knorr, K.; Mayer, H. M.; Lampert, G. *Materials Science Forum* **2001,** *378,* 288-293.

(22) Straumanis, M.E.; Riad, S.M. *Transactions of the Metallurgical Society of Aime* **1965,** 233.

(23) Marciniak, B. K., J. and Paszyc, S. *Bulletin of the Polish Academy of Sciences Chemistry* **1979,** 27, 843-845.

(24) Fragala, M. E.; Malandrino, G.; Puglisi, O.; Benelli, C. *Chemistry of Materials* **2000**, *12*, 290-293

(25) Yvon, K. B.; Tissot, P.; Fischer, P. *Journal of Solid State Chemistry* **1986,** *65,* 225-230.

(26) Bullen, H.A.; Garrett, S. J. *Chemistry of Materials* **2002,** *14,* 243-248.

(27) Warren, B.E., *X-ray Diffraction* Dover Publications, Inc., New York, **1990**.

(28) Srinivasa Rao, S.; Anantharaman, T.R. *Current Science* **1963**, *32*, 262-263.

(29) Brese, N.E.; O'Keeffe, M.; Ramakrishna, B.L.; Von Dreele, R.B *Journal of Solid State Chemistry* **1990,** *89,* 184-190.

(30) Seshan, K.; Park Ridge, N. J. *Handbook of Thin-film Deposition Processes and Techniques: principles, methods, equipment, and applications* Noyes Publications **2002,** 2nd Edition.

(31) Lide, D. R. *CRC Handbook of Chemistry and Physics,* 87th Edition, **2006-2007**, 12-40.

(32) Hauder, M.; Gstottner, J.; Hansch, W.; Schmitt-Landsiedel, D. *Applied Physics Letters* **2001**, *78*, 838-840.

(33) Luo, E. Z.; Heun, S.; Kennedy, M.; Wollschlaeger, J.; and Henzler, M. *Physical Review B: Condensed Matter and Materials Physics* **1994,** *49,* 4858-4865.

(34) Lide, D. R. C*RC Handbook of Chemistry and Physics,* 87th Edition, **2006-2007,** 5-4.

CHAPTER 4:
KINETICS AND MECHANISM OF SOLID-STATE DECOMPOSITION OF A FILM OF (1,1,1-TRIFLUOROACETYLACETONATO)SILVER(I)

4.1. Introduction

The kinetic and mechanistic study of decomposition of a solid-state film on the surface of substrates by spectroscopic method is of scientific importance because the spectroscopic method can determine concentrations of the reactants with high accuracy and reliability. Although heterogeneous reactions between gases or liquids with solid catalysts have been well reported in the literature,[1] little research has been reported on the kinetic study of the reactions of solid-state films of metal organic complexes occurring on substrate surfaces. In particular, spectroscopic investigation of the kinetics and mechanism of a silver organic complex film has not been reported in the literature. Although zero-order reaction was reported in the solid-state decomposition of some metal-containing polymers,[2,3] a mixed-order reaction of a solid-state film of a metal organic complex has not been reported. On the other hand, the deposition of silver and silver oxide films directly from metal organic complexes has been studied intensively due to their unusual properties.[4-8] However, deposition of a silver and silver(II,III) oxide composite film under ambient conditions from silver organic complex has not been reported.

In this chapter of the thesis, thermal decomposition of a solid-state film of (1,1,1-trifluoroacetylacetonato)silver(I) is investigated. The thermal products are characterized by mass spectrometry, AES, and XRD. The kinetics between the film and water and its reaction mechanism is explored in detail.

4.2. Investigations

4.2.1. Characterization of thermal products

In order to understand the thermal decomposition of a solid-state film of Ag(I)tfa, identification of the thermal products is critical. The volatile products produced from the film were analyzed by mass spectrometry, and the residual products on the substrate were analyzed by AES and XRD.

4.2.1.1. Identification of volatile products

The volatile gases produced from a solid-state film of Ag(I)tfa on a substrate in the dark were analyzed by mass spectrometry. The collected mass spectrum is shown in Figure 4.1. The inset on the right corner is a plot from 60.0 to 170.0 with y values magnified fifty times.

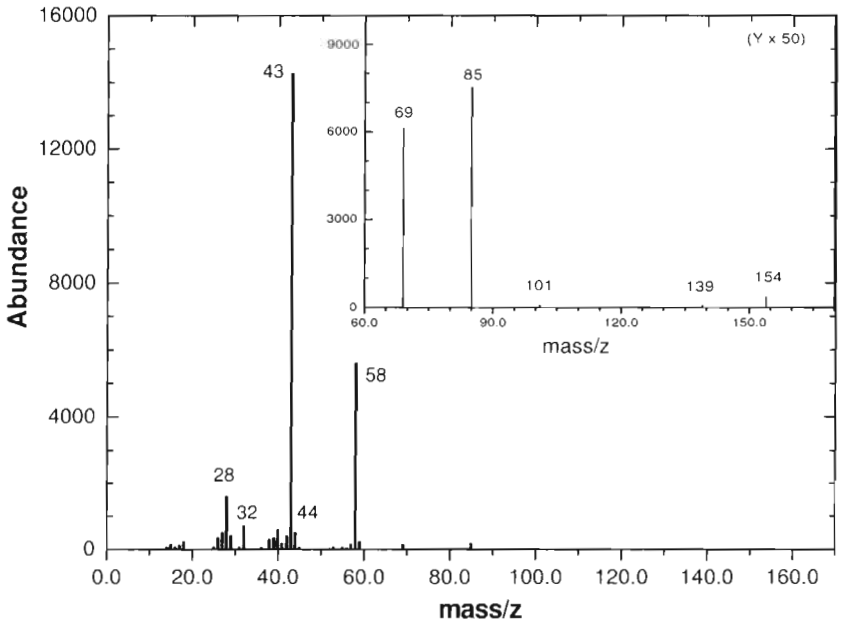

Figure 4.1 Mass spectrum of the volatile gases produced from a solid-state film of Ag(I)tfa in the dark.

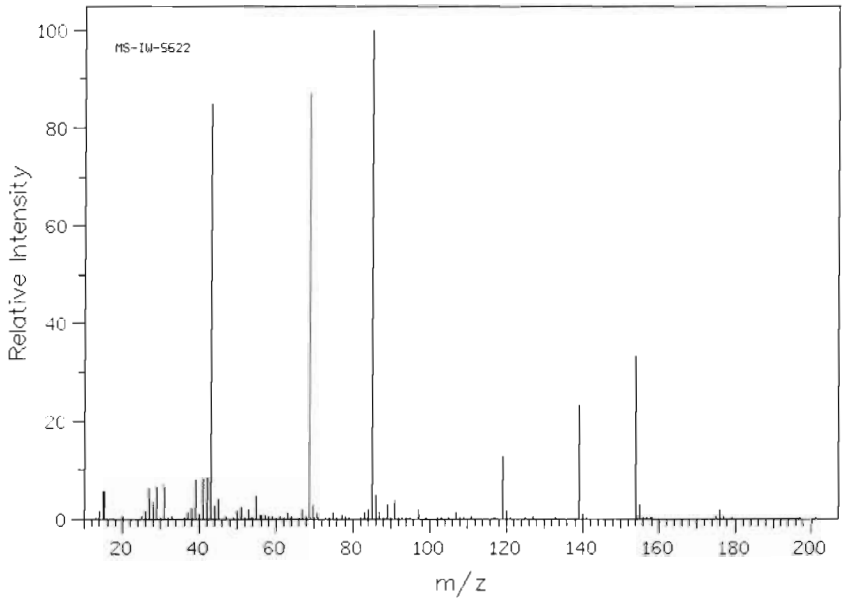

Figure 4.2 Mass spectrum of 1,1,1-trifluoroacetylacetone from the literature,[9] reproduced by permission.

The most abundant peak was found at mass/z 43.0, which is the most common species in the mass spectra of other metal β-diketonate complexes. The most

likely structure is $[CH_3CO]^+$. The second most abundant species was found at mass/z 58.0, which could be due to acetone or the other fragments. The highest mass/z species was found to be 154, which could be the molecular ion of the ligand (Htfa). The other species found at mass/z 139, 85, 69, and 43 are found in the mass spectrum of Htfa in the literature[9] (Figure 4.2). Therefore, Htfa is believed to be one of the thermal products.

4.2.1.2. The composition of the deposited film

A solid-state film of Ag(I)tfa was kept in the dark under ambient condition until the FT-IR absorption spectrum of a reference film of Ag(I)tfa appeared as a flat line. The chemical composition of the deposited film was analyzed by Auger electron spectroscopy. The spectrum of the film after surface cleaning for 30 seconds by argon sputtering is shown in Figure 4.3.

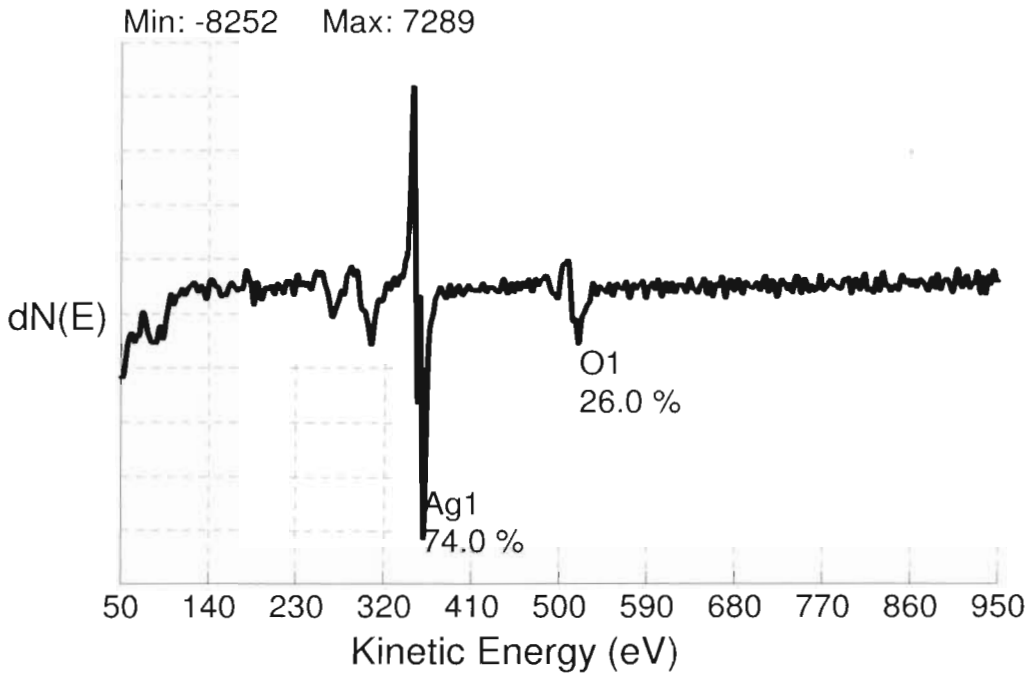

Figure 4.3 Auger electron spectrum of a film converted from Ag(I)tfa in the dark at 24 ℃.

Figure 4.3 shows that the deposited film comprised of 74(±6) mol% silver and 26(±7) mol% oxygen. As discussed in a previous chapter, the signal at 91 eV is believed to be a contribution from the silicon substrate. The ratio between the atomic concentrations of silver and oxygen is greater than that of the known silver oxides. This suggests that the deposited film includes metallic silver as well as silver oxide.

4.2.1.3. XRD of a thermally decomposed film of Ag(I)tfa

. An XRD pattern of the deposited film on a silicon substrate was recorded. An XRD pattern of a bare identical silicon substrate was recorded as background.

The pattern shown in Figure 4.4 is a result of the sample data subtracted by the background.

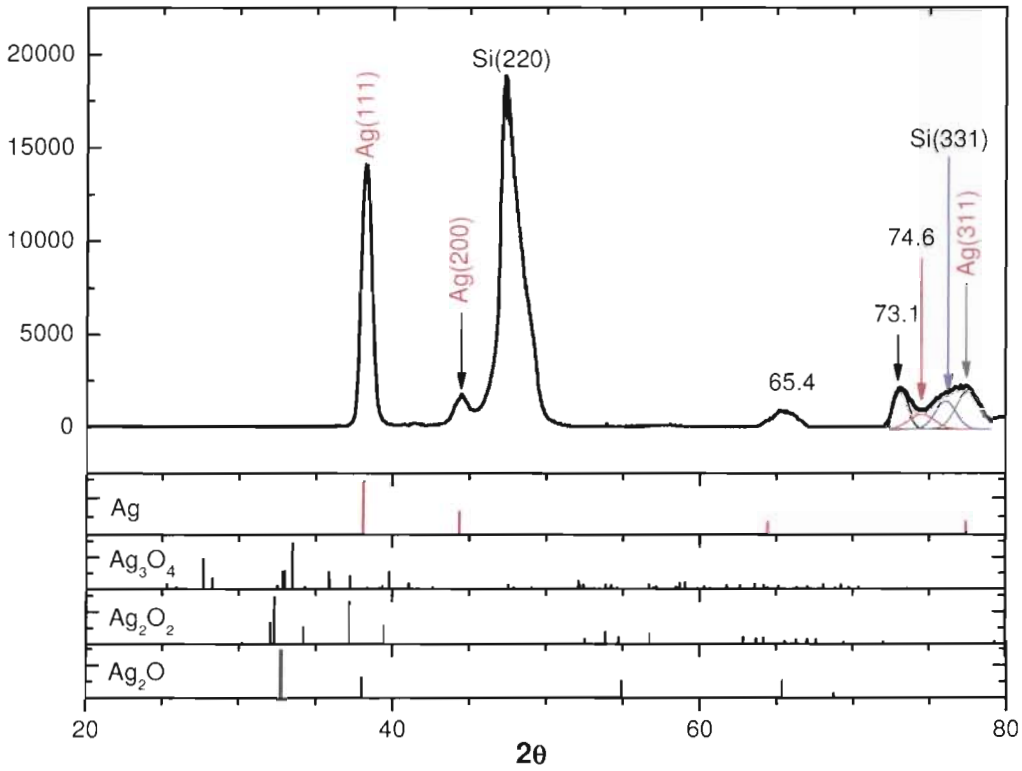

Figure 4.4 An XRD pattern of a thermal decomposed film of Ag(I)tfa in the dark under ambient conditions (RT: 24 ℃ and RH 26%).

The peaks in Figure 4.4 clearly indicate that the thermally deposited film is composed of more than one type of crystalline material. A group of broad peaks observed in the range from 72° to 80° were deconvoluted to four best fit peaks by using Gaussian functions centred at 73.1°, 74.6°, 76.4°, and 77.5°. The peaks observed at 38.2°, 44.4°, and 77.5° are believed to be attributed to metallic silver. An intense and broad peak at 47.3° is attributed to the silicon substrate. The peak at 76.4° should have a contribution of Si(331) as well.

The observed peaks appear to match well with those of Ag_3O_4 as listed in Table 4.1. However, due to the absence of many major intense peaks, these peaks may not be due to this oxide but to some other unidentified impurity.

Table 4.1 The diffraction peaks detected from the film compared with selected peak values of Ag_3O_4, Ag_2O_2, Ag_2O, and silicon from literature.

The film	Peaks (°)		**38.2**	**44.4**	**65.4**	**73.1**	**74.6**	**76.1**	**77.5**
	I[f]		1000	124	60	150	60	135	160
Ag	Peaks (°)		38.1	44.3	-	-		-	77.4
	I		1000	468	-	-		-	272
Ag_3O_4	Peaks (°)	33.5	**38.4**	**44.4**	**65.4**	**73.2**	**74.8**	**76.1**	**77.7**
	I	1000	31	18	3	14	1	11	0
Ag_2O_2	Peaks (°)	32.3	37.2	43.2	65.6	73	74.6	76.1	77.7
	I	1000	908	1	**57**	1	0	0	0
Ag_2O	Peaks (°)	32.8	38.0	-	65.4	-	75.1	-	-
	I	1000	425	-	366	-	1	-	-
Si	Peaks (°)	28.4	-	47.3		-			76.4
	I	1000	-	600		-			130

.

4.2.2. Surface structure of the converted film

The surface structure of the film containing silver is of interest. The surface morphology of a thermally converted film of Ag(I)tfa was investigated by SEM. The SEM image of the film is shown in Figure 4.5.

[f] Relative intensity of the diffraction peaks.

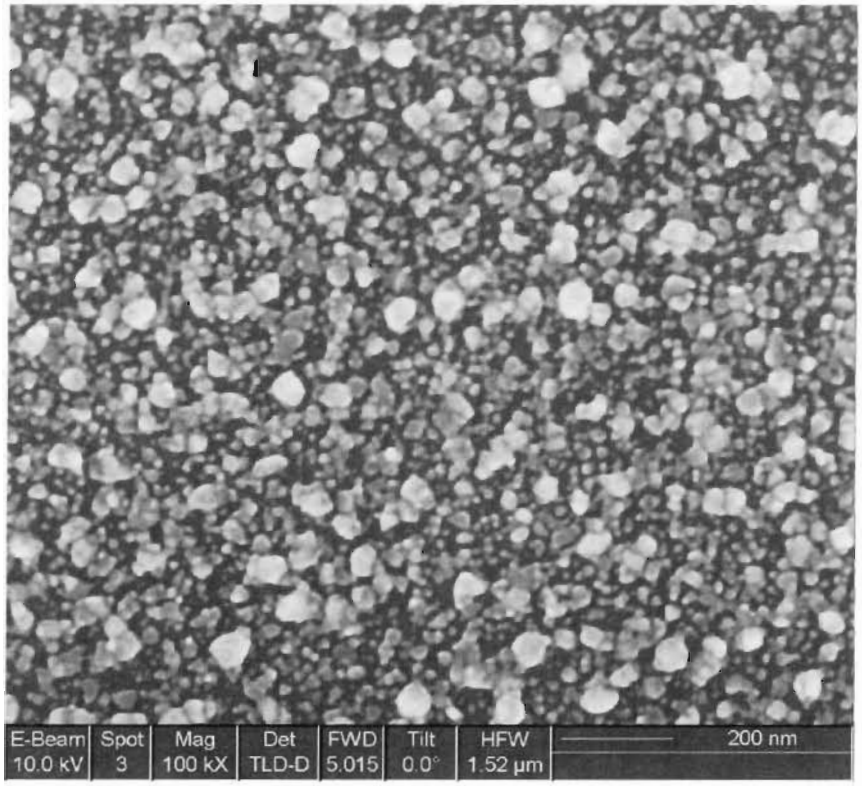

Figure 4.5 SEM image of a film deposited thermally from a solid-state film of Ag(I)tfa kept in the dark (RT: 22 °C, RH: 26%).

The SEM image shows that the film is composed of many irregular shaped nanoparticles with a size range from 12 to 85 nm. The separation between the nanoparticles are clearly observed as well as stacking on top of each other. These observations suggest that the film is loosely packed. The separations or pores could have been formed during the volatilization of the organic species from the film.

4.2.3. The involvement of water

It was found that the reaction rates of the solid-state films of (1,1,1-trifluoroacetylacetonato)silver(I) changed with the relative humidity of the reaction chamber in air. This change could be caused by water, or by oxygen in air, or both. To investigate this, the changes of the films under different relative humidity levels were monitored by FT-IR spectroscopy. First, the water involvement in the reaction was examined. Moistures of nitrogen and water vapour were used to control the relative humidity levels so that the possible oxygen effect could be minimized. Eight films were prepared under identical conditions, and each film was investigated separately under different relative humidity levels. Each individual film was kept in the sample chamber of the FT-IR spectrometer in the dark, in which the sample chamber was purged by nitrogen and maintained at a constant relative humidity level of 13 %, 15 %, 17 %, 18 %, 20 %, 22 %, 24 %, or 30 %. The FT-IR spectra of each film were collected at fixed time intervals. All the spectra decreasing in intensity with time for each film were overlaid and are shown in the following figures.

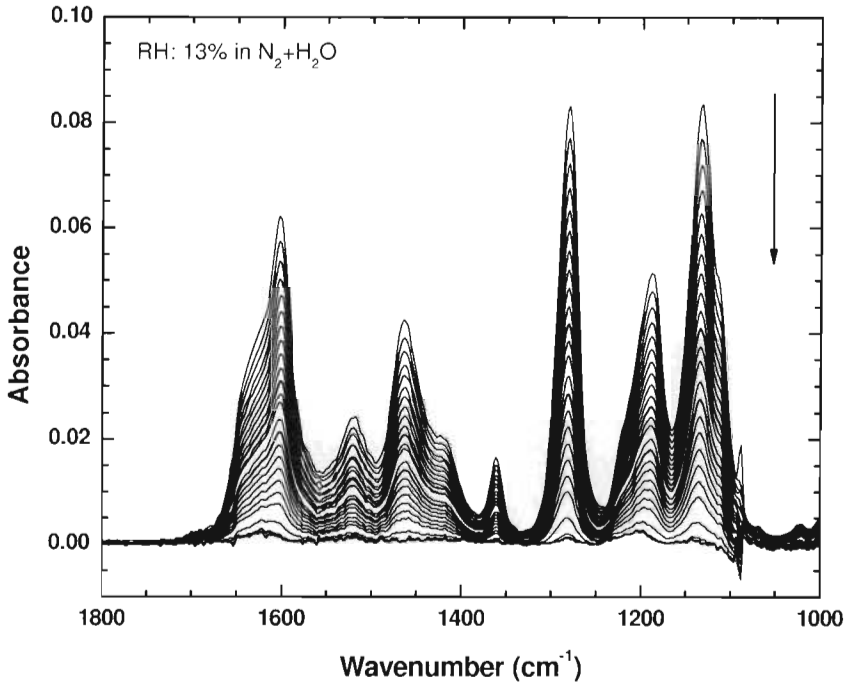

Figure 4.6 FT-IR spectra of a solid-state film of Ag(I)tfa recorded in the dark under relative humidity (RH) 13 % every 10 minutes from 0 to 300 minutes.

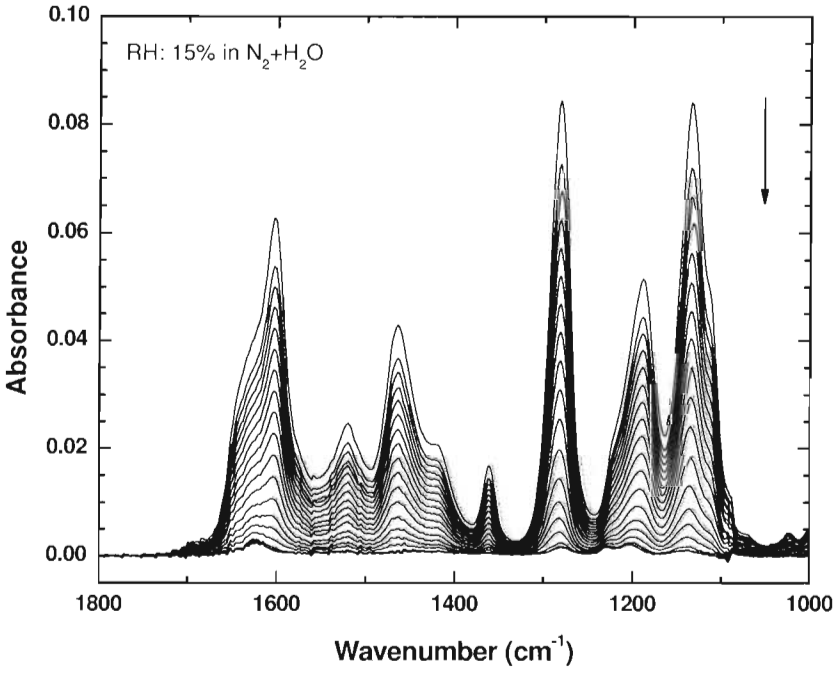

Figure 4.7 FT-IR spectra of a solid-state film of Ag(I)tfa recorded in the dark under relative humidity 15 % every 4 minutes from 0 to 72 minutes.

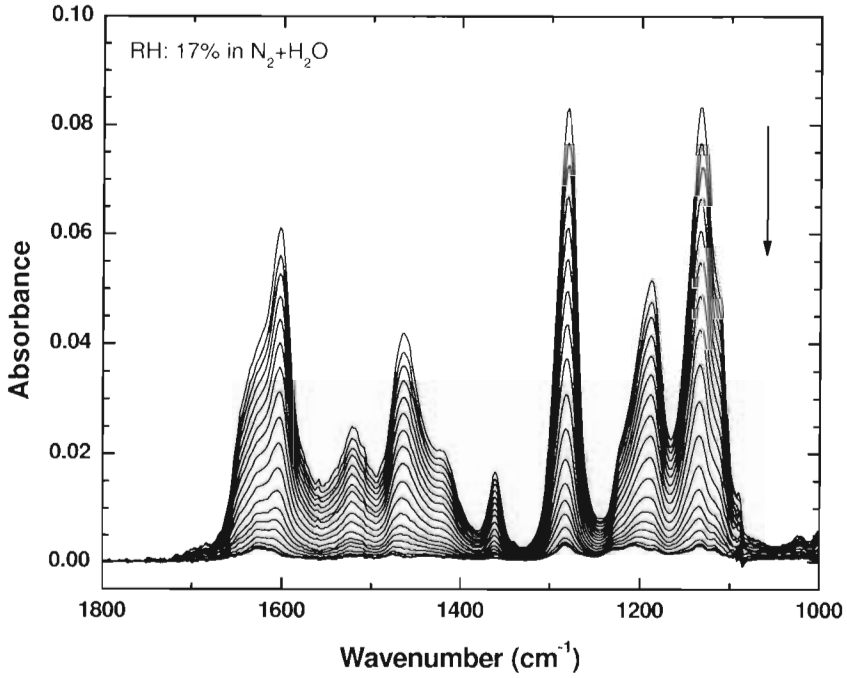

Figure 4.8 FT-IR spectra of a solid-state film of Ag(I)tfa recorded in the dark under relative humidity 17 % every 2 minutes from 0 to 40 minutes.

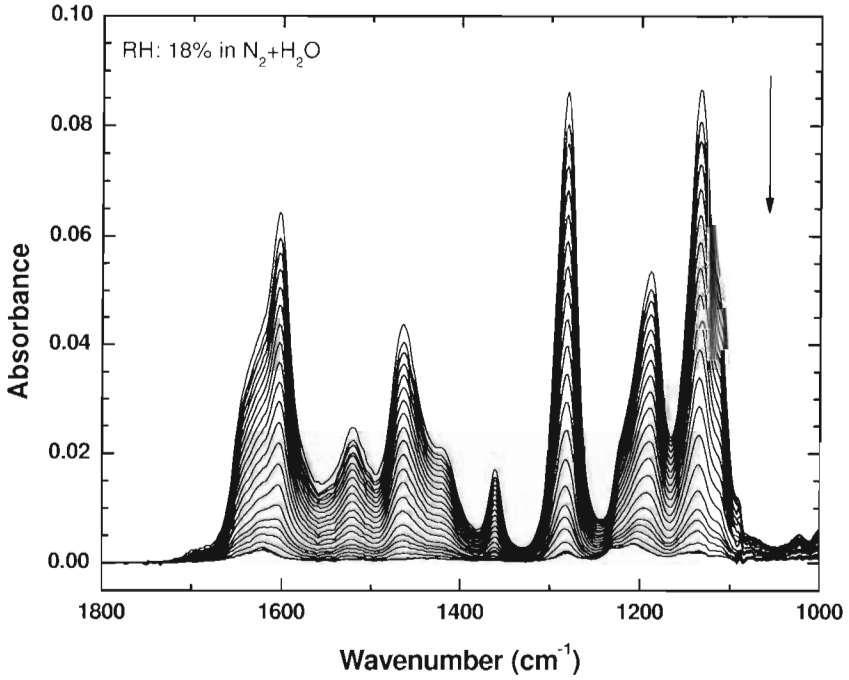

Figure 4.9 FT-IR spectra of a solid-state film of Ag(I)tfa recorded in the dark under relative humidity 18 % every 2 minutes from 0 to 38 minutes.

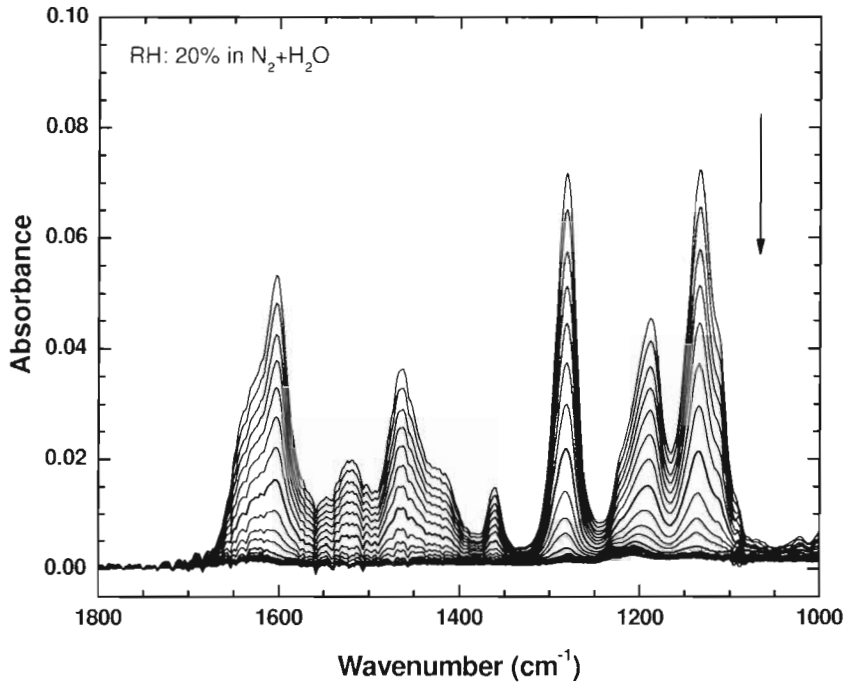

Figure 4.10 FT-IR spectra of a solid-state film of Ag(I)tfa recorded in the dark under relative humidity 20 % every 2 minutes from 0 to 28 minutes.

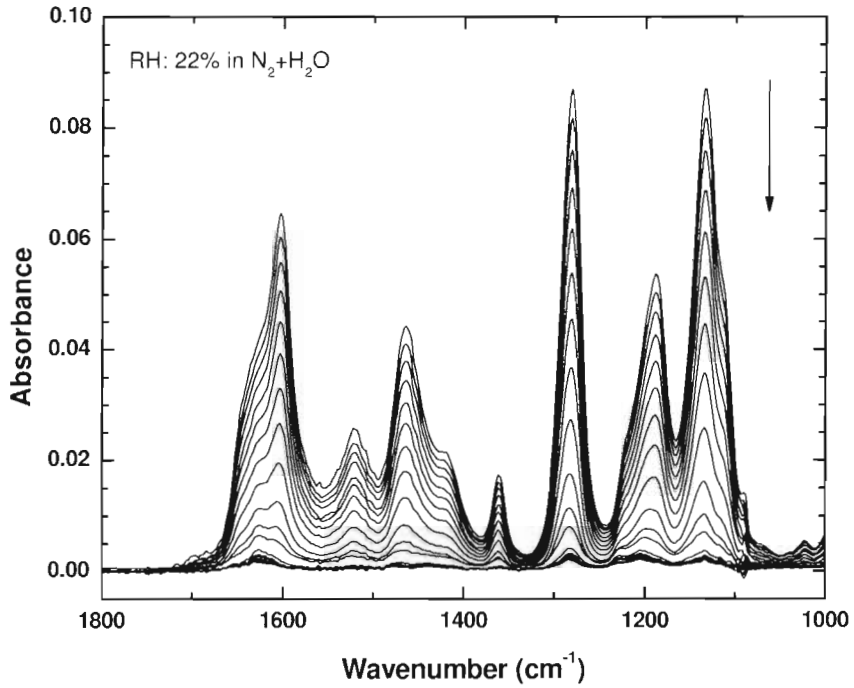

Figure 4.11 FT-IR spectra of a solid-state film of Ag(I)tfa recorded in the dark under relative humidity 22 % every 2 minutes from 0 to 36 minutes.

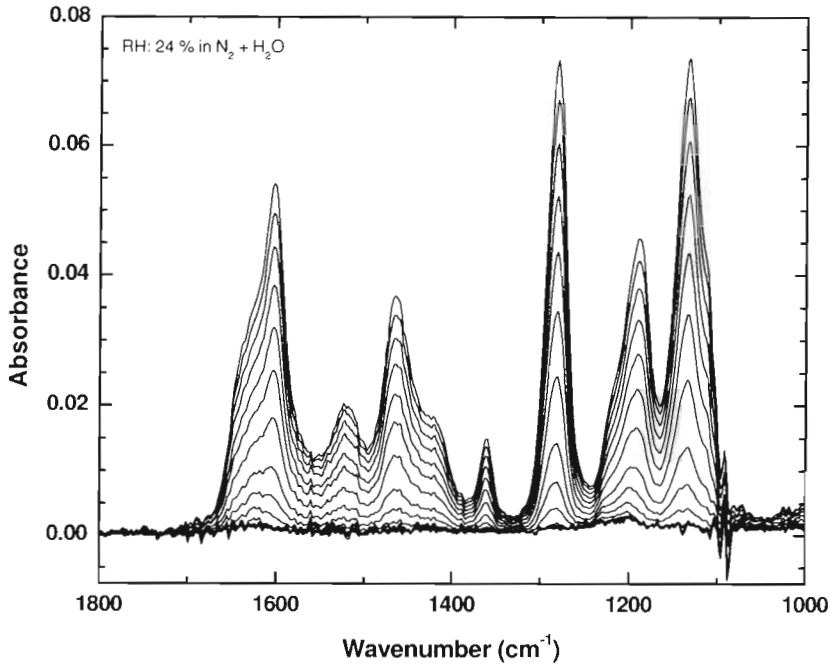

Figure 4.12 FT-IR spectra of a solid-state film of Ag(I)tfa recorded in the dark under relative humidity 24 % every 2 minutes from 0 to 26 minutes.

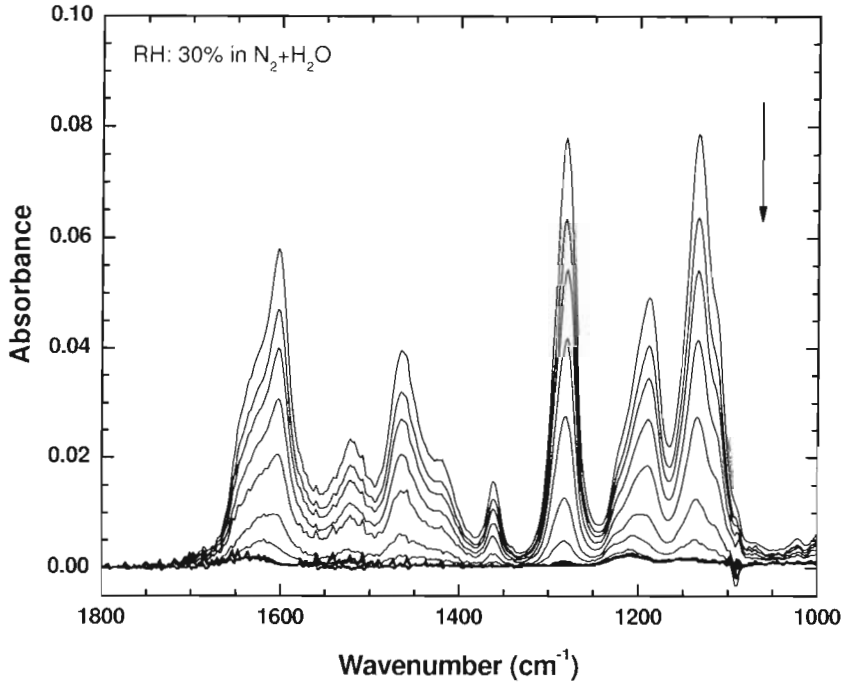

Figure 4.13 FT-IR spectra of a solid-state film of Ag(I)tfa recorded in the dark under relative humidity 30 % every 2 minutes from 0 to 20 minutes.

Two important features of the reaction of the films are observed. First, in each figure, the absorbance of each film decreased with time and no new absorption bands were observed. Some small shifts of the absorption bands were noticed at the later stage of decomposition. These shifts could be due to the interaction between the metal nanoparticles and the metal organic complex, which can affect the bond strength or molecular structures. Secondly, the films decomposed faster with higher relative humidity levels. Table 4.2 lists the time for the initial absorbance of the band at 1283 cm^{-1} to decay 98 % for each film kept under different relative humidity levels.

Table 4.2 The relationship between the times for the absorption band at 1283 cm^{-1} to decay 98% in intensity and the relative humidity levels.

Relative Humidity	**15 %**	**17 %**	**18 %**	**20 %**	**22 %**	**24 %**	**30 %**
Reaction time (minutes)	73	60	41	32	32	21	14

It is apparent that the decay time of the film decreased while the relative humidity level in the environment increased. This result suggests that water was involved in the decomposition of the silver complex films. The relationship between the reaction rate and relative humidity will be discussed in section 4.3.1.

4.2.4. The effect of oxygen

Oxygen could be involved in the decomposition of the solid-state film of Ag(I)tfa if the film was kept in air. To investigate this, the changes of the films kept in air were monitored by FT-IR spectroscopy. Two films of Ag(I)tfa prepared under identical conditions were examined. The spectra of the films kept under relative humidity level 20 % and 24 % were recorded in the same sample chamber at 30 ℃ and are shown in Figure 4.14 and Figure 4.15.

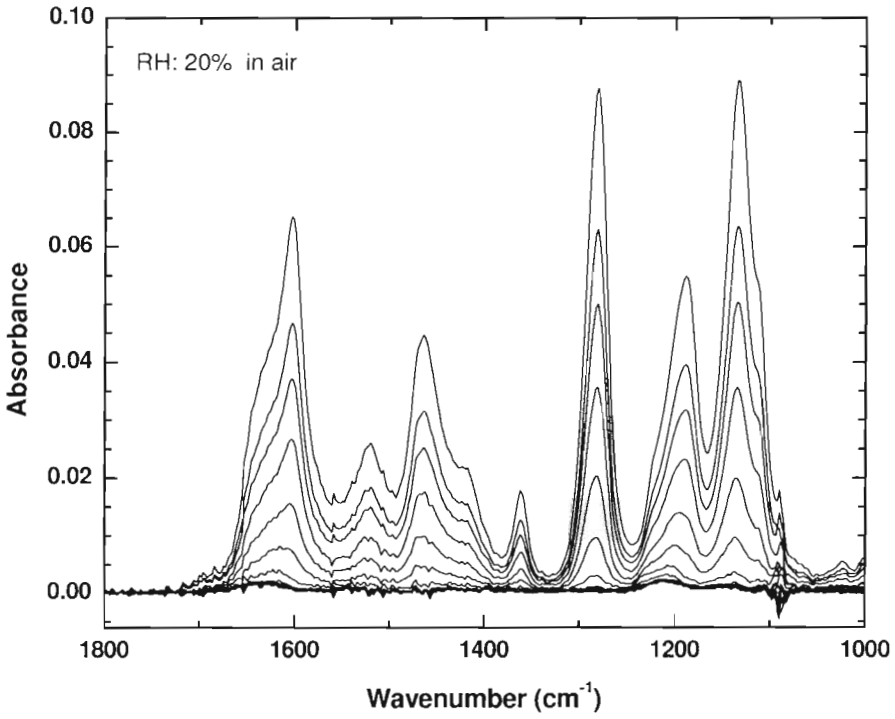

Figure 4.14 FT-IR spectra of a solid-state film of Ag(I)tfa recorded under relative humidity 20 % in air every 4 minutes from 0 to 32 minutes.

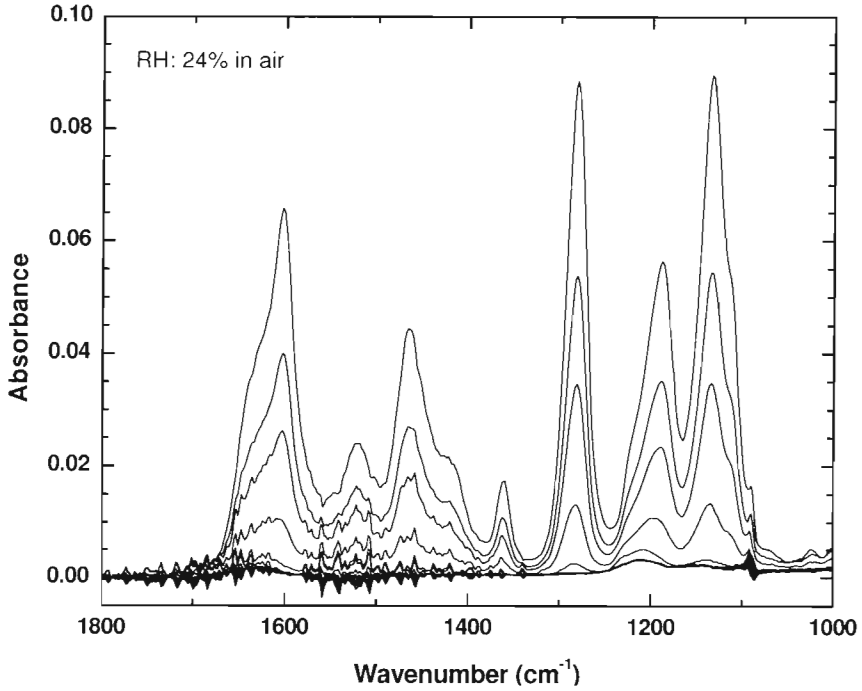

Figure 4.15 FT-IR spectra of a solid-state film of Ag(I)tfa recorded under relative humidity 24 % in air every 2 minutes from 0 to 36 minutes.

The spectra of two films kept under identical relative humidity levels in nitrogen are shown in Figure 4.10 and Figure 4.12. The difference between the films kept under different gases will be discussed in section 4.3.2.

4.2.5. The molar extinction coefficient

According to the Beer-Lambert law,

$$A = \log \frac{I_0}{I} = \varepsilon C l \qquad [4.1]$$

where A is the absorbance; I_0 the intensity of the incident light, I the intensity of the transmitted light, ε the molar extinction coefficient (molar absorptivity); C the concentration of the substance in mol/L; and l the thickness of the sample in cm.

In this work, by assuming that the film is uniform, the concentration of the solid-state film of Ag(I)tfa is given by the moles of the Ag(I)tfa divided by the volume. Therefore, the absorbance equation changes to the following,

$$A = \varepsilon \frac{n}{V_{\text{film}}} l = \varepsilon \frac{n}{(\pi r^2 l)_{\text{(liters)}}} l_{\text{(cm)}} \qquad [4.2]$$

where n is the number of moles of Ag(I)tfa in the film, r the radii of the circle area of Ag(I)tfa film. In equation [4.2] , the absorbance of the film is linearly proportional to the moles of Ag(I)tfa since the area is a fixed value. In order to verify the validity of the Beer-Lambert law for the films of Ag(I)tfa, different thicknesses of films of Ag(I)tfa were prepared individually in a circular well (diameter 1.44 cm and depth 0.05 cm) on a substrate of single-crystal sodium chloride from a stock solution. The FT-IR spectrum of each film was recorded and are shown in Figure 4.16.

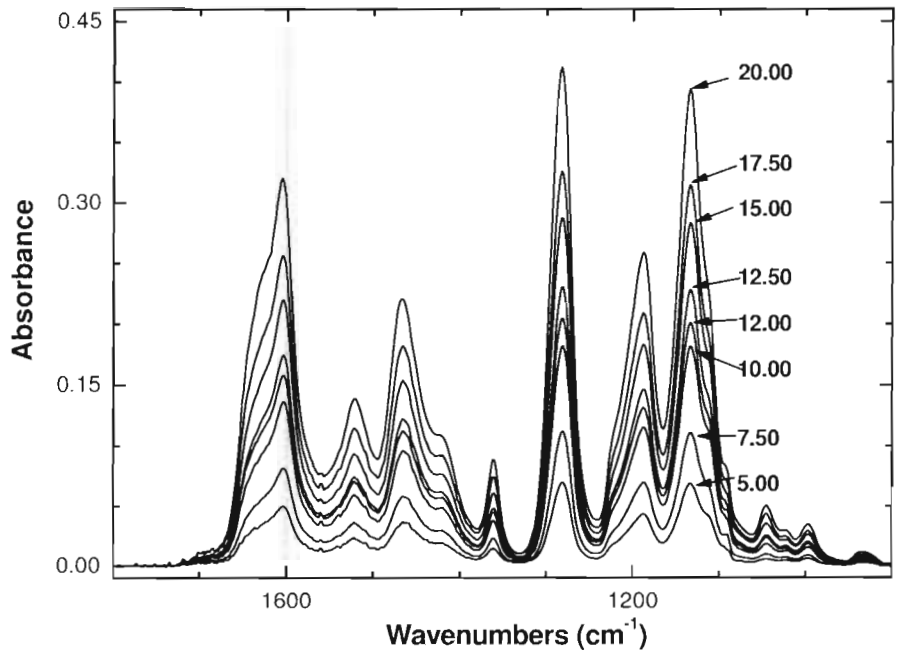

Figure 4.16 FT-IR spectra of different thicknesses of films prepared from Ag(I)tfa solution (RT: 24 ℃ and RH: 26 %). The numbers are the used volumes of the stock solution in microliters.

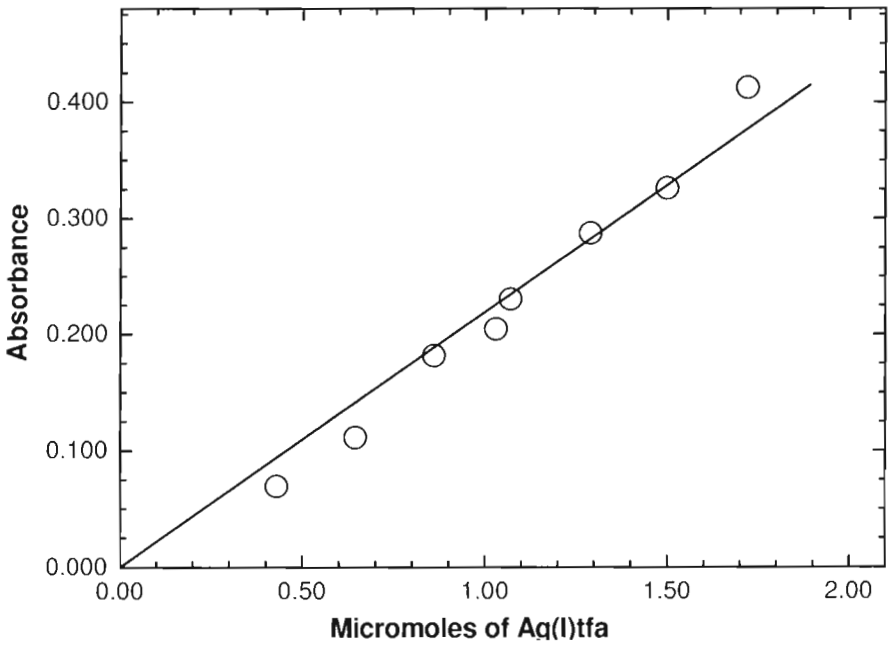

Figure 4.17 A plot of the absorbance at 1281 cm^{-1} versus the moles of Ag(I)tfa.

Figure 4.16 shows that the absorbance of the films increased with volume of the solution of Ag(I)tfa used. The increased volumes of the solution meant that larger amounts of Ag(I)tfa were deposited in the well. A linear relationship between the absorbance and the amount of Ag(I)tfa was obtained from a plot of the absorbance at 1281 cm^{-1} versus the moles of Ag(I)tfa (Figure 4.17). The linear fitting equation is the following.

$$A = 0.219(\pm 0.007) \times 10^6 n \qquad [4.3]$$

According to the equation [4.2], the slope of the linear line is $\frac{\varepsilon l}{v}$, then

$$\varepsilon = \frac{A\pi(r^2 l)_{(\text{in liters})}}{n l_{(\text{in cm})}} n = 10 \times slope \times \pi r^2_{(\text{in meters})}$$
$$= 0.219 \times 10^6 \times \pi \times (0.0144/2)^2 \times 10 \approx 357$$

The molar extinction coefficient is 357(±11) $(mol/L\ cm)^{-1}$.

The linear relationship indicates that the Beer-Lambert law is valid in the measured concentration range. As the experimental spectroscopic data were acquired within this range, the Beer-Lambert is valid to be used to describe the relationship between the absorbance and the concentration of Ag(I)tfa in the film.

4.3. Discussion

4.3.1. Reaction orders of thermal decomposition of the film of Ag(I)tfa

Based on the rate law, if a plot of the concentration of one of reactants or products versus time is a linear line, the reaction has zero-order kinetics. If the plot is an exponential decay curve, the reaction is a first-order reaction. By analyzing such plots one can deduce the reaction order of the decomposition of the film of Ag(I)tfa. It is very difficult to measure the concentration of products or Ag(I)tfa in the film. However, as described previously, the absorbance is linearly proportional to the concentration of the film of Ag(I)tfa. Therefore, a plot of the absorbance versus time can be used to investigate the possible reaction order(s) of the film decomposition. The plot of the absorbance at 1281 cm^{-1} versus time for each film based on the spectra shown in from Figure 4.6 to Figure 4.13 are shown in Figure 4.18 and Figure 4.19. In these figures, the symbols represent experimental values, while the solid lines, the dotted lines, and the dashed lines represent linear fits, first order decay over the entire time range, and first order decay over a selected time range.

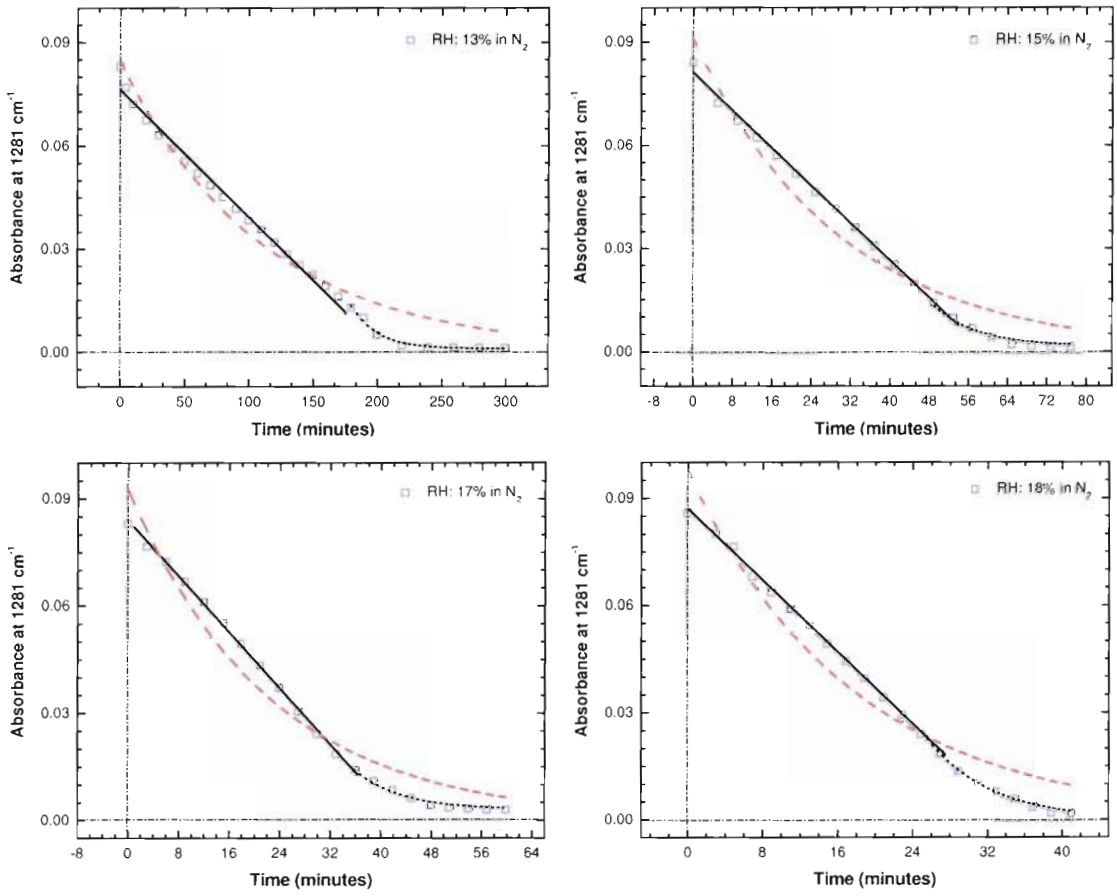

Figure 4.18 Absorbance at 1281 cm^{-1} as a function of time plotted for the films of Ag(I)tfa kept under different relative humidity levels (a) 13 %, (b) 15 %, (c) 17 %, and (d) 18 %. The open squares are the experimental data; the blue solid lines are the best linear fit; the dotted lines are first-order decay curves; the red dashed lines are the first-order curved for the whole datasets for each film.

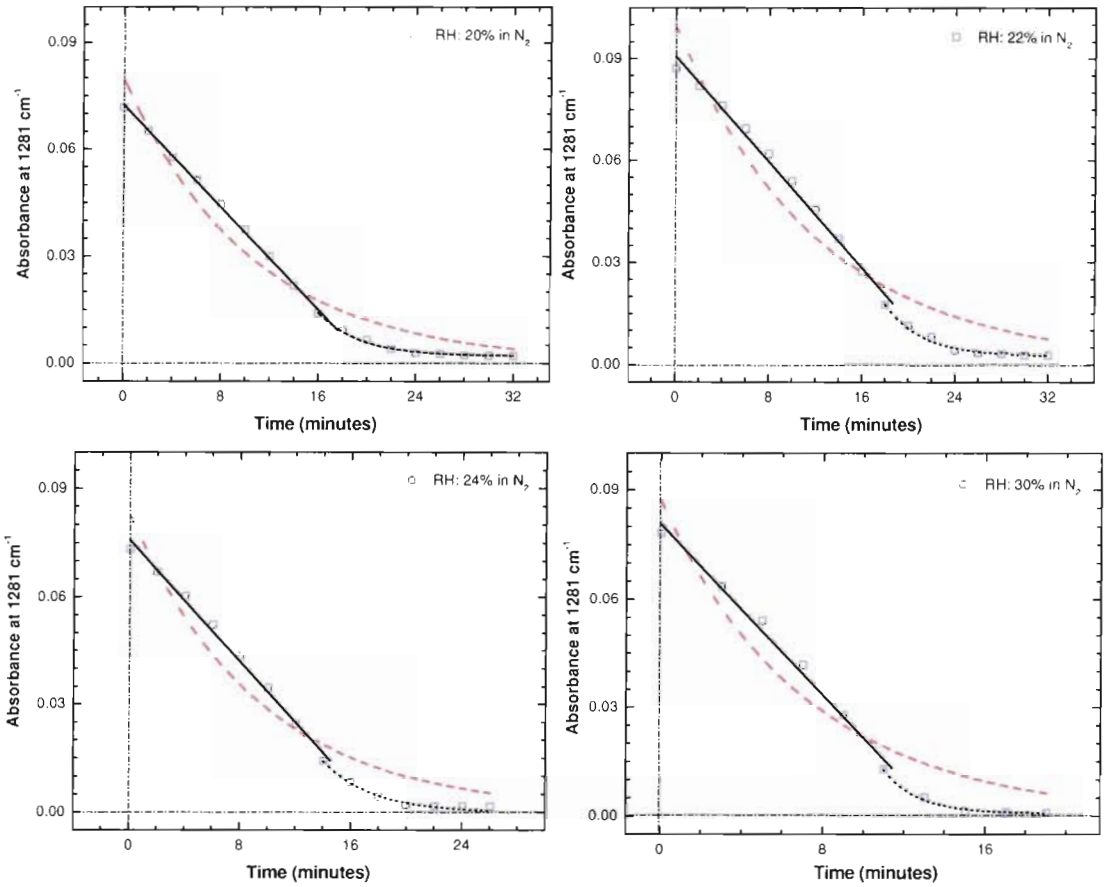

Figure 4.19 Absorbance at 1281 cm^{-1} as a function of time plotted for the films of Ag(I)tfa kept under different relative humidity levels (e) 20 %, (f) 22 %, (g) 24 %, and (h) 30 %. The open squares are the experimental data; the blue solid lines are the best linear fit; the dotted lines are first-order decay curves; the red dashed lines are the first-order curved for the whole datasets for each film.

The decay plots in Figure 4.18 and Figure 4.19 show that the reaction rate of the film does not fit a linear line or simple first-order decay, rather a combination of both. For a thermal decomposition reaction, a first order reaction is normally expected. However, from the experimental data, it appears that a zero-order reaction took place initially and a first-order reaction occurred at a later stage. A zero-order reaction is normally expected for some catalytic or photochemical reaction, in which the reaction was either controlled by the presence of catalyst

or the light intensity that excited the molecules. Since the film was kept in the dark without light irradiation, a photochemical reaction is excluded. No catalyst was employed in the film preparation or in air. The zero-order character of the decomposition suggests that other possible factor(s) are involved.

4.3.2. The effect of oxygen on the reaction rate

It is apparent that the reaction rate of the film increased with increasing the relative humidity level of the environment. It is important to understand whether oxygen could have been involved in the reaction of the film. Plots of the relative absorbance versus time for two films kept under different gas environments are shown in Figure 4.20 and Figure 4.21. The open squares represent the data acquired from the film kept in air and the filled circles data acquired under nitrogen.

In both figures, the two sets of data points overlap with each other very well. The insignificant difference suggests that the oxygen enriched or deficient in the surrounding environment has negligible effect on the decomposition rate of the film.

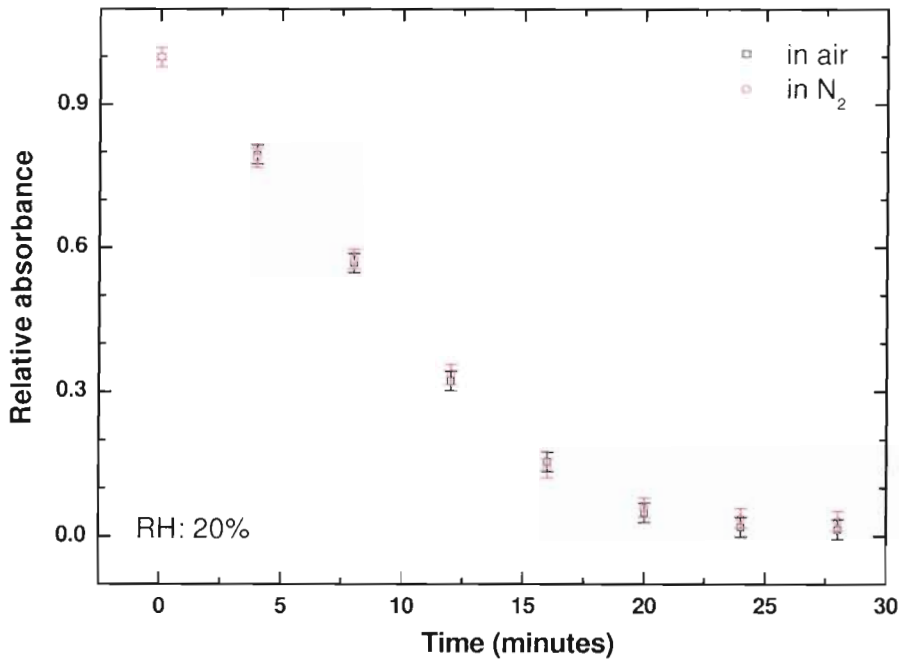

Figure 4.20 A plot of relative absorbance at 1281 cm^{-1} versus time for two films kept in different gases, air (open squares) or N_2 (filled circles), and under RH: 20 %. The error bars are ±0.02 in height.

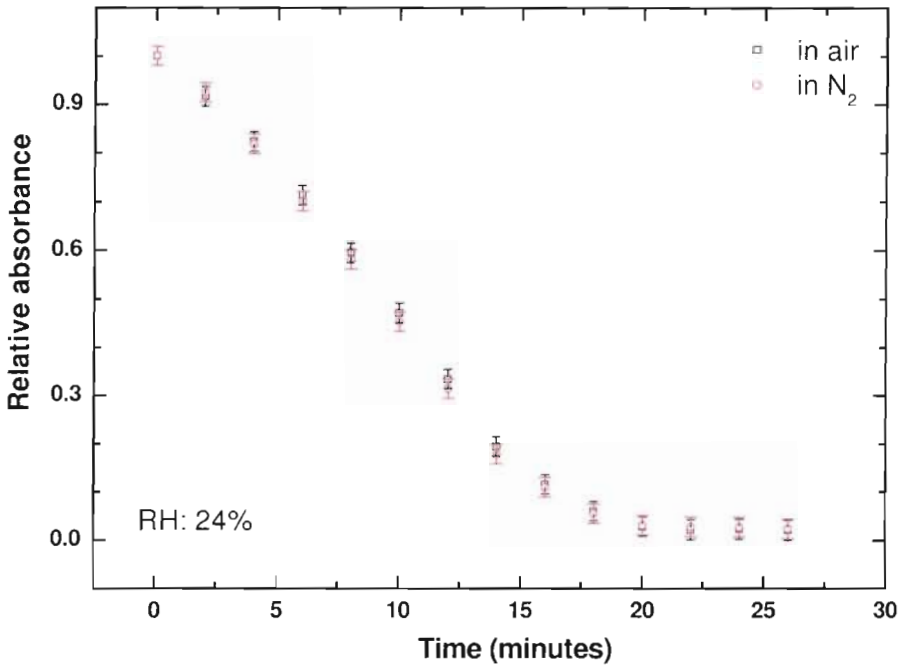

Figure 4.21 A plot of relative absorbance at 1281 cm^{-1} versus time for two films kept in different gases, air (open squares) or N_2 (filled circles) and under RH 24 %. The error bars are ±0.02 in height.

Nitrogen is an inert gas to common metal organic complexes, and involvement of nitrogen in the reaction of the film of Ag(I)tfa is unlikely.

4.3.3. A mechanistic investigation of chemical kinetics of the solid-state film of Ag(I)tfa

Since the reaction rate of the solid-state film of Ag(I)tfa increases with increasing water concentration, an understanding of how this reaction occurs is important. Before a proposal of the reaction mechanism, a brief discussion of the film structure is important.

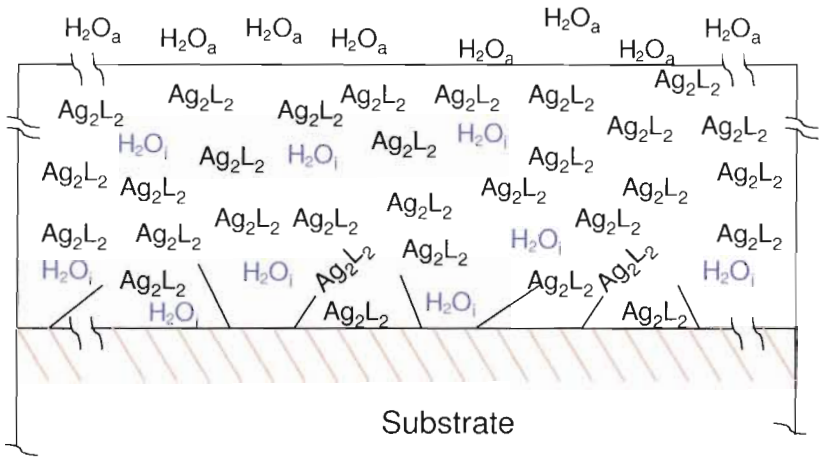

Scheme 4.1 A schematic diagram of the environment of the reaction between Ag(I)tfa and water molecules.

4.3.3.1. A possible scheme of the film structure

A solid-state film of Ag(I)tfa prepared on a substrate was determined to be amorphous from its X-ray powder diffraction pattern shown in Chapter 2 section 2.3.3.2. From the FT-IR spectrum of the film presented in Chapter 2, the film could be composed of polymeric molecules of Ag(I)tfa. It is difficult to define the

molecular structure or formula of the silver complex in this amorphous state. According to the discussion in Chapter 2 section 2.3.3.3, the formula Ag_2L_2 could be assumed to represent the silver complex in the amorphous film. A possible environment for the reaction between Ag_2L_2 and water is depicted in Scheme 4.1. In the scheme, H_2O_a represents the water molecules in air, and H_2O_i represents the water molecules diffused into the film.

The collected data and obtained results provided qualitative information of the thermal decomposition of the solid-state film of Ag(I)tfa and water. The reaction between the film and water involves water absorption, water diffusion into the solid-state film, and disproportionation reactions of Ag(I)tfa. Such a heterogeneous and complex system needs extra information and data in order to derive a potential kinetic model to describe the reaction profile. Based on the limited information, a sound theoretical model is not available. However, a simplified kinetic model is presented in the appendix. Although the model and data fitting may explain the experimental results and data, the fit may not be unique and that does not assure we have understood the kinetics of the decomposition of solid-state film of Ag(I)tfa with water.

4.4. Future work

Although a two-step kinetic model of the reaction between the amorphous film of Ag(I)tfa and water has been proposed, how the water involvement affects the contents of silver and silver oxide in the deposited film is unclear. Furthermore, it is very interesting whether this involvement would change the composition of the film, such as different silver oxides. The physical state of silver and silver oxide could be determined by X-ray powder diffraction if they are polycrystalline. The identity of silver oxide(s) is very interesting as well. Expanded research could explore the answers to these interesting questions.

Secondly, an investigation of the reaction of the film under absolute zero humidity may reveal a very different reaction mechanism or kinetics. The thermal products of the film under zero humidity are interesting. A thermogravimetric analysis under nitrogen environment would assist in understanding how the film decomposes without water and oxygen.

Thirdly, the temperature dependence of film-decay in air could explore the activation energy of the reaction and add much understanding to the thermal decomposition of (1,1,1-trifluoroacetylacetonato)silver(I).

4.5. Experimental

4.5.1. Materials and instruments

The compound, (1,1,1-trifluoroacetylacetonato)silver(I) was synthesized as reported in this thesis. The hygrometer combined with a digital thermometer was purchased from Fisher Scientific. (Only new materials are listed.)

The used instruments have been listed in the previous chapters.

4.5.2. The FT-IR spectra of the films with different thicknesses

A solution was prepared in a vial by dissolving (1,1,1-trifluoroacetylacetonato)-silver(I) (0.0315 g) in absolute ethanol (0.2892 g). This solution was filtered by a Millex syringe filter unit and used as a stock solution cooled in an ice-water bath. A circular well with a diameter 1.44 cm and a depth of 0.50 mm on one side of a single-crystal sodium chloride plate was used as the sample substrate. A measured amount of the stock solution was added by micro syringe into this circular well. A solid-state film was formed after the solvent evaporated from the well. A FT-IR spectrum of this film was recorded. The substrate was rinsed thoroughly with reagent grade acetone. Then, the second desired amount of the stock solution was added into this circular well. A solid-state film was formed after the solvent evaporated from the well. A FT-IR spectrum of the film was recorded. The same process was repeated for the FT-IR spectra of the films prepared from the desired amounts of the stock solution.

4.5.3. Procedures for FT-IR monitoring of the thermal decomposition of a solid-state film of Ag(I)tfa

All the experiments on thermal decomposition of the solid-state films of Ag(I)tfa were conducted in the following setup.

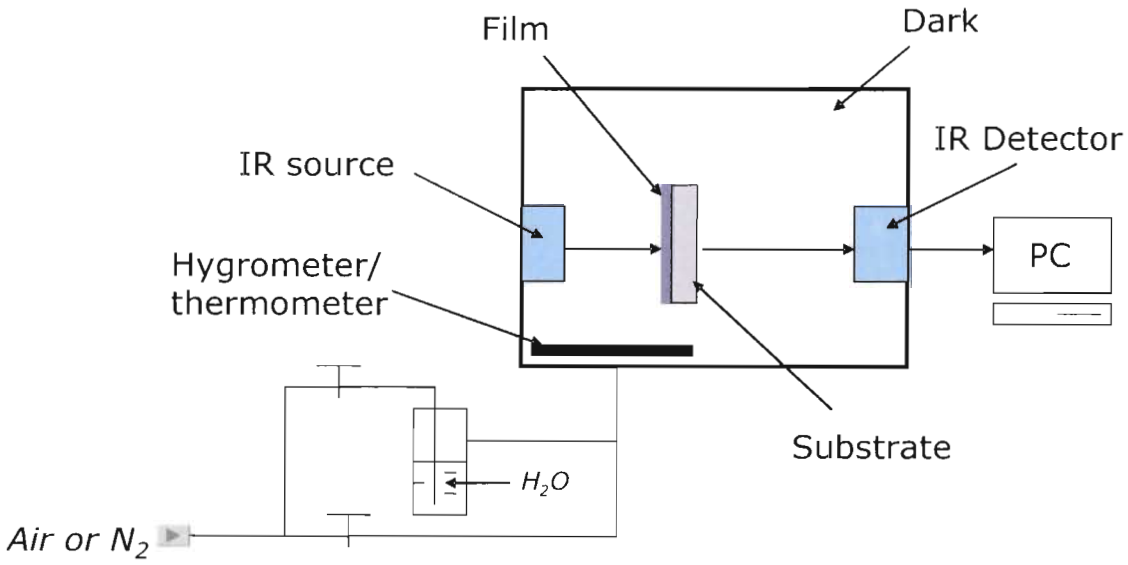

Figure 4.22 Experimental setup for the kinetic study of a solid-state film by FT-IR spectroscopy under controlled humidity.

A stock solution was prepared by dissolving (1,1,1-trifluoroacetylacetonato)-silver(I) 0.1235 g in absolute ethanol 0.9452 g. The solution was filtered by a syringe filter unit with a pore size of 0.22 micron. The stock solution was kept in an ice-water bath. A solid-state film was prepared by spin coating a CaF_2 substrate with this stock solution at a spin speed of 5000 rpm. Each time, the surface of the substrate was saturated with the stock solution before spin coating. This sample was mounted on a sample holder and placed in a FT-IR spectrometer sample chamber purged by nitrogen or dry air. The relative humidity level in the FT-IR spectrometer sample chamber was controlled by mixing dry air or nitrogen gas with the portion of the gas that passed through a water bubbler. The relative humidity and temperature in the sample chamber

was monitored by a digital hygrometer and a digital thermometer. The relative humidity level in the FT-IR spectrometer sample chamber was stabilized at least for half an hour prior to any data acquisition. The relative humidity levels were varied from 13 % to 15 %, 17 %, 18 %, 20 %, 22 %, 24 %, and 30 %. The FT-IR spectra of the film under each relative humidity level were monitored and recorded.

The effect of the different gaseous environments was studied with the films kept separately at a relative humidity level of 20 % and 24 % in the FT-IR spectrometer sample chamber using dry air instead of nitrogen.

The temporal evolution of infrared absorption of the films was monitored by FT-IR spectroscopy. The reference spectra of the bare substrate kept under individual relative humidity level were recorded before the film was coated on the substrate. All the FT-IR spectra were collected in the dark, due to the tendency of the precursor film to decompose when exposed to the light. The temperature in the FT-IR spectrometer sample chamber was stable in a range from 29.4(±0.2) to 30.0(±0.2) ℃.

4.5.4. Mass spectrum

A solution was prepared by dissolving (1,1,1-trifluoroacetylacetonato)silver(I) (0.1258 g) in absolute ethanol (1.056 g) in a vial. The solution was filtered by a Millipore syringe-driven unit with a pore size of 0.22 micron before use. A film was prepared by spin coating this solution onto a silicon substrate, which had an

area of 2.0 cm by 0.8 cm. The sample was inserted into a quartz cell wrapped completely with aluminium foil. The cell was pumped for one hour by a roughing pump. Then, the film was kept for an additional two hours inside the quartz cell wrapped with aluminium. A mass spectrum of the volatiles in the cell was obtained on an HP GCMS-5945A mass spectrometer with an electron impact source.

4.6. Reference list

(1) Belfiore, L. A.; Sun, X.; Das, P.; Lee, J. Y. *Polymer* **1999**, *40*, 5583-5599.

(2) Cardenas T, G.; Munoz D, C.; Tagle D, L. H. *Journal of Thermal Analysis* **1995**, *44*, 123-132.

(3) Cardenas T, G.; Gonzalez G, M. *International Journal of Polymeric Materials* **1997**, *35*, 71-81.

(4) Dufour, L. C.; Bertrand, G. L.; Caboche, G.; Decorse, P.; El Anssari, A.; Poirson, A.; Vareille, M. *Solid State Ionics* **1997**, *101-103*, 661-666.

(5) Brus, J.; Spirkova, M. *Macromolecular Symposia* **2005**, *220*, 155-164.

(6) Gulbransen, E. A.; Ruka, R. *Journal of Industrial and Engineering Chemistry* (Washington, D. C.) **1951**, *43*, 697-703.

(7) Johnson, C. D.; Noh, M.; Sellinschegg, H.; Schneidmiller, R.; Johnson, D. C. *Handbook of Nanostructured Materials and Nanotechnology* **2000**, *1*, 251-294.

(8) Schwarz, R. B.; Rubin, J. B. *Materials Research Society Symposium Proceedings* **1992**, *230*, 15-20.

(9) Retrieved on January 22 **2007** from http://*www.aist.go.jp/RIODB/SDBS*, SDBS #3695.

(10) Retrieved on February 6 **2007** from http://*hyperphysics.phy-astr.gsu.edu/hbase/kinetic/watvap.html*.

CHAPTER 5: SUMMARY

A silver organic complex (1,1,1-trifluoroacetylacetonato)silver(I) has been used to deposit silver/silver oxide composite films on various substrates.

(1,1,1-trifluoroacetylacetonato)silver(I) was synthesized from silver(I) oxide and 1,1,1-trifluoroacetylacetone in a ligand-enol-form promoted by the solvent, dichloromethane. Crystallization of the product was carried out in an alcohol solvent. The product was characterized by single-crystal X-ray diffraction, FT-IR spectroscopy, ^{1}H and ^{13}C NMR spectroscopy, and TGA techniques. The crystal structure was determined to be orthorhombic, space group *Fddd*. The shortest distance between two silver atoms was found to be 2.877(3) Å. Both Ag-O and Ag-C bonds were deduced in the structure and their corresponding absorption bands in the FT-IR spectrum were assigned. Identification of those bands in the FT-IR spectrum of a solid-state amorphous film suggests that the film could be a polymeric silver complex.

The proton and ^{13}C NMR spectra of Ag(I)tfa in solution were also reported. All the chemical shifts observed are similar to those of the ligand ion of Htfa. These data suggest that the silver complex dissociates as ions in solution.

Thermogravimetric investigation of the crystalline product indicated that Ag(I)tfa starts to decompose above 40 °C. The final product above 300 °C is believed to be silver.

The photochemical deposition of a silver and silver oxide film from a solid-state film of Ag(I)tfa was investigated by FT-IR, UV-vis, mass spectrometry, Auger electron spectroscopy, X-ray powder diffraction, electron diffraction, SEM, and HRTEM. The course of the photochemical reaction was monitored by FT-IR spectroscopy. From the changes of the infrared spectra, four different intermediates or products were identified. The volatile photoproducts of the film were identified by mass spectrometry, from which no parent molecular ions were identified. The solid products remaining on the substrate were characterized to be polycrystalline silver and unidentified silver oxide. The XRD pattern of the film is also in agreement with this result. The Auger spectra of the films before and after sputtering with argon revealed that the observed carbon and chlorine signals were mainly due to surface contamination. The resistivity of a 250 nm-thick film was 2.1 $\mu\Omega$ cm, which is close to the bulk silver value despite the presence of silver oxide. However, single-processed films on silicon substrates showed high sheet resistances due to their loosely packed structure and rough surfaces, which were revealed by their HRTEM and SEM images. A photochemical mechanism is not available at this time due to the unverified structure of the silver complex in amorphous state and unknown identities of the multiple intermediates. However, photolithographic patterns developed from solid-state films of Ag(I)tfa were obtained and the desired aspect ratio was achieved. No distortion and cracks of the patterns were observed.

Due to the thermal sensitivity of the amorphous film of Ag(I)tfa, the kinetics and mechanism of the decomposition of solid-state films of Ag(I)tfa in the dark were

investigated by FT-IR spectroscopy, mass spectrometry, Auger electron spectroscopy, XRD, and scanning electron spectroscopy. The mass spectrum of the volatile products suggested that Htfa was present in the volatile products. The chemical composition of the film was determined to be Ag 74 mol% and oxygen 26 mol% by Auger electron spectroscopy. The XRD data revealed that the film was composed of metallic silver and other unidentified crystalline products. The surface morphology of the deposited film was revealed to be composed of many separated nanoparticles in a loosely packed structure. The reaction rates of the films were found to increase with increasing relative humidity of the environment. The possibility of oxygen involvement in the decomposition of the film of Ag(I)tfa was eliminated by experiments with and without oxygen. Due to the complexity and heterogeneity of the system, it is not possible to develop a rational kinetic model of the decomposition of solid-state films of Ag(I)tfa at this time.

In summary, this thesis work has discovered that films composed of metallic silver and silver oxides can be prepared by different reactions, thermal and photochemical, from the same solid-state film of Ag(I)tfa. The successful preparation of crystalline Ag(I)tfa, structure characterization by various techniques, and detailed spectroscopic experimental work have added much value to the exploration of the reaction mechanisms of deposition of these silver and silver oxide films. The possible reaction mechanisms and application of these films should be explored in the future.

APPENDICES

Appendix 1 The procedure for indexing an electron diffraction pattern

The diameters ($2R$) of rings in the electron diffraction pattern were measured with a millimeter ruler with a precision of 0.5 mm on a negative film of the electron diffraction pattern. The camera length (L) was set at 1.225 meters when the image was recorded. The wavelength (λ) of the electron beam with excitation voltage 200 keV is 0.00275 nm. The d-spacing (d) was calculated from the following equation:

$$R*d = \lambda*L$$

where d is the d-spacing, that is the space between two lattice planes. At the Bragg condition,

$$\frac{2\sin\theta}{\lambda} = \frac{1}{d_{hkl}}$$

where h, k, l are the reciprocal lattice indices. For a cubic structure,

$$\frac{1}{d_{hkl}^2} = \frac{h^2+k^2+l^2}{a^2}$$

where a is the lattice parameter of a cubic crystal structure.

Appendix 2
A proposed simplified kinetic model of thermal decomposition of solid-state film of Ag(I)tfa

A brief summary of the results is listed in the following. The solid-state film of Ag(I)tfa reacts with the moisture in surrounding to produce a silver and silver(II,III) oxide film. One of the volatile thermal products could be Htfa. Due to that he reaction rates increased with increasing relative humidity in surrounding, a diffusion step of water molecules from surrounding into the silver complex film (Scheme 4.1) is reasonable. Therefore, based on these results, a reaction kinetic model for thermal decomposition of the film of Ag(I)tfa in a wet environment is proposed in the following.

$$(1) \qquad H_2O_a \underset{k_{-d}}{\overset{k_d}{\rightleftharpoons}} H_2O_i$$

$$(2) \quad Ag_2L_2 + H_2O_i \xrightarrow{k_2} Ag + AgO_x + \text{byproducts}$$

$$\text{Overall:} \quad Ag_2L_2 + H_2O_a \longrightarrow Ag + AgO_x + \text{byproducts}$$

This postulated mechanism includes two elementary steps. In the first step, the water molecules (H_2O_a) in the environment diffuse into the film to become the interface water (H_2O_i). In the second step, the molecules of Ag_2L_2 react with the diffused water to produce metallic silver, silver oxide, and by products. If silver oxide was an oxidation product of silver, the reaction in the second step should produce metallic silver and the by-products. This modification should not affect the derivation of the rate equation for $[Ag_2L_2]$.

The rate equation for $[Ag_2L_2]$ can be expressed by the following equation,

$$-\frac{d[Ag_2L_2]}{dt} = k_2[Ag_2L_2][H_2O_i] \qquad [4.4]$$

The rate equation for $[H_2O_i]$ is

$$\frac{d[H_2O_i]}{dt} = k_d[H_2O_a] - k_{-d}[H_2O_i] - k_2[Ag_2L_2][H_2O_i] \qquad [4.5]$$

If it is assumed that the concentration of H_2O_i changes slowly, the steady state approximation condition can be applied. Then, solving $[H_2O_i]$,

$$[H_2O_i] = \frac{k_d[H_2O_a]}{k_{-d} + k_2[Ag_2L_2]} \qquad [4.6]$$

Substituting $[H_2O_i]$ into equation [4.4],

$$-\frac{d[Ag_2L_2]}{dt} = \frac{k_2k_d[H_2O_a][Ag_2L_2]}{k_{-d} + k_2[Ag_2L_2]} \qquad [4.7]$$

If the absorbance is due to Ag_2L_2 only, then, from the Beer-Lambert law,

$A = k[Ag_2L_2]$

where $k = \varepsilon l$, and

$$\frac{d[Ag_2L_2]}{dt} = \frac{1}{k}\frac{dA}{dt}$$

The differential rate equation [4.7] changes to the following,

$$-\frac{dA}{dt} = \frac{k_2k_d[H_2O_a]A}{k_{-d} + k_2A/k} \qquad [4.8]$$

Integrating this differential equation [4.8] from the absorbance (A_0) at time zero to the absorbance (A_t) at time t,

$$\int_{A_0}^{A_t} -\frac{k_{-d} + k_2 A / k}{k_2 k_d [H_2O_a] A} dA = \int_0^t dt$$

The integrated rate equation is

$$t = -\frac{(A_t - A_0)}{k k_d [H_2O_a]} - \frac{k_{-d}}{k_2 k_d [H_2O_a]} \ln\left(\frac{A_t}{A_0}\right) \qquad [4.9]$$

under the assumption that the water concentration in the chamber($[H_2O_a]$) is constant. Mathematically, this equation has no explicit solution for A_t as a function of time.

A.2.1 Prediction of the differential rate equation

The experimental results suggest that the reaction of the film has initially zero-order kinetics followed by first-order kinetics at a later stage to the end. Whether the deduced differential rate equation can predict this trend is important. The differential equation of the reaction between the Ag(I)tfa film and water is shown as equation [4.8]. If it is assumed that $k_{-d} << k_2 A / k$, then the rate equation reduces to the following.

$$-\frac{1}{k}\frac{dA}{dt} = -\frac{d[Ag_2L_2]}{dt} = k_d[H_2O_a] \qquad [4.10]$$

This equation [4.10] describes zero-order kinetics. It also predicts that the reaction rate of AgL increases with increasing water concentration [H_2O_a]. These predictions are qualitatively consistent with the experimental results.

If it is assumed that $k_{-d} >> k_2A/k$, then the rate equation reduces to

$$-\frac{1}{k}\frac{dA}{dt} = -\frac{d[Ag_2L_2]}{dt} = \frac{k_2k_d[H_2O_a]}{k_{-d}}[Ag_2L_2] \qquad [4.11]$$

As k_2, k_d and k_{-d} are rate constants, this equation [4.11] describes first-order kinetics. This also suggests that the change of reaction order from zero-order to first-order is related to the kinetics of diffusion of water into the film. Furthermore, the relative magnitudes of k_{-d} and k_2A/k depend on the absorbance and can cause the reaction order to change. This is consistent with the experimental results, in which the first-order reaction always appeared at the later stage of the reaction of the films.

A.2.2 Data fitting with the integrated rate equation

It is important to test whether the integrated rate equation [4.9] fits the experimental data. For simplification of the data fitting, let,

$a_1 = kk_d$, $a_2 = k_{-d}/(k_2k_d)$

Then, the integrated rate equation changes to,

$$t = -\frac{A_0(A_t/A_0 - 1)}{a_1[H_2O_a]} - \frac{a_2}{[H_2O_a]}\ln\left(\frac{A_t}{A_0}\right) \qquad [4.12]$$

Eight datasets collected under different relative humidity levels were tested. The values of the right side of the equation were calculated based on the experimental data. The water concentration ($[H_2O_a]$) was calculated from the measured relative humidity levels. All the data were acquired at temperatures near 30.0 °C and the saturated water vapor density ($[H_2O_a]_s$) of 30.4 g/m^3 was taken from the literature.[10] Chi-square minimization was used to fit the calculated values of theoretical reaction time ($t_{(calc)}$) to the values of the experimental decay time ($t_{(expt)}$). The reduced chi-square (χ^2) is defined by the following equation.

$$\chi^2 = \frac{1}{n-p}\sum_n \left(\frac{(t_{(calc)i} - t_{(expt)i}}{\delta_i} \right)^2 \qquad [4.13]$$

where n is the total number of data points, p the number of fitting parameters, and δ the error associated with $t_{(calc)}$ that was propagated by the following methods.

$$\delta_i = t_{(calc)} \sqrt{\left(\frac{s_{(rh)}}{(RH)_{fitted}} \right)^2 + \left(\frac{s_{(A)i}}{A_i} \right)^2} \qquad [4.14]$$

where $s_{(rh)}$ is the error (2 %) of the relative humidity, $s_{(A)}$ the error associated with each absorbance. For each set of spectral data, the RH and $s_{(A)}$ are assumed constant. The values of $s_{(A)}$ are chosen from a range between 0.0005 and 0.002 based on the noise of the spectra. The best-fit values of the parameters ($a_1$and a_2) are listed in Table A.

In Table A, the reduced chi-square values for the data obtained under relative humidity 13% is large and this data set was rejected. This could be due to

erroneous reading of the hygrometer at this low level. A control experiment showed that the hygrometer did not respond correctly after it was kept in dry nitrogen overnight. The other reduced chi-square values are close to unity after some adjustment of the relative humidity levels. These variations are believed due to the errors of the response of the hygrometer and/or possible unstable humidity control of the reaction chamber.

Table A The best-fit parameters for the integrated rate equation for the kinetic decay of films kept under different relative humidity levels.

Parameters	**Fitting values**	**Experimental RH±2 (%)**	**Fitted RH (%)**	χ^2
a_1	11	13	3.0	~~1.54~~
a_2	0.00060	15	11	0.99
		17	15	0.99
		18	17	0.99
		20	22	0.99
		22	24	0.99
		24	25	0.99
		30	40	0.99

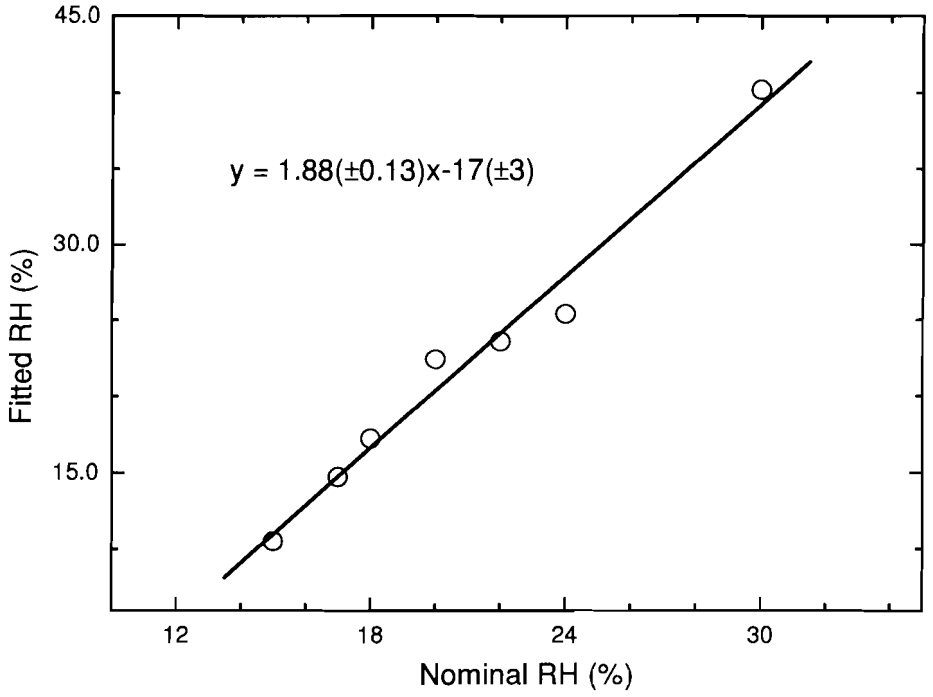

Figure A1 The relationship between the experimental and fitted values of relative humidity (RH).

In order to examine whether the fitted RH values could have a meaningful relationship with the experimental RH values, a plot of the fitted values versus the nominal relative humidity is shown in Figure A1. The figure shows that the data points fall on a line. This linear relationship suggests that the hygrometer responded linearly with increasing relative humidity. Therefore, the fitted values of relative humidity are believed to be reasonable.

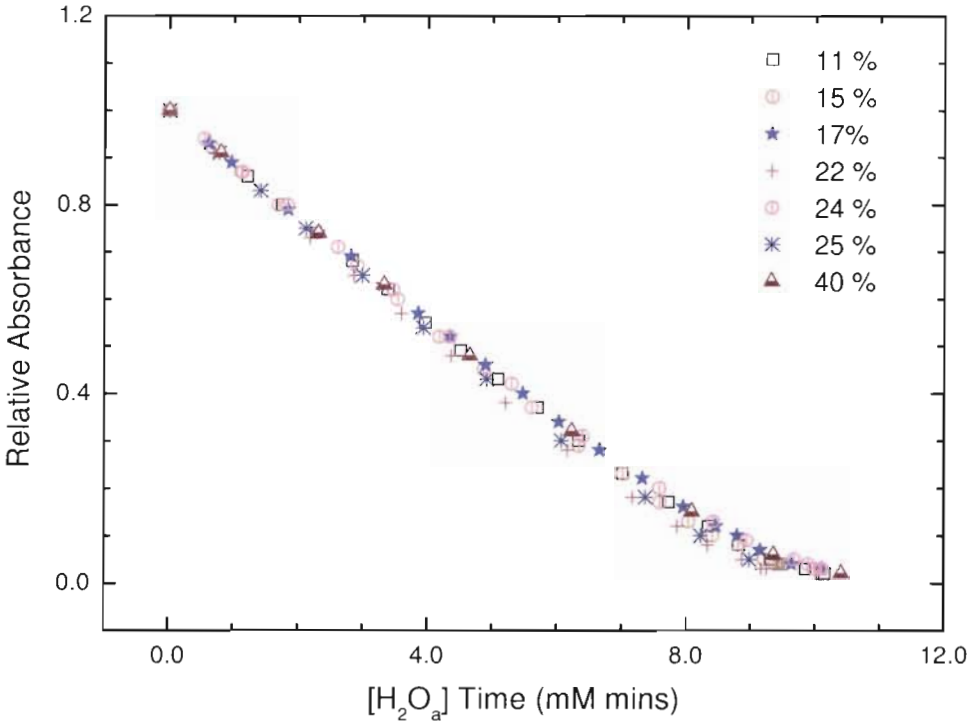

Figure A2 Plots of relative absorbance versus ([H_2O_a] Time) for the data sets obtained under different fitted values of relative humidity.

According to equation [4.12], plots of relative absorbance versus the values of ([H_2O_a] Time) for each dataset should give the same profile, which means the plots of the films kept under different humidity levels should overlap with each other. This is a further test of whether the data fit is reasonable. Plots of relative absorbance versus the values of ([H_2O_a] Time) for seven datasets (the one acquired under RH 13 % was excluded.) are displayed in Figure A2. The plots overlap with each other very well with considering that the average percentage error of readings of RH is about 10%. Therefore, the fitting result supports that the deduced rate equation can be used to explain the experimental results.

The data fitting could be further improved if accurate humidity measurements were made. Since the reaction rate is sensitive to the relative humidity, an

instantaneous recording of the relative humidity could provide valuable information.

A.2.3 Justification of the fitting parameters

The fitted values of a_1 and a_2 ($a_1 = kk_d$, $a_2 = k_{-d}/(k_2k_d)$) can be used to justify whether the assumptions used to predict the reaction orders are reasonable. The two conditions are $k_{-d} << k_2A/k$ and $k_{-d} >> k_2A/k$. Rearranging gives,

$$\frac{kk_{-d}}{k_2} << A, \text{and } \frac{kk_{-d}}{k_2} >> A,$$

The product of (a_1 a_2) is $\frac{kk_{-d}}{k_2}$. Therefore, the conditions correspond to $a_1a_2 << A$ and $a_1a_2 >> A$, respectively. From the results in Table A, the product (a_1 a_2) is 0.0066. The average initial absorbance (A) of the films of Ag(I)tfa is no less than 0.0807, which is one order greater than 0.0066. This suggests that the first condition is valid. If the absorbance decreases to 0.0066, this condition becomes invalid, and with further decrease, the second condition becomes valid. During the whole course of the decomposition, the absorbance of the film of Ag(I)tfa decreases continually because of the decomposition of the film. The fitted parameters are in good agreement with the assumptions used in the predictions.